NASA TECHNICAL MEMORANDUM

NASA TM-77293

EXPERIMENTAL DETERMINATION OF GAP FLOW-CONDITIONED FORCES AT TURBINE STAGES AND THEIR EFFECT ON THE RUNNING STABILITY OF SIMPLE ROTORS

Raimund Wohlrab

Translation of "Experimentelle ermittlung spaltstromungsbedingter krafte an turbinenstufen und deren einfluss auf die laufstabilitat einfacher rotoren", Muenchen, Technische Universitaet, Fachbereich Maschinenwesen, Doctoral Dissertation, Munich, (West Germany), 1975, pp 1-161

NATIONAL AERONAUTICS AND SPACE ADMINISTRATION
WASHINGTON, D.C. 20546 CCTOBER 1983

STANDARD TITLE PAGE

1. Report No. NASA TM-77293	2. Government Accession No.	3. Recipient's Catalog No.
4. Title and Subtitle EXPERIMENTAL DETERMINATION OF GAP FLOW-CONDITIONED FORCES AT TURBINE STAGES AND THEIR EFFECT ON THE RUNNING STABILITY of SIMPLE ROTORS		5. Report Date OCTOBER 1983 6. Performing Organization Code
7. Author(s) Raimund Wohlrab		8. Performing Organization Report No. 10. Work Unit No.
9. Performing Organization Name and Address SCITRAN Box 5456 Santa Barbara, CA 93108		11. Contract or Grant No. NASw- 3542 13. Type of Report and Period Covered Translation
12. Sponsoring Agency Name and Address National Aeronautics and Space Administration Washington, D.C. 20546		14. Sponsoring Agency Code

15. Supplementary Notes

Translation of "Experimentelle ermittlung spaltstromungsbedingter krafte an turbinestufen und deren einfluss auf die laufstabilitat einfacher rotoren", Muenchen, Technische Universätaet, Fachbereich Maschinenwesen, Doctoral Dissertation, Munich (West Germany), 1975, pp 1-161 (A76-42648)

16. Abstract

Instabilities in turbine operation can be caused by forces which are produced in connection with motions involving the oil film in the bearings. An experimental investigation regarding the characteristics of such forces in the case of three typical steam turbine stages is conducted, taking into account the effect of various parameters. Supplementary kinetic tests are carried out to obtain an estimate of flow forces which are proportional to the velocity.

17. Key Words (Selected by Author(s))	18. Distribution Statement
	Unclassified - Unlimited

19. Security Classif. (of this report)	20. Security Classif. (of this page)	21. No. of Pages	22. Price
Unclassified	Unclassified	198	

This dissertation originated in the context of the research project "Rotor instability due to gap excitation", of the Research Association for Internal Combustion Engines, being implemented at the Institute for Thermal Power Systems of the Technical University of Munich. Numerical calculations were performed at the Leibnitz Computer Center of the Bavarian Academy of Sciences.

I am especially grateful to the Institute's director, Prof. Dr. H.-J. Thomas, whose interest in this study's progress was always an ecouragement for this study, and who made it possible for me to complete this task while I was an assistant to his chair. I would like to thank Prof. Dr. K. Magnus for the interest he contributed to this effort, as co-reporter.

I am deeply grateful to Dr. K. Urlichs for stimulating discussions and invaluable suggestions for the design of the test installation. I am also indebted to engineer E. B. Leie for his assistance during tests and their evaluation. My gratitude also goes to the member companies of the Research Association for Internal Combustion Engines, who undertook the fabrication of the major components of the test installation and made the test stages available. In addition, my gratitude is due the Institute's machine shops, who contributed substantially to the success of this effort.

Munich, December 1975

Raimund Wohlrab

TABLE OF CONTENTS

1 INTRODUCTION

The rotor's vibration behavior plays an essential role in the operating safety of turbomachines of any kind. The interfering running disorders can be divided here into those depending on the rotation rate and those unrelated to it. Rotation frequency related motions are forced vibrations of the rotor system, caused by mechanical or thermal unbalance. They have been in the foreground of consideration for many years. Today, due to significant improvements in balancing techniques, a more precise knowledge of the thermal behavior of rotors and more precise pre-calculations of resonance velocities and amplitudes, there is a sufficient availability of methods to avoid operation interruptions due to forced vibration. Today, interruption or restriction of operations caused by rotor vibrations unrelated to the rotation frequency are becoming increasingly important. The cause of such vibrations is overwhelmingly to be found in system self-excitation, and hence they are indicative of rotor motion instability.

One instability of this kind - particularly serious, when it occurs - is the so-called "oil whip". The cause of this phenomenon which has been extensively studied, these past years, lies in the anisotropic elastic and damping characteristics of the bearing's lubricating film. In this case, instability occurs above a certain rotation velocity. Exceeding a certain output may trigger the occurrence of another, equally dangerous form of self-excited rotor vibration. In view of the worldwide effort to increase the output of machine units, in turbomachine engineering, it seems necessary to investigate the kind and magnitude of output-dependent excitation mechanisms more intensively than has been done.

---

* Numbers in the margin indicate foreign pagination

/2

1.1. Current research status

While numerous experimental and theoretical studies are available regarding the problem of bearing instability, there are few publications on the problem of output-dependent excitation mechanisms. Thomas [1] first pointed out the possibility of stimulation of self-excited vibration caused by variable seal-losses along the perimeter, in thermal turbomachines (gap or clearance excitation). Gasch [2] expanded the stability study of rigidly supported shafts by taking into consideration the internal damping and determined the excitation force as in [1], but using newer gap loss equations, from [17]. In addition to the transverse forces caused by eccentric rotor positioning, pressure differences can arise in the seal gaps - due to variable leakage along the perimeter - that generate stimulating forces [3, 4, 5, 19, 20]. If we consider, under simplifying assumptions, the rotor stressing that is produced for small deflections and deflection velocities of the shaft, as a consequence of modified flow conditions at tne rotor, then we can calculate a series of forces and moments [6].

Theoretical stability considerations for both simple and complex rotor systems that take into account friction bearing and fluid forces can be found in a number of publications [7 through 14], while in the area of experimental studies regarding gap excitation we have only Winter's [15] and, in a more limited way, Pollmann's [9] studies. However, from the stability limits found in these studies, it is possible only to determine conditioned gap excitation forces, since the required sufficiently exact determination of the damping forces occurring in test installations presents considerable difficulties.

/3

1.2. Objective

It seems necessary - from the development of turbomachines to ever greater unit output - to be able to calculate the output-dependent self-excited vibrations more precisely than had been possible. This would provide information to the designer to enable him to build the rotor in such a manner that a sufficient safety margin to the stability limit can be maintained. Besides suitable calculation procedures to determine the stability limits, it is necessary to ready realistic coefficients for the calculation of the external forces acting on the shafts. Voluminous test data are already available for the bearing-related forces (for instance. [16]), while only theoretical bases exist for flow generation-related coefficients.

Within the context of this study, flow-dynamic force coefficients proportional to the deflection are experimentally determined for three typical steam turbine stages, as a function of various stage parameters. To this end, the forces and moments acting on the rotor are measured for eccentric positioning with respect to the housing (force measurements). In these measurements, the gap excitation forces - which for rotor misalignment manifest themselves as stationary transverse forces vertical to the direction of deflection - are in the foreground. To a lesser extent are measured the forces acting in the direction of deflection, as well as the momenta acting on the rotor; the coefficients for the vibration calculations are derived from these measurements.

Supplementary kinetic tests are intended to estimate the effect of fluid forces proportional to the velocity. The foundation for these measurements is a detailed theoretical consideration on the damping behavior of a vibration model corresponding to the test installation.

This study concludes with an analytical investigation of the effect of the fluid forces measured on the stability behavior of a simple, friction bearing supported model rotor.

2 THEORETICAL FOUNDATION

2.1 General definitions

We wish to describe the changes in the forces and momenta acting through the flow medium on the rotor of a turbomachine, when the latter moves with respect to its stationary position.

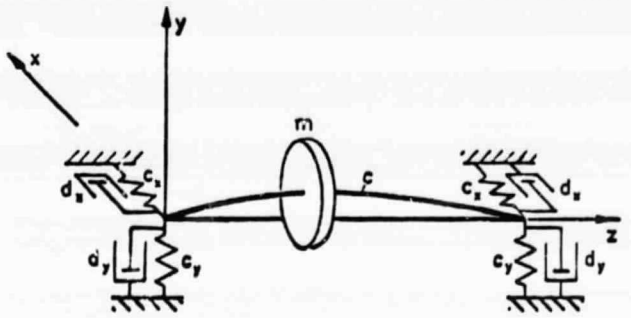

Figure 2.1 Rotor model and coordinate system

Figure 2.1, above, shows the spatial coordinate system x,y,z to be used. The z axis falls on the line combining the centers of the trunnions during stationary equilibrium. The rotation of the rotor is described by the angular velocity vector $(0,0,\omega)$.

If we represent the deformed shaft center-line in top and side projection (Figure 2.2, below), then we have, for the bending angle,

$$\varphi_x = -\frac{\partial y}{\partial z}, \quad \varphi_y = \frac{\partial x}{\partial z}. \qquad (2.1)$$

The external forces acting on the rotor are defined as positive in the direction of the coordinates, as usual. The same convention is applied to the right-handed system chosen for the external momenta.

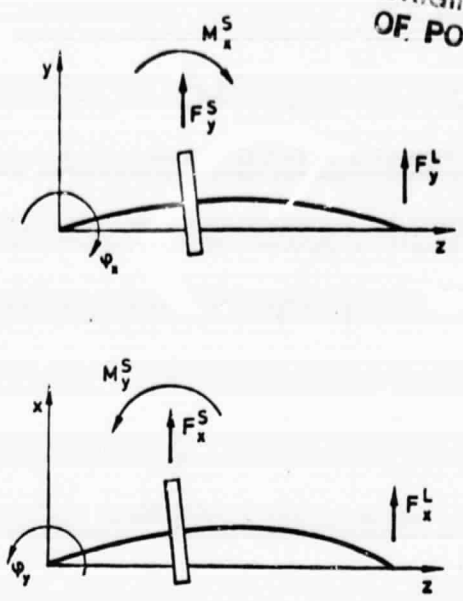

Figure 2.2 Definition of forces on the rotor model

Assuming small dynamic displacements, the external forces and momenta present besides the stationary stress can as a first approximation be taken as linear with respect to the motion. /5
In conformance with this linear theory, the load vector $\mathfrak{y}$ can be described in matrix notation, as a function of the movement vector w, as follows:

$$\mathfrak{y} = \mathfrak{R} w + \mathfrak{k} \frac{\partial w}{\partial t} . \quad (2.2)$$

The load vector $\mathfrak{y}$ and the movement vector w are defined as

$$\mathfrak{y} = \begin{bmatrix} F_x \\ F_y \\ M_x \\ M_y \end{bmatrix}, \quad w = \begin{bmatrix} x \\ y \\ \varphi_x \\ \varphi_y \end{bmatrix}, \quad (2.3)$$

while the coefficient patterns of the deflection matrix $\mathfrak{R}$ and the velocity matrix $\mathfrak{k}$ are as follows:

$$\mathcal{R} = \begin{bmatrix} r_{11} & r_{12} & r_{13} & r_{14} \\ r_{21} & r_{22} & r_{23} & r_{24} \\ r_{31} & r_{32} & r_{33} & r_{34} \\ r_{41} & r_{42} & r_{43} & r_{44} \end{bmatrix}, \quad \mathcal{K} = \begin{bmatrix} k_{11} & k_{12} & k_{13} & k_{14} \\ k_{21} & k_{22} & k_{23} & k_{24} \\ k_{31} & k_{32} & k_{33} & k_{34} \\ k_{41} & k_{42} & k_{43} & k_{44} \end{bmatrix}. \qquad (2.4)$$

Because of the problem's isotropy, the two-row, two-column matrices outlined have certain symmetry characteristics: the elements of the principal diagonals are the same; the elements of the secondary diagonals differ only in their sign.

In a dimensionless representation of flow-conditioned forces and momenta in turbine stages, equation (2.2) can be written as follows:

$$\mathcal{L}_S^* = \mathcal{R}_S \cdot \mathcal{W}^* + \mathcal{K}_S \cdot \dot{\mathcal{W}}^*$$

or

$$\begin{bmatrix} \frac{F_x^S}{U_s} \\ \frac{F_y^S}{U_s} \\ \frac{2M_x^S}{d_m U_s} \\ \frac{2M_y^S}{d_m U_s} \end{bmatrix} = \begin{bmatrix} K_1 & -K_2 & K_3 & K_4 \\ K_2 & K_1 & -K_4 & K_3 \\ L_1 & -L_2 & L_3 & L_4 \\ L_2 & L_1 & -L_4 & L_3 \end{bmatrix} \cdot \begin{bmatrix} \frac{x}{l''} \\ \frac{y}{l''} \\ \frac{\varphi_x d_m}{2l''} \\ \frac{\varphi_y d_m}{2l''} \end{bmatrix} + \begin{bmatrix} A_1 & -A_2 & A_3 & A_4 \\ A_2 & A_1 & -A_4 & A_3 \\ B_1 & -B_2 & B_3 & B_4 \\ B_2 & B_1 & -B_4 & B_3 \end{bmatrix} \cdot \begin{bmatrix} \frac{2\dot{x}}{d_m \omega} \\ \frac{2\dot{y}}{d_m \omega} \\ \frac{\dot{\varphi}_x}{\omega} \\ \frac{\dot{\varphi}_y}{\omega} \end{bmatrix}. \qquad (2.5)$$

Here U_s is the isentropic peripheral or tangential force, d_m the average diameter, l'' the blade length and ω the rotor's angular velocity. The matrices $\mathcal{R}_S$ and $\mathcal{K}_S$ contain dimensionless coefficients of the flow-conditioned forces and momenta, in which the above symmetry condition has already been taken into account. The coefficients' signs depend on the shaft's direction of rotation and the fluid's direction of flow through the rotor.

The signs defined in (2.5) are applicable to positive direction of rotation and of flow (in the direction of the z axis).

It is possible to represent the bearings' dynamic restoring forces in a similar manner, in the coordinate system x, y. The symmetry condition mentioned above is not satisfied here, as a rule. In contrast, assuming punctiform support, the external moments vanish. In addition, in general forces due to the bearings' cant are usually neglected. We thus have

$$\mathfrak{F}_L = -\mathfrak{R}_L \varphi - \mathfrak{D}_L \dot{\varphi} ,$$

or

$$\begin{bmatrix} F_x^L \\ F_y^L \end{bmatrix} = -\begin{bmatrix} c_{xx} & c_{xy} \\ c_{yx} & c_{yy} \end{bmatrix} \cdot \begin{bmatrix} x \\ y \end{bmatrix} - \begin{bmatrix} d_{xx} & d_{xy} \\ d_{yx} & d_{yy} \end{bmatrix} \cdot \begin{bmatrix} \dot{x} \\ \dot{y} \end{bmatrix} . \qquad (2.6)$$

/7

The bearings' characteristic magnitudes are composed of four force and damping constants or coefficients, whose sign is established by the system of coordinates adopted above. For the usual friction bearings voluminous measurement results are already available, from Glienicke [16]. It should be pointed out that in [16] the positive direction of rotation is defined inversely, with the consequent sign change in the coupling term, when the coefficients c_{ik} and d_{ik}, respectively, are transferred into the coordinate system here adopted.

2.2. Calculation of flow-conditioned forces

During a displacement of the turbine rotor in the housing, necessarily different gap width along the perimeter of the stator and the rotor will be caused, at the non-contact seal gaps. This changes the gap loss and the distribution of the

tangential forces over the rotor; as a consequence, a resulting force will act on the shaft. At the same time, the pressure distribution in the seal gaps will become asymmetrical, also generating a force to act on the rotor. In a vibration calculation, both portions - the transverse force Q_S due to the gap loss and that arising from the pressure distribution, Q_D - must be added. Since the deflections are the same, the coefficients of the deflection matrix α_S^* will also be composed of two portions,

$$Q = Q_S + Q_D , \quad K = K_S + K_D . \qquad (2.7)$$

From another viewpoint, one could start, with Piltz [6], from the premise that rotor displacements cause a variation in the local flow cross-sectional areas and velocities, and hence, that due to modifications in the triangle of velocities, forces and momenta act on the rotor.

Due to the isotropy of flow-conditioned forces, it is sufficient to determine the coefficients in a co-rotating system for displacements in only one direction. Below, this direction is identified by subscript "1", while the axis perpendicular to it is characterized by a "2".

/8

2.2.1. Forces due to variable seal losses caused by eccentric rotor position

A first physicl explanation for the generation of an excitation force [1] starts from the premise that, as shown in Figure 2.3 below, a turbine rotor that suffers a deflection e will exhibit uneven tangential forces. For a small local seal gap ($\phi = 0$), due to the smaller gap loss a larger tangential force will occur; this force will be correspondingly smaller at the diametrically opposed location.

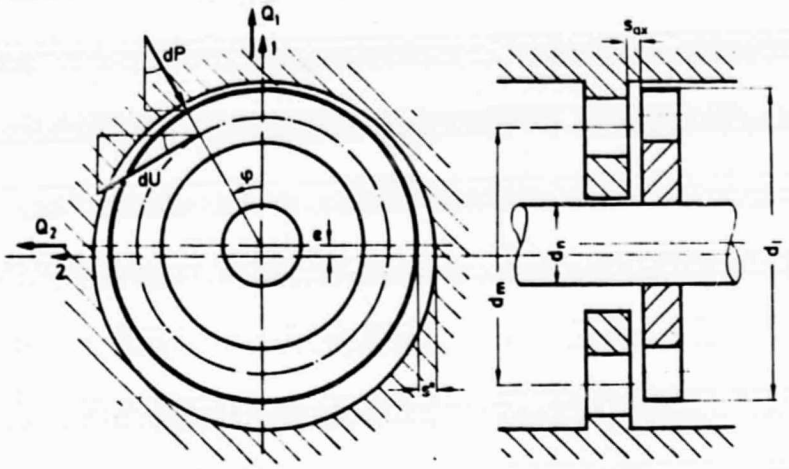

Figure 2.3 Derivation of the gap excitation forces

The tangential force U_i at a turbine stage results from the specific work $\underline{a}_i$, the throughput $\dot{m}$ and the tangential velocity $\underline{u}$

$$U_i = \frac{a_i \dot{m}}{u} . \qquad (2.8)$$

The dependence of the internal tangential force U_i on the gap width can be described either by the reduced work a_{sp} - as in [17] - or as in [1], due to the loss of volume $\dot{m}_{sp}$. Both effects can be combined in the tangential force lost in the gap,

$$U_{sp} = U_u - U_i \qquad (2.9)$$

/2

where U_u is the tangential force without gap loss. If we define with U_s the isentropic tangential force that could be attained in a loss-free flow, then the inner and the tangential efficiency, as well as the gap loss, can be defined as force ratios:

$$\eta_u = \frac{U_u}{U_s} , \quad \eta_i = \frac{U_i}{U_s} , \quad \zeta_{sp} = \frac{U_{sp}}{U_s} . \qquad (2.10)$$

The local tangential force then becomes

$$dU = \frac{U_1}{2\pi}\cdot d\varphi = \frac{U_s}{2\pi}\cdot(n_u - \zeta_{sp})\cdot d\varphi \,. \qquad (2.11)$$

Integrating along the rotor perimeter, from Figure 2.3 we obtain the transverse forces

$$\left.\begin{aligned} Q_{1S} &= -\int_0^{2\pi} dU\cdot\sin\varphi\, d\varphi = \frac{U_s}{2\pi}\int_0^{2\pi}\zeta_{sp}(\varphi)\cdot\sin\varphi\, d\varphi \,, \\ Q_{2S} &= \int_0^{2\pi} dU\cdot\cos\varphi\, d\varphi = -\frac{U_s}{2\pi}\int_0^{2\pi}\zeta_{sp}(\varphi)\cdot\cos\varphi\, d\varphi \,. \end{aligned}\right\} \quad (2.12)$$

As a first approximation, the gap loss $\zeta_{sp}(\phi)$ for the stator and the rotor can be set as proportional to the local gap width

$$s'(\varphi) = s' - e\cos\varphi \,, \quad s''(\varphi) = s'' - e\cos\varphi \qquad (2.13)$$

of the stator or respectively, rotor seal:

$$\zeta_{sp}(\varphi) = k'\cdot s'(\varphi) + k''\cdot s''(\varphi) \,. \qquad (2.14)$$

Hence, the transverse forces are

$$\left.\begin{aligned} Q_{1S} &= 0 \,, \\ Q_{2S} &= \tfrac{1}{2}\cdot U_s\cdot(k' + k'')\cdot e \,. \end{aligned}\right\} \qquad (2.15)$$

The magnitudes k' and k" can be determined, for instance, from gap loss equations in Traupel [17]; for blading with labyrinth seals we obtain

$$k' = \frac{K'_{II}}{\sqrt{z'}}\cdot\frac{d_n}{d_m l'\sin\alpha_1} \,, \quad k'' = \frac{K''_{II}}{\sqrt{z''}}\cdot\frac{d_1}{d_m l''\sin\beta_2} \,. \qquad (2.16)$$

Here α_1 and β_2 designate the angles of emergence, l' and l" the blade lengths of the stator and, respectively, the rotor, z' and

z" the number of seal peaks in the stator and respectively, rotor labyrinths and K'_{II} and K''_{II} are gap loss coefficients /10 that can be taken from Figure 2.4 below as a function of the

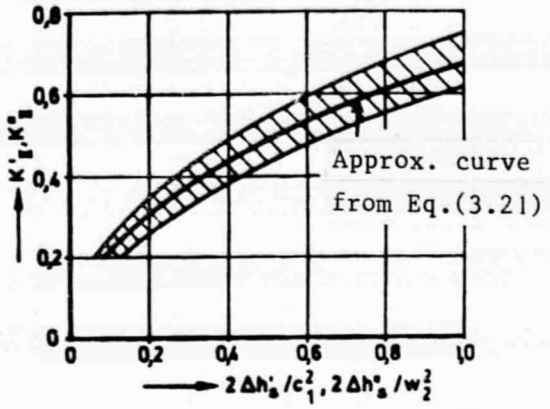

Figure 2.4 Gap loss coefficient K_{II} for labyrinth seals, from [17]

relative gradient $2\Delta h'_s/c_i^2$ for the stator, or respectively, $2\Delta h''_s/w_2^2$ for the rotor. Here, for the stator we must use the gradient $\Delta h'_{si}$ at the foot of the blade, and for the rotor, the gradient $\Delta h''_{sa}$ at the head of the blade. For a dimensionless description it seems appropriate to relate the deflection e to the length l" of the rotor blade; we thus obtain

$$\frac{Q_{2S}}{U_s} = K_{2S} \cdot \frac{e}{l''} , \qquad (2.17)$$

where

$$K_{2S} = K'_{2S} + K''_{2S} = \frac{1}{2} \cdot \left(\frac{K'_{II}}{\sqrt{z'} \sin\alpha_1} \cdot \frac{d_n}{d_m} \cdot \frac{l''}{l'} + \frac{K''_{II}}{\sqrt{z''} \sin\beta_2} \cdot \frac{d_1}{d_m} \right). \qquad (2.18)$$

The so-called gap excitation coefficient K_{2S} reflects the slope of the relative excitation force Q_{2S}/U_s over the relative eccentricity e/l". For the opposite direction of rotation we obtain a sign reversal for K_{2S}, but the flow direction has no effect.

The transverse forces and coefficients, respectively, due to a variable axial gap loss caused by an inclination of the rotors, can be calculated in a similar manner [20].

/11

2.2.2. Forces arising out of the pressure distribution in the seal gap

For a seal gap that is not uniform along the perimeter, under flow conditions the throughput and the pressure will change with the local gap width. For a purely axial flow, a characteristic pressure distribution results along the perimeter, with a maximum at the narrowest width (cf. curve in Figure 2.5, below).

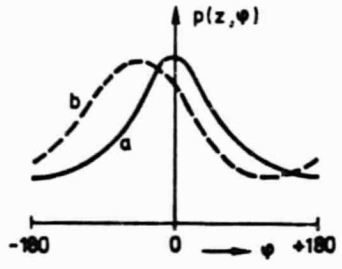

Figure 2.5 Qualitative pressure curve
a) Purely axial flow
b) Torsionally affected flow

This pressure course, described by Lomakin [18] for a smooth gap, gives rise to a transverse force against the direction of deflection.

It is not possible, in general, to start from a purely axial flow through the seal gap, with thermal turbomachines. The runner's rotation can impart a tangential component to the gap flow, analogous to that of gas bearings [24]. However, because of the relatively large gap widths or respectively, large chamber height in labyrinths, as well as the low tangential

rotor velocity, this effect will be small in stage sealing. In contrast, with turbines there will be a strong torsional effect on the flow in the direction of rotation, especially before the rotor gap. Considering the changes in the seal gap flow caused by this, the smallest flow will occur already before the narrowest gap ($\phi = 0$), and as illustrated in Figure 2.5 above, in curve b, the pressure maximum will occur before the narrowest gap. The integration of this pressure curve along the perimeter results not only in a force opposed to the direction of reflection, but also a vibration exciting force perpendicular to the deflection.

Considerations similar to these for a smooth rotor gap can be transferred also to the labyrinth seals customary in turbines.

/12

According to Alford [3], forces are also caused by the shaft's vibrational motion, if the gap width at the entrance seal peaks is smaller than that at the exit. However, in a recent publication Spurk [4] comes to the opposite conclusion when he takes the equalizing flow in tangential direction into account. Under the assumption that the velocity energy is completely turbulent at a seal peak, Kostyuk [5] derived vibration exciting forces, generated in a labyrith seal for shaft inclination. However, displacements parallel to the axis do not generate transverse forces, under the assumption of complete turbulence.

Assuming an oblique flow across the gap, which may be the result of shaft rotation or also of torsional effects on the incident flow, Rosenberg [19] investigated the pressure distribution in labyrinths both theoretically and experimentally, for eccentric rotor positioning (spiral effect). Qualitatively he obtained the pressure curve described in Figure 2.5 b, for torsional flow. Rosenberg's calculation of the pressure distribution is based on knowledge of the course of the flow lines, in the seal gap; however, usually this course is not known.

The processes occurring in turbine stage seal gaps under torsional flow were extensively studied by Urlichs [20]. By means of adjacently placed stream tubes of variable cross-section, it is possible to describe almost any arbitrary geometry, characterized in turbines by means of a radial entrance, a radial gap that is variable for eccentric positioning, and a radial exit. From the tangential velocity c_{uE} before the gap and the pressure gradient Δp_B between gap entrance and exit, it is possible to describe a relative afflux energy

$$c_E^x = \frac{\rho c_{uE}^2}{2\Delta p_B} \qquad (2.19)$$

for the incident flow. It is characteristic of the flow-line course and the pressure distribution within the gap.

/13

By means of the pressure differential Δp_B, the diameter d_1 and the gap width $\underline{b}$ (or respectively, that of the shroud band), as well as the relative eccentricity $\underline{e}$ - referred to the radial gap width $\underline{s}$ - it is possible to calculate the maximum attainable compressive force,

$$Q_B = \frac{1}{8} \cdot \Delta p_B d_1 \pi b \cdot \frac{e}{s}. \qquad (2.20)$$

If we now relate the force Q_{2D} stemming from the pressure distribution to this force, then we obtain the course as a function of the relative afflux energy shown in Figure 2.6, valid for the gap shape of stage C, to be investigated later. In the calculation according to [20], we have assumed here that the velocity energy generated at the peaks is not fully turbulent in the labyrinth chamber. At increased turbulence - i.e., increasing ζ_s - weaker forces are obtained, which vanish completely for complete turbulence, $\zeta_s = 1$. While for an axial incident flow to the gap - $C_E^x = 0$ - there also is no excitation

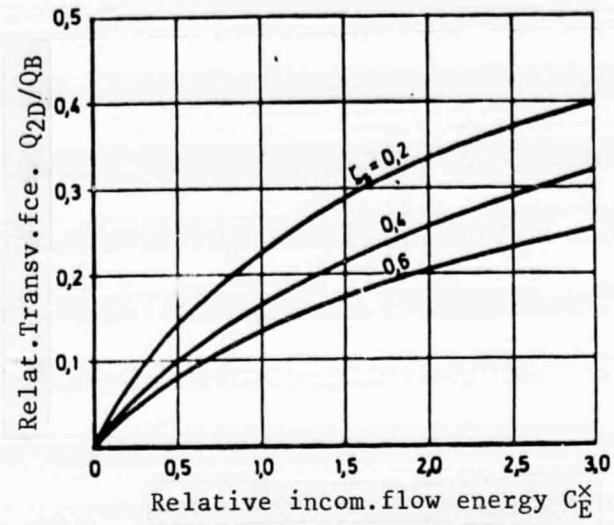

Figure 2.6 Relative excitation force from [20] for a rotor shroud band with three seal peaks (d_1 = 500 mm, b = 27 mm) and different loss coefficients ζ_s

force Q_{2D} generated in the pressure distribution, a strong increase results as C_E^x increases. It follows from this that constant pressure stages are particularly endangered by excitation forces out of the pressure distribution, since they are characterized by large C_E^x values. However, because of the greater pressure gradient and lower incident flow torsion, reaction stages have smaller C_E^x values and hence, considerably smaller excitation forces out of the pressure distribution. /14

Although Urlichs [20] obtained good agreement between measurements and theory for a constant pressure stage, we shall not draw on the calculation procedure for extensive comparison studies, here. His calculations presuppose knowledge of the loss coefficients that describe the complex flow processes in the gap. Fundamental parameter studies for this have already been performed, in [20], which provide qualitative agreement with the measurements here presented, as shall be shown in section 3.6.4.

2.2.3. Rotor stressing according to Piltz

Starting with several simplifying assumptions, Piltz [6] derived the stress to the rotor of a chamber turbine stage due to deflection, inclination, deflection velocities and inclination velocities of the shaft. This made it possible to determine theoretically all the coefficients for the matrices $\mathfrak{R}_S$ and $\mathfrak{K}_S$. However, while considering the flow conditions at the rotor, several correction coefficients are introduced, without any indication as to their magnitude, since they had to be determined experimentally. Since as has been shown also in [13], only the coefficient K_2 has a substantial effect on a turbo-rotor's stability behavior, we shall only provide its value, here. According to equation (33) in [6], and using the designations in Figure 2.3 for the transverse force Q_2, we obtain

$$Q_2 = \frac{3}{4} \cdot \gamma_{21} \cdot \frac{U}{l_w} \cdot e \,. \qquad (2.21)$$

/15

Here $U = \dot{m}\Delta c_u$ is the tangential force for central positioning and γ_{21} is a correction factor for the change in the axial velocity component for shaft deflection $\underline{e}$. By means of the factor γ_{21} - which can be only experimentally determined - we could also take into account any effects caused by the as yet disregarded stator gland flow. Taking (2.5) into consideration and the definition of the internal efficiency η_i given in (2.10), we obtain the gap excitation coefficient K_{2P}, after Piltz:

$$K_{2P} = 0{,}75\, \gamma_{21} \eta_i \,. \qquad (2.22)$$

Comparison to K_{2S} values from (2.18) show relatively good agreement when only the rotor seal is taken into consideration, if we assume $\gamma_{21} \approx 1$.

The remaining values are readily provided by means of a

coefficient comparison, but because of the unknown correction factors, there seems to be no purpose in the practical calculation, for comparison. To this must be added that all the coefficients were derived disregarding a possible flow asymmetry at the stator's exit, and finally, forces from an uneven pressure distribution over an eventually used shroud band were also disregarded.

2.3. Measurement procedures to determine the flow-conditioned forces

In principle, flow-conditioned forces could be determined by means of so-called limiting output tests. These can be envisioned such that the tangential force of a turbine rotor is increased, using either known or computable bearing data, until instability just sets in. However, a reasonably precise determination of the excitation forces acting at the stability limit is possible only when the remaining magnitudes affecting the vibrational system are sufficiently well-known. Here, an essential role must be assigned the damping forces whose pre- /16
cise pre-determination still presents considerable difficulties. Making such tests even more difficult is the fact that in general the stability limit can not be precisely measured.

A better hope for correct measurement results is offered by the so-called damping tests, in which a turbine rotor is stimulated to eigen-vibrations by means of the appropriate device, for various operating conditions; the damping of that vibration provides a measure of the system damping. By correlation of the damping factors measured at different outputs with a theoretically determined course, it then becomes possible to establish gap excitation coefficients. The advantage of these tests over limiting output measurements is that any desired

number of measurement points can be used, with differing excitation and otherwise unchanged system parameters. Here, the calculation of system damping and stability limits is based on linear equations for the elastic, damping and excitation forces. Hence it must be assumed, in damping tests, that the springs and dampers used have linear characteristics. The excitation determined from kinetic tests, however, always represents the totality of possible excitation and damping forces, due to all the coefficients indicated in the matrices $\mathfrak{R}_S$ and $\mathfrak{A}_S$.

A separate determination of individual coefficients of the matrix $\mathfrak{R}_S$ proportional to the deflection is possible, corresponding to their definition, through static measurements. In these so-called force measurements, the forces acting on a turbine rotor are determined, as a function of its relative position with regard to the housing. In similarity to the stator tests, first measurements can be taken with a standing rotor (static tests), then passing on to tests with rotating runner (quasi-static measurements). The result of the force measurements is the course of the forces acting on the runner, as a function of its position with regard to the housing. The coefficients of the deflection matrix $\mathfrak{R}_S$ are then determined from the slope of the forces as a function of the deflection. /17 This measurement procedure allows it to individually determine the coefficients of the deflection matrix, by measuring the forces or respectively, the momenta, in the direction of deflection and perpendicular to it. It is suitable here to fix in space the rotor at which the forces are to be measured, and to displace the housing correspondingly. This procedure has the advantage that for a corresponding housing design, through separate adjustments of the stator and rotor seals, respectively, their individual contributions to the gap excitation force can be measured separately, in accordance with equation (2.18). In addition, the inclination of the rotor with respect to the housing can be studied independently of any eccentricity. Although in a real turbine both cases would not

occur alone, they facilitate obtaining knowledge essential to the theory of gap excitation. A further advantage of quasi-static force measurements is that at the housing, pressure distributions in the seal gap are relatively easy to measure. Last but not least, the measurement procedure above allows the verification of the assumption of linearity for the forces over the deflection, made for the vibration calculation.

Since we expected considerably more differentiated results from the force measurements, they were performed very thoroughly, in the context of this study.

3 FORCE MEASUREMENTS (Quasi-static tests) /18

The goal of these measurements is the determination of coefficients proportional to the deflection, to calculate flow-conditioned forces and momenta for various realistic turbine stages, with the highest possible precision; this, in turn, will make it possible to reliably calculate the stability limits of actual high-power turbines. To this end, for several operating conditions of the test turbine, different eccentricities are obtained by displacing the external housing in relation to the spatially fixed, rotating runner, and then measuring the transverse forces acting on the rotor. Using equipment with two pressure gauges at the rotor's front and back ends, under translational displacement of the external housing it is possible to measure, besides the coefficients K_1 and K_2, also the moment coefficients L_1 and L_2. The measurement of the inclination coefficients K_3 and K_4 on a small constant-pressure stage is reported in [21].

3.1. Test arrangement

Figures 3.1 and 3.2 below show the arrangement of the test turbine, with a reaction stage drawn in as an example. The rotor a is fastened to the relatively rigid shaft b by means of hoop tension elements. The shaft is supported by roller bearings c, whose outer ring d is suspended vertically from flat keep springs e and in horizontal direction by prestressed pressure gauges f. Oil supply and drainage tubes are installed for bearing lubrication. However, the oil mist lubrication planned was somewhat cumbersome during test operation, since the environmental pressure at the two bearings varied considerably corresponding to the stage's inlet and back pressures; hence, grease lubrication was adopted. The axial thrust is received by

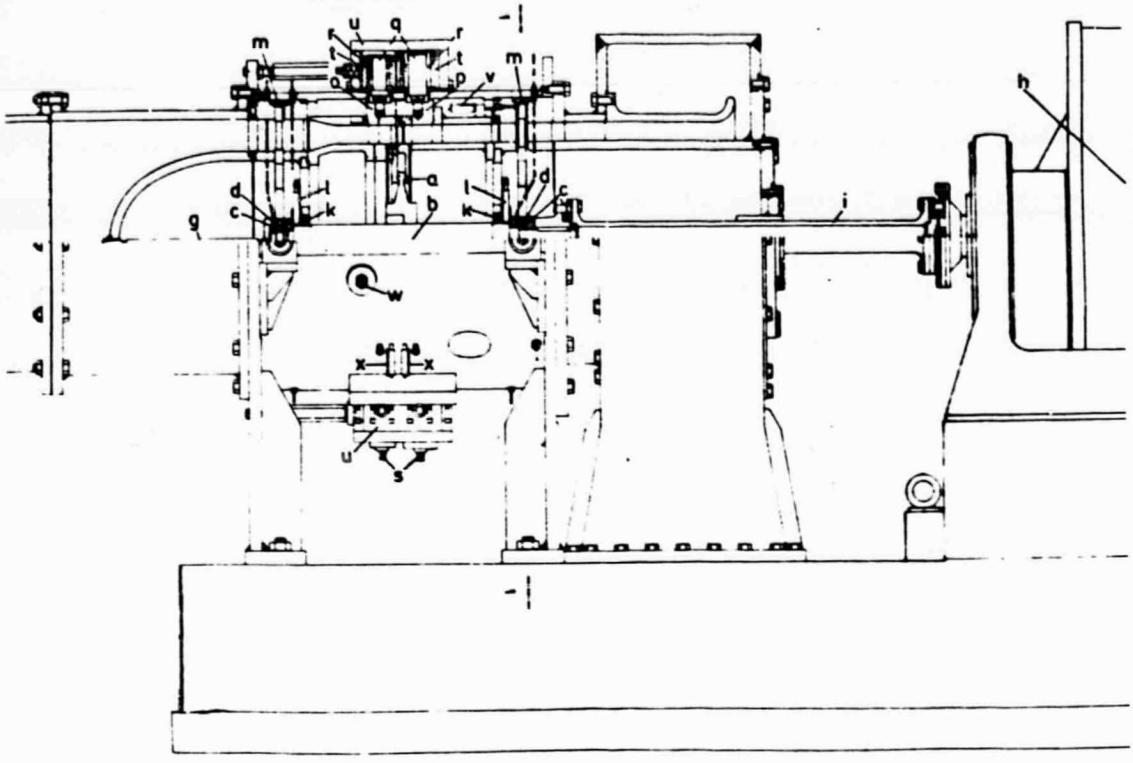

Figure 3.1 Longitudinal section of the test installation

the external housing via the front bearing in conjunction with a bending tensile bar g. For subsequent tests, this tensile bar was replaced by a steel cable, which could be retightened from the outside, during operation. The transfer of the output to the eddy-current brake h was accomplished nearly free of transverse forces by means of a multiple-disk clutch i. After the first measurement series, this clutch was replaced with a diaphragm clutch, which insured smaller disturbing effects on the rotor /20 suspension. The cushioning bearings k prevent excessive rotor deflection; they are controlled by means of non-contact, temperature compensated inductive transmitters l. The shaft's central position with respect to the cushioning bearings can be adjusted by means of spindles on the spring joint pins m and the pressure gauge mounting n. The rotor's eccentricity is adjusted by means of internal housing displacements. For this purpose, the two unsplit inner rings o, p are supported by means of two pins q each in vertical longitudinal ball bearings r. Through

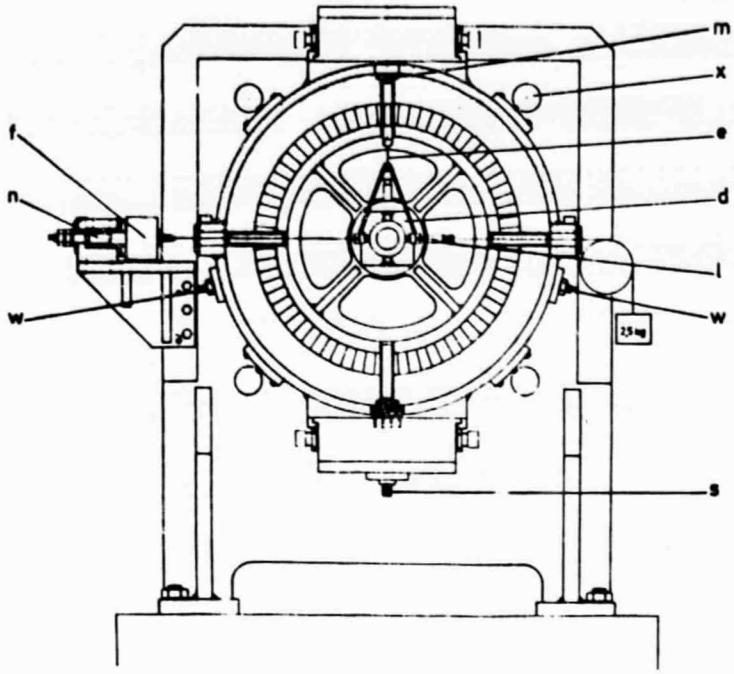

Figure 3.2 Test turbine cross-section

rotation of the spindles s - on which the lower pins stand - the internal rings can be jointly or individually adjusted in vertical direction. The ball boxes are fastened in plates t /21 by means of conical adapter sleeves for no-play adjustment. By displacing the plates perpendicularly to the plane of the drawing, within the boxes u, adjustment in horizontal direction becomes possible. Finally, by axial displacement of the boxes u, the axial gap can be modified. The position of the inner rings perpendicular to the rotor axis is verified by means of four dial gauges v and corrected using the cam followers w. The radial position of the inner rings with respect to the fixed rotor can be controlled via four dial gauges x.

The turbine was assembled vertically on a mounting plate. After mating the individual rings and placing the rotor, the rings are firmly bolted to the upper part of the housing and the mounting plate; after rotation to a horizontal position and removal of

the plate, the assembly is placed in the lower part of the housing. During these operations the shaft is fixed to the front bearing bracket through the cushioning bearings and a crosstie.

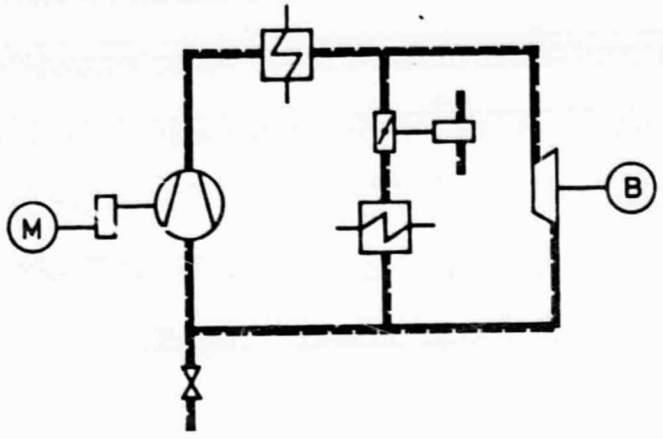

Figure 3.3 Test installation circuit diagram

The test turbine is built into a closed air circuit as shown in Figure 3.3, above. The maximum pressure is 7 bar and the mass flow can be increased to 26,000 m^3/h under standard conditions, with regulation of both mass and gradient possible over a very wide range (rate of rotation of the driving motor can be /22 regulated to 70% of nominal velocity, torsion throttle regulation of the radial compressor and finally, bypass pipeline). The highest power of the eddy-current brake B is 400 kW at a rotation rate of 5500/min.

3.2. Equipment and instruments

Considering the multiplicity of measurements, the most extensive automation of measurement data recording and processing seemed indicated; however, this was possible only within the limitations of the measurement instruments available. All measurement magnitudes are transformed into electrical values by

means of appropriate sensors and recorded by a printer through a selector switch coupled to a digital voltmeter. The printer tape is read optically and the values are stored on magnetic tape for subsequent processing by an EDP*.

Figure 3.4, below, shows the arrangement of the measurement

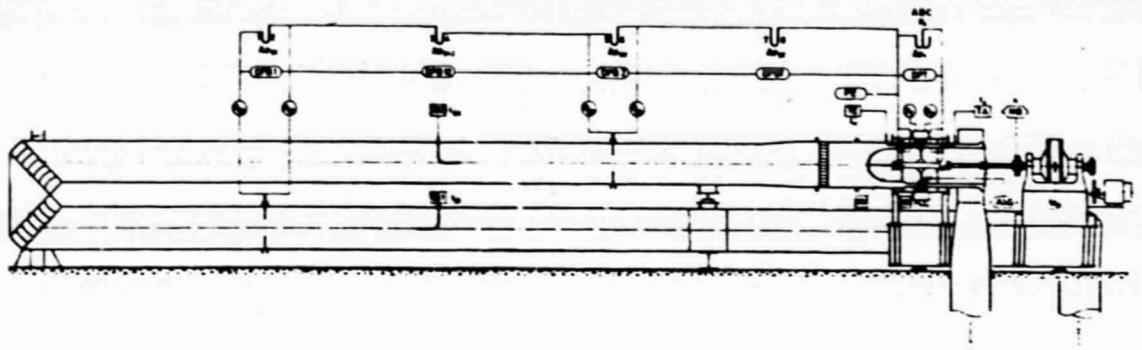

Figure 3.4 Test installation measurement point schematic

points. The temperatures t_{B1} and t_{B2} at the measurement orifices 1 and 2 are obtained from 3 mm diameter iron-constantan thermoelements. Four 3mm diameter iron-constantan elements, displaced by 90° with respect to each other and connected as one thermoelement are used to determine the temperatures $\underline{t}_e$ and $\underline{t}_a$ before and after the turbine. The cold junctions of all thermoelements are in a common ice-water mixture.

The pressure sensors at the measurement orifices are annular chambers with annular slots (see Figure 3.5, below). The pressure before the turbine and the static pressure gradient are determined at the inner and outer flow-guides before and after the blading. Since the pressure differences in tangential direction at the measurement points were very small even for eccentric positioning, the four measurement drill-holes could be connected by means of a ring conduit.

---

* EDV = elektronische Datenverarbeitung = electronic data processing = EDP

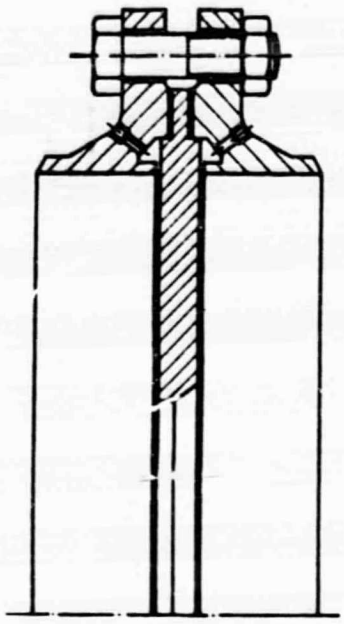

Figure 3.5 Measurement orifice adapter

Since the evaluation refers to average values, it is sufficient to form an average with the pressures at the inner and outer limits, by interlocking them. The schematic for the connection of the pressure line can be seen in Figure 3.4.

/24

U-tubes were built as a parallel indication to the pressure transducers; this was necessary for verification of the pressure transducer system calibration. Table 3.1, below, provides a survey of the pressure transducer systems used.

Measurement of horizontal forces (KV and KH) acting on the rotors is accomplished via two prestressed pressure gauges (0 - 50 N); that of the tangential force U_B at the brake, with a pressure gauge (0 - 2000 N). The force measurement is based on a resistance variation in a glued-on wire-strain gauge, proportional to the change in length of a measurement element; this resistance change is transformed into a voltage pulse proportional to the acting force by means of a Wheatstone bridge circuit and a carrier frequency amplifier. To eliminate the

TABLE 1. Review of pressure transducer systems used

Designation	Measurement range	Operation
DPB 1	0 - 0.2 b	The movements of a multiple return spring capsule are transmitted directly to the slider on a carbon-fil potentiometer with practically infinite resolution. The resistance proportional to the measurement value can then be taken from the potentiometer slider.
DPB 12 DPBT	±5000 Pa ±2500 Pa	The deformation of a pressure capsule is transferred mechanically to the slider of a miniature precision wire potentiometer. The resistance proportional to the measurement value can then be taken from the potentiometer slider.
DPB 2 DPT	0 - 1 bar 0 - 4 bar	The movement of the valve stem of a Barton cell is transferred to an inductive sensing system and then transformed into a voltage pulse proportional to the measurement value.
PE	0 - 6 bar	The pressure applied causes a proportional, tangential deflection at a Bourdon tube pressure gauge, which is transferred to an inductive sensing system and then transformed into a voltage pulse proportional to the measurement value.

out-of-balance force - which is proportional to the rate of rotation - the amplifier output pulses pass through a low-pass filter before reaching the selector switch. In addition, the three forces are recorded in triplicate at each measurement point; an average value is obtained during evaluation. The magnitude and direction of the eccentricity of the inner rings selected for a measurement point is indicated in each case by two inductive transmitters displaced by 90° with respect to each other, which measure the position of the inner rings with respect to the outer housing in non-contact manner. The control of the axial gap is accomplished via four axial dials that can be read through plexiglass windows during testing, in addition to a non-contact distance indicator that measures the position of the rotor with respect to the fixed housing. From the dial readings and the value on the axial transmitters, the actual axial gap is then obtained, with the distance from the rotor shroud band to the inner ring's front edge, $\underline{p}$, measured directly

during assembly. Monitoring of the rotor's rate of rotation is accomplished by means of a digital frequency counter and a pulse generator placed across from a disk with 60 marks along the perimeter. The rate of rotation is kept constant during a measurement series through a regulator built into the eddy-current brake's control instrument.

Normally, a measurement sequence proceeds as follows:

First, the inner rings are perfectly centered with respect to the rotor, by turning the spindles s (with the system at rest) for the vertical direction and the plates t for the horizontal direction, until contact is just made with the rotor: due to the sensitive pressure gauges, this is immediately recognizable; the radial dials are then set to 0. From the maximum possible displacements - which can be measured during the operation above - the gap widths at the stator and rotor seals are obtained simultaneously. Once the compressor and the turbine have attained operating condition and a certain period of time has elapsed to achieve thermal balance in the circuit, the desired turbine rotation rate and tangential force are adjusted. Within a measurement sequence, several measurement series at various pressure values for the turbine may be run; the variation in the pressure value is accomplished either by changing the turbine's rate of rotation or - more frequently - by increasing or decreasing the pressure for the stage. An additional increase in output can be obtained by a stepwise increase in the circuit's load. Each measurement series of a measurement sequence is composed of three parts:

1. One or more measurement points, with simultaneous reading of the pressures on the U-tubes, to determine the calibration curve for the pressure transducer.

2. Measurement points at differing inititial stressing forces - with the approximate magnitude of the expected excitation

forces - of the pressure gauges KV and KH, to determine the applicable calibration curve.

/26

3. Measurement points for various eccentric positions of the inner housing with respect to the rotor, that can be adjusted by means of rotation of the spindles s at the lower box or respectively, by displacement of the plates t.

The pressure gauge calibration that precedes each force measurement at any selected operating condition and central rotor positioning, has the advantage that during the actual force measurement, the horizontal, stationary rotor deflection - which results from the transverse forces acting on it and the rigidity of the force measuring devices - need not be compensated for by displacing the pressure gauge attachment. This would be necessary, since for horizontal rotor deflections flow-conditioned forces could be generated in the direction of deflection, that would falsify the transverse force to be measured. By means of the pressure gauge calibration it is simultaneously possible to take into consideration any changes in the rigidity of the frontal suspension due to differing axial forces, as well as any eventually occurring restoration forces, through the coupling at the rotor's back end.

For each measurement point, the electrical initial readings of all pressure transducers, thermoelements, transmitters for eccentricity and axial gap measurements, and the pressure gauges are recorded - with a code number - on the printer tape. With the triplicate force measurements, this results in 24 values.

After transferring the numerical values to magnetic tape by reading with an optical scanner, a preliminary program sorts the data in such a manner that a data file results for each measurement sequence, containing all the data necessary to the evaluation program, with exception of the reference magnitudes.

3.3. Evaluation

It is assumed for evaluation purposes that the fluid behaves like an ideal gas. The starting point for the computation of the essential turbine or respectively, stage data is the determination of the mass flow $\dot{m}$, measured by means of two sequentially arranged measurement orifices. According to DIN* 1952 we have

$$\dot{m} = \alpha\varepsilon\mu \cdot \frac{D^2\pi}{4} \cdot \sqrt{2\Delta p_B \rho} \,, \qquad (3.1)$$

where D is the pipe diameter and μ the aperture ratio d^2/D^2 of the orifice, at the operating temperature. The density ρ is obtained from the equation, since pressure and temperature at the orifice are known. The expansion coefficient $\varepsilon = \varepsilon(p_2/p_1, \mu^2)$, and the flow coefficient $\alpha = \alpha(Re, \mu^2)$ are obtained by linear interpolation between the values tabulated in DIN 1952 ($\kappa = 1.4$). For the calculation of Reynold's number Re we set the dynamic viscosity of air at

$$\eta_L = 1{,}72 \cdot 10^{-5} \cdot \left(\frac{T_B}{273{,}15}\right)^{0{,}76} \left[\frac{Ns}{m^2}\right] \qquad (3.2)$$

The dependence of Reynold's number on the resulting mass flow requires an iterative calculation of the throughput.

From the pressure and temperature at the turbine entrance and the turbine's pressure gradient, we obtain the isentropic gradient

$$\Delta h_s = \frac{\kappa R T_e}{\kappa - 1} \cdot \left[1 - \left(1 - \frac{\Delta p_T}{p_e}\right)^{\frac{\kappa-1}{\kappa}}\right] \qquad (3.3)$$

* DIN = Deutsche Industrienorm = German Industrial Standard

and from it and the mass flow obtained from equation (3.1), the reference magnitude chosen for the measured forces, the isentropic tangential force

$$U_s = \frac{\dot{m}\Delta h_s}{u} \qquad (3.4)$$

where u is the tangential velocity in the central section.

The effective turbine output P is derived from the force U_B that acts on the lever arm h_a, at the brake:

$$P = 2h_a U_B n\pi, \qquad (3.5)$$

/28

where n is the rotation rate.

The turbine's measured effective efficiency is

$$\eta_e = \frac{P}{\dot{m}\Delta h_s}, \qquad (3.6)$$

where we have set the entrance velocity c_o equal to the exit velocity c_2, for simplification purposes. Correspondingly, from the measured temperatures before (subscript e) and after the turbine (subscript a) we can determine the inner turbine efficiency,

$$\eta_i = \frac{c_p(t_e - t_a)}{\Delta h_s}. \qquad (3.7)$$

Once the turbine data have been calculated, we can continue with the calculation of data for the stage. For a single-stage turbine, the entrance and exit conditions become conditions "0" and "2", before and after the stage. For a multistage arrangement, a suitable gradient subdivision must be found. For the case of a three-stage group studied here, this subdivision is performed corresponding to the different tangential

velocities $\underline{u}$ at the rotor center, assuming a constant pressure coefficient ψ and disregarding the heat recovery (very low, here):

$$\Delta h_{s\nu} = \frac{\psi}{2} \cdot u_\nu^2, \quad \Sigma \Delta h_{s\nu} = \Delta h_s, \quad \nu = 1,2,3. \qquad (3.8)$$

To determine the temperatures, we shall further assume, in conformance to Figure 3.6, below, that they behave as the isentropic gradient does:

$$\Delta h_{s1} : \Delta h_{s2} : \Delta h_{s3} = \Delta t_1 : \Delta t_2 : \Delta t_3,$$
$$\Delta t_1 + \Delta t_2 + \Delta t_3 = t_e - t_a. \qquad (3.9)$$

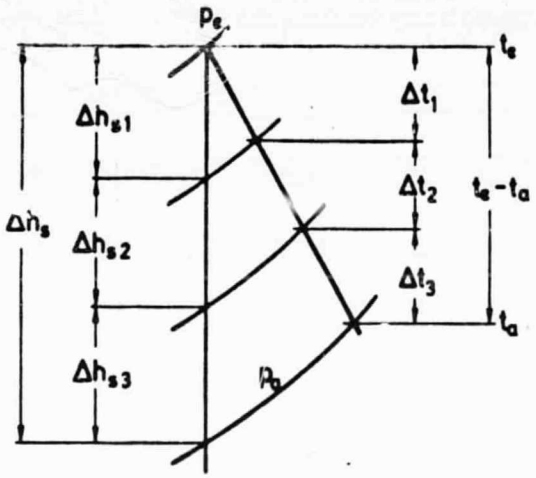

Figure 3.6 Gradient subdivision for a 3-stage group (ideal gas)

A more precise determination of the gradient subdivision for a multi-stage group does not appear necessary here, since it is used only for the calculation of the gap loss coefficients for the individual stages, from which an average excitation force for all stages is computed, for comparison with measurement data.

To estimate the excitation forces derived from the gap loss

using the existing theory, it was necessary to know the triangles of velocities for the individual stages; first the pressure p_1 and the velocity c_1 at the stator exit are calculated. For c_1 we obtain, with the blading efficiency η' of the stator buckets /29

$$c_1^2 = \eta' \cdot \left(2RT_o \cdot \frac{\kappa}{\kappa-1} \cdot \left[1 - \left(\frac{p_1}{p_o}\right)^{\frac{\kappa-1}{\kappa}}\right] + c_o^2\right), \qquad (3.10)$$

where the velocity c_o is obtained from the mass flow and the stator's condition

$$c_o = \frac{\dot{m} T_o R}{p_o d_m l' \pi}. \qquad (3.11)$$

Assuming an ideal gas (c_p = const.), we obtain the temperature T_1 at the stator exit from the energy equation:

$$T_1 = \frac{1}{R} \cdot \left[\frac{c_1^2}{2} \cdot \frac{1-\eta'}{\eta'} \cdot \frac{\kappa-1}{\kappa} + RT_o \cdot \left(\frac{p_1}{p_o}\right)^{\frac{\kappa-1}{\kappa}}\right]. \qquad (3.12)$$

With the continuity equation, we finally obtain

$$\frac{p_1}{RT_1} \cdot c_1 d_m \pi l' \sin\alpha_1 = \dot{m} - \dot{m}'_{sp}, \qquad (3.13)$$

/30

where $\dot{m}_{sp}$ refers to the gap loss at the stator seal, calculated according to Traupel [17]. From equations (3.10) to (3.13) we obtain the quantities p_1 and c_1, by iteration. From the pressure p_1 we derive the percentage reaction

$$r = \frac{\Delta h_s^*}{\Delta h_s} = \frac{\left(\frac{p_1}{p_o}\right)^{\frac{\kappa-1}{\kappa}} - \left(\frac{p_2}{p_o}\right)^{\frac{\kappa-1}{\kappa}}}{1 - \left(\frac{p_2}{p_o}\right)^{\frac{\kappa-1}{\kappa}}}. \qquad (3.14)$$

Assuming a flow distribution in agreement with the potential vortex law we obtain the percentage reaction values below for the blade base, r_i and the blade head, r_a

$$r_i = 1 - \frac{d_m^2}{(d_m - 1")^2} \cdot (1 - r) \ , \quad r_a = 1 - \frac{d_m^2}{(d_m + 1")^2} \cdot (1 - r) \ . \quad (3.15)$$

With the now known velocity c_1, the flow angles α_1 and β_2 as well as the blading efficiency $\eta"$ for the rotor, we now obtain, corresponding to Figure 3.7, below,

$$\left.\begin{aligned} \beta_1 &= \arctan\frac{c_1 \sin\alpha_1}{c_1 \cos\alpha_1 - u} \ , \quad w_1 = \sqrt{c_1^2 + u^2 - 2uc_1\cos\alpha_1} \ , \\ w_2 &= \sqrt{\eta"(2r\Delta h_s + w_1^2)} \ , \quad c_2 = \sqrt{w_2^2 + u^2 - 2uw_2\cos\beta_2} \ , \\ \alpha_2 &= \arctan\frac{w_2 \sin\beta_2}{w_2\cos\beta_2 - u} \ , \quad \Delta c_u = c_1\cos\alpha_1 + c_2\cos\alpha_2 \ . \end{aligned}\right\} (3.16)$$

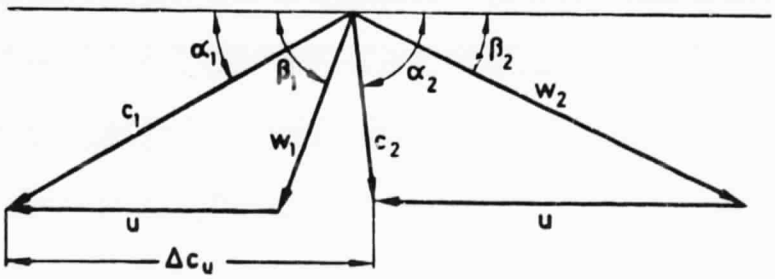

Figure 3.7 Triangle of velocities

/31

The peripheral efficiency η_u becomes

$$\eta_u = \frac{u\Delta c_u}{\Delta h_s + \frac{c_0^2}{2} - \frac{c_2^2}{2}} \ , \quad (3.17)$$

as well as the pressure coefficient

$$\psi = \frac{2\Delta h_s}{u^2} \quad (3.18)$$

and the throughput coefficient

$$\varphi = \frac{c_{2ax}}{u} = \frac{c_2 \sin\alpha_2}{u} . \qquad (3.19)$$

The gap loss can now be calculated with the equations in section 2.2.1. For the gradient at the blade base or head, respectively, we have

$$\Delta h'_{si} = \Delta h_s \cdot (1 - r_i) , \quad \Delta h''_{sa} = \Delta h_s r_a . \qquad (3.20)$$

from which we obtain the gap loss coefficients with an approximate curve corresponding to Figure 2.4

$$K' = 0{,}685 \cdot \sqrt{\frac{2\Delta h'_{si}}{c_1^2}} , \quad K'' = 0{,}685 \cdot \sqrt{\frac{2\Delta h''_{sa}}{w_1^2}} . \qquad (3.21)$$

It then becomes possible to provide calculated gap excitation coefficients K_{2S}, from the gap loss, in accordance with equation (2.18).

Applying the method of the least squares, a straight line $y = a + bx$ is then fitted to the measured forces y_i as a function of the displacement, x_i. For the estimated values of the coefficients, with n as the number of measurement points, we obtain, according to [22],

$$\left.\begin{aligned} a &= \bar{y} - \frac{\Sigma(x_i - \bar{x}) \cdot \Sigma(y_i - \bar{y})}{\Sigma(x_i - \bar{x})^2} \cdot \bar{x} , & b &= \frac{\Sigma\left[(x_i - \bar{x}) \cdot (y_i - \bar{y})\right]}{\Sigma(x_i - \bar{x})^2} , \\ \bar{x} &= \frac{1}{n} \cdot \Sigma x_i , & \bar{y} &= \frac{1}{n} \cdot \Sigma y_i , \end{aligned}\right\} \qquad (3.22)$$

where the sums must always range from i = 1 to i = n. In excitation force measurements, the slope b corresponds then to the so-called excitation constant q_2, from which the gap excitation coefficient

$$K_2 = q_2 \cdot \frac{1''}{U_s} \cdot \text{sign}(\omega) \qquad (3.23)$$

is calculated. The factor sign (ω) takes into account the direction of rotation of the different stages, since the sign of the gap excitation coefficient depends on the direction of rotation. From the measured values we also obtain a slope p_1 for the moment curve as a function of the eccentricity, from which the moment coefficient L_1 is obtained /32

$$L_1 = p_1 \cdot \frac{21''}{U_s d_m} . \qquad (3.24)$$

For appropriately adjusted rotor positions, we obtain the coefficients K_1 and L_2 in a similar manner. For separate adjustments, it is also possible to determine coefficients for the stator and rotor, individually.

In the evaluation program, for each measurement sequence first a pressure sensor calibration takes place, in which the values y_i read on the U-tubes and the simultaneously recorded electric signals x_i of the pressure transducers are used to obtain a straight line $y = a + bx$, by the least squares method. The coefficients a and b are calculated using Equation (3.22). An example of pressure sensor calibration is provided in Table A1, in the Appendix. For each calibration point are listed the values read on the U-tubes, the resulting pressures at the pressure transducers, and the corresponding electrical values. The uncertainties indicated for each calibration factor correspond to the standard deviation of the parameters fitted. For control purposes, a diagram is plotted for each pressure transducer, recording the individual calibration points and the calculated calibration curve (see Figure 3.8, below). From the recorded electrical values and the corresponding calibration line, all essential pressures in the circuit are obtained, for each measurement point. The temperatures are calculated by /33 means of conversion factors determined in separate experiments, before the thermoelements or respectively, thermoelement chain,

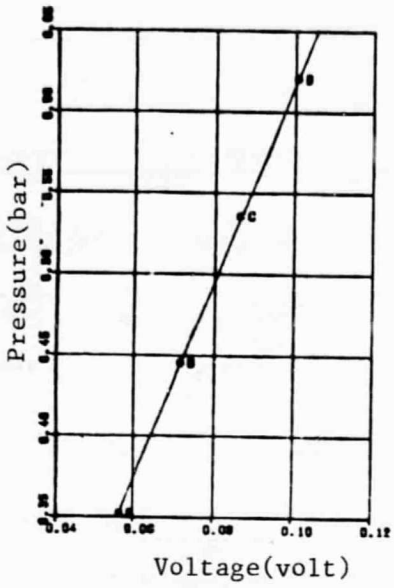

Figure 3.8 Calibration of pressure transducer PE

is built into the installation. The calibration curves for the non-contact distance gauges, necessary to determine the eccentricity as well as the axial gap, are also obtained in the corresponding test measurements, as is the sensitivity of the tangential force pressure gauge U_B. We are now ready for the evaluation of the individual measurement points. The mass flow is calculated from the conditions reported at the two measurement orifices and equations (3.1) and (3.2). An average of the two values is obtained and used in subsequent calculations. Control is provided by an expression of the deviation of the mass flow as a percentage of the average. Further data for the stage group are computed from equations (3.3) through (3.7). All the essential data for a stage group are reported in tabular form, with a simultaneous computation of the mean value, $\bar{x}$, as well as the standard deviation of the mean in units of $s_{\bar{x}}$ and as percentages, $s_{\bar{x}\%}$, for the $\underline{n}$ measurement points of the series

$$\bar{x} = \frac{1}{n} \cdot \Sigma x_i \quad , \quad s_{\bar{x}} = \sqrt{\frac{\Sigma (x_i - \bar{x})^2}{n(n-1)}} \quad , \quad s_{\bar{x}\%} = 100 \cdot \frac{s_{\bar{x}}}{\bar{x}} \quad . \qquad (3.25)$$

For the so-called pressure gauge calibration, a corresponding curve is calculated from equation (3.22), using the electrical values of the two pressure gauges KV and KH and the corresponding weights; the coefficients obtained are stored. Control is provided by a table listing the calibration weights supplied (KV[N]), the recorded values (KV[volt]) and the forces obtained therefrom, using the calibration curve (KVG[N]). Table A2 compiles the stage group's calculated data, as well as the pressure gauge calibration for measurement series 293. Appended to the Table with the individual values for the pressure gauge are listed the coefficients of the regression curve determined. To complete the picture, there is a listing of the standard deviations (= uncertainties) for the line and the coefficients. It is also possible, for linearity verification, to use a reference variable and prepare a plot with the calibration points and the straight line fitted through them (see Figure 3.9, below). The calibration factors thus determined may be valid for several consecutive measurement series, if no substantial changes occurred in the turbine's operating conditions (pressure coefficient, rotation rate, load). As a rule this is the case for three measurement series (stator, rotor and stage adjustment) in a given parameter combination. /34

In an actual force measurement, the data for the stage group are again calculated for each measurement point. The calculation of the stage data in a measurement series that are essential to the excitation forces, start from the mean values for the stage group. This seems appropriate, in view of the very small deviations of individual measurement values in a measurement series, to reduce the calculation time. For a multi-stage arrangement, the averages are obtained for the data for each stage, for comparison. Table A3 shows the results for the stage group and individual stage calculations, for measurement series 490, corresponding to a three-stage arrangement.

For the evaluation of forces and momenta, distinctions are made

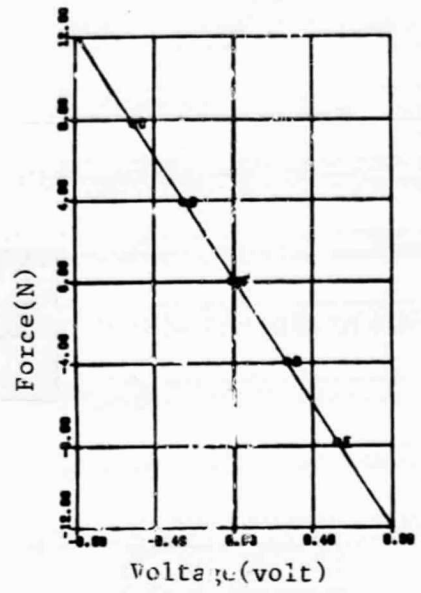

Figure 3.9 Calibration of pressure gauge KV (MR 293)

between stator, rotor and stage adjustment, based on the measured eccentricities of the stator or rotor ring, respectively. Next to the chosen deflection indicated for each measurement point, are reported the theoretically computable excitation forces

$$Q'_{2S} = \frac{Y'}{l^*} \cdot U_s K'_{2S} \ , \quad Q''_{2S} = \frac{Y''}{l^*} \cdot U_s K''_{2S} \ , \quad Q_{2S} = Q'_{2S} + Q''_{2S} \qquad (3.26)$$

as well as the measured forces and momenta

$$Q_2 = KV + KH \ , \quad M_1 = -KV \cdot A + KH \cdot B \ . \qquad (3.27)$$

/35

Here, A and B refer to the distance between the rotor and the front, or respectively, back bearing. Using equation (3.22) we then calculate - by linear regression on the displacements and the forces measured - the corresponding excitation coefficients q_2 or respectively, moment slopes p_1, as well as the therefrom resulting gap excitation coefficients K_2 from equation (3.23), or respectively, moment coefficients L_1 from equation (3.24).

Table A4 shows, as an example, the evaluation of measurement series 293, with stator adjustement.

In order to be able to provide tabulated surveys, all parameters and average values of a measurement series are stored in data files arraged by measurement series number. The equally stored data for displacement and force, or moment, respectively, for each measurement point can be used, as a control of the course of forces or momenta, respectively, to obtain a graphical record by means of a separate plotter program.

3.4. Error computation

As a measure of possible random error in the excitation force measurements, in correspondence with DIN 1319 we shall use the measurement uncertainty f, with the understanding that we shall always refer to the 95% confidence level for the measured magnitude. Because of the calibration measurements performed in each measurement sequence or series, respectively, systematic errors are excluded. Only the cold junctions necessary to temperature measurements by means of thermoelements could cause small, systematic deviations, since in the ice-water mixture used, small upward temperature variations are conceivable due to incomplete thermal equilibrium; this could make the temperatures indicated slightly low. However, the small temperature fluctuations at the cold junctions can be neglected here, since even deviations of 1.5 K in temperatures near 300 K represent an error of only 0.5%. Additional possibilities of error may exist at the temperature measurement locations (due to radiation, heat conduction, flow velocity), which can be neglected however, as shown by estimations, for the measurements performed here at relatively low temperatures and velocities.

/36

The measurement uncertainty $f_{\bar{x}}$ at the 95% confidence level is obtained from the standard deviation $s_{\bar{x}}$ of the measured variable $\bar{x}$, obtained as the mean value of $\underline{n}$ measurements,

$$f_{\bar{x}} = t_{95\%}^{n-1} \cdot s_{\bar{x}} . \qquad (3.28)$$

Here $t_{95\%}^{n-1}$ represents the 95% confidence limit in a Student distribution for n-1 degrees of freedom. For the linear regression y = a + bx corresponding to equation (3.22), the estimated values for the standard deviation from [22] are

$$\left.\begin{aligned} s_y &= \sqrt{\frac{\Sigma (y - y(x_i))^2}{n-2}} , \quad s_a = s_y \cdot \sqrt{\frac{1}{n} + \frac{\bar{x}^2}{\Sigma (x-\bar{x})^2}} , \\ s_b &= s_y \cdot \sqrt{\frac{1}{\Sigma (x-\bar{x})^2}} , \end{aligned}\right\} \qquad (3.29)$$

as well as 95% confidence ranges

$$f_y = t_{95\%}^{n-2} \cdot s_y , \quad f_a = t_{95\%}^{n-2} \cdot s_a , \quad f_b = t_{95\%}^{n-2} \cdot s_b , \qquad (3.30)$$

where in this case the 95% limit of the Student distribution for n-2 degrees of freedom is relevant. If the measurement result is a function of one or more measurement variables, then the uncertainty in the measurement results is determined by the rules of error propagation and

$$y = F(x_i) , \quad f_y = \sqrt{\sum \left(f_{xi} \frac{\partial F}{\partial x_i} \right)^2} . \qquad (3.31)$$

An external EDP program was written for the throughput calculations, which performed an error computation for every pressure sensor calibration point, whose result could be used as the measurement uncertainty in the mass flow corresponding to the measurement series of which this point was a part. An error propagation calculation does not seem necessary for each point, since there was little scattering in the values within a given

measurement series (see Tables A2 and A3). The measurement tolerance for the throughput is given in DIN 1952 for individual measurements, as

$$\tau_q = \pm\sqrt{\tau_i^2 + \tau_\varepsilon^2 + \frac{1}{4}\tau_{\Delta p} + \frac{1}{4}\tau_\rho + \tau_D^2\left(2\frac{\mu^2}{\alpha}\right)^2 + \tau_d^2\left(2+2\frac{\mu^2}{\alpha}\right)^2} \quad (3.32)$$

/37

Since τ_q is valid with a statistical certainty that can be assumed higher than 95%, τ_q well corresponds to the measurement uncertainty mentioned above. We thus obtain

$$f_{\dot{m}\%} = \tau_q \,, \quad f_{\dot{m}} = \frac{\dot{m}}{100}\cdot\tau_q \,, \qquad (3.33)$$

where $f_{m\%}^{\cdot}$ designates the mass flow uncertainty in % and $f_m^{\cdot}$ that in mass flow units. From DIN 1952, the tolerance of the throughput coefficient α is then

$$|\tau_\alpha| = |\tau_o| + |\tau_{sp}| + |\tau_{ex}| + |\tau_{fr}| = \pm\left[0{,}35 + \mu^2 + 0{,}3\mu(\lg(Re)-6)^2\right]\% \,, \qquad (3.34)$$

where due to the measurement orifice adapter (see Figure 3.5, page 26) τ_{sp}, τ_{ex} and τ_{fr} can be taken = 0. Furthermore, for the tolerance of the expansion constant ε we have

$$\tau_\varepsilon = \pm 4\,\frac{\Delta p_B}{p_B}\,\% \,. \qquad (3.35)$$

During the pressure sensor calibration we obtain the measurement uncertainty f_y for each pressure transducer for the calibration curve, from equation (3.22), corresponding to equations (3.29) and (3.30). Therefore

$$\tau_{\Delta p} = \frac{f_{\Delta pB}}{\Delta p_B}\cdot 100 \,. \qquad (3.36)$$

To determine the measurement uncertainty in the density ρ before the measurement orifice, we must first determine the

uncertainties in the pressure p_B and the temperature T_B before that orifice. Since the absolute value of the pressure p_B is calculated by addition of several pressure differences to the measured absolute pressure p_e, we obtain from the error propagation law (3.31),

$$\left.\begin{aligned} f_{pB1} &= \sqrt{f_{BA}^2 + f_{pe}^2 + f_{\Delta pBT}^2 + f_{\Delta pB2}^2 + f_{\Delta pB12}^2 + f_{\Delta pB1}^2} \,, \\ f_{pB2} &= \sqrt{f_{BA}^2 + f_{pe}^2 + f_{\Delta pBT}^2 + f_{\Delta pB2}^2} \,. \end{aligned}\right\} \quad (3.37)$$

Here f_{BA} is the measurement uncertainty in the barometer reading, approximately 30 Pa. The magnitudes f_{pe}, $f_{\Delta pBT}$, $f_{\Delta pB2}$, $f_{\Delta pB12}$ and $f_{\Delta pB1}$ are obtained from the 95% confidence limits for the fitted straight lines derived from the pressure sensor calibration. Corresponding to the calibration tests for the thermoelements, the uncertainty f_{TB} can be assumed to be 0.5 K; we finally obtain /38

$$f_\rho = \sqrt{\left(\frac{1}{RT_B}\cdot f_{pB}\right)^2 + \left(\frac{p_B}{RT_B^2}\cdot f_{TB}\right)^2} \,, \quad \tau_\rho = \frac{f_\rho}{\rho}\cdot 100 \,. \quad (3.38)$$

The tolerances τ_D and τ_d for the pipe and measurement orifice diameters are negligibly small, in comparison to the other tolerances. Table A5 compiles the results of the error calculations for a measurement sequence. The uncertainty for the average mass flow is obtained from the individual uncertainties of the two measurement orifices,

$$f_{\dot m} = \frac{1}{\sqrt{\left(\frac{1}{f_{\dot m1}}\right)^2 + \left(\frac{1}{f_{\dot m2}}\right)^2}} \,. \quad (3.39)$$

Starting with this value, the uncertainty for the measured gap excitation coefficient is calculated for each measurement series: first, the measurement uncertainty of the isentropic gradient must be determined. It is obtained from the uncertainties f_{pe}, $f_{\Delta pT}$, f_{Te} applying the law of error

propagation to equation (3.3), where we can disregard the scatter of the mean values of Δh_s and U_s, since they are small in comparison to the measurement uncertainty.

$$f_{\Delta hs} = \sqrt{\left(\frac{\kappa}{\kappa-1}\cdot R\left[1-\left(1-\frac{\Delta p_T}{p_e}\right)^{\frac{\kappa-1}{\kappa}}\right]\cdot f_{Te}\right)^2 + \left(\frac{RT_e}{p_e}\cdot\left(1-\frac{\Delta p_T}{p_e}\right)^{-\frac{1}{\kappa}}\cdot f_{\Delta pT}\right)^2 + \left(\frac{RT_e\Delta p_T}{p_e^2}\cdot\left(1-\frac{\Delta p_T}{p_e}\right)^{-\frac{1}{\kappa}}\cdot f_{pe}\right)^2} \quad . \qquad (3.40)$$

In the same manner we obtain for the isentropic tangential force, corresponding to equation (3.4)

$$f_{Us} = \sqrt{\left(\frac{\Delta h_s}{u}\cdot f_{\dot m}\right)^2 + \left(\frac{\dot m}{u}\cdot f_{\Delta hs}\right)^2} \qquad (3.41)$$

and finally

$$f_{K2} = \sqrt{\left(\frac{q_2 l^n}{U_s^2}\cdot f_{Us}\right)^2 + \left(\frac{l^n}{U_s}\cdot f_{q2}\right)^2} \quad . \qquad (3.42)$$

/39

For f_{q2} we must use the 95% confidence limit obtained for the standard deviation of the slope of the regression line. The measurement uncertainty thus determined for the gap excitation coefficient may be considered representative only if the course of the excitation force curve has a linear tendency. For some of the measurements, however, the course was more "s" shaped than linear; while fitting a straight line to all points yielded K_2 values, their 95% confidence limit, calculated as shown above, did not contain the various possible slopes. In such cases, slopes and uncertainties should be calculated only for more or less linear segments.

The measurement uncertainties for the deflection and moment coefficient are obtained by similar procedures.

3.5. Test program

The design of the test installation allows the investigation of different turbine stages. In the context of this study, we shall report on the force measurements of three typical single stages /40

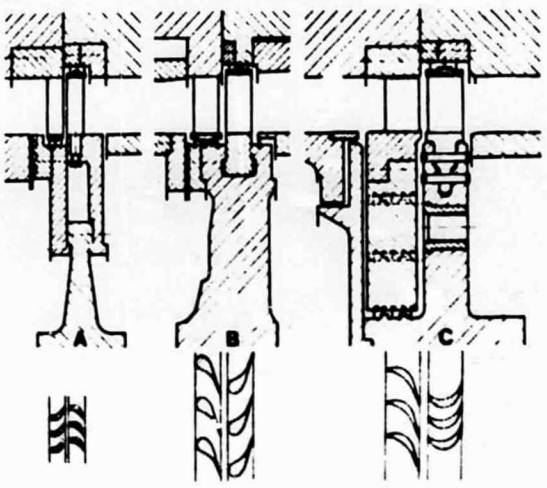

Figure 3.10 Stages studied

(see Figure 3.10, above) and one three-stage group (see Figure 3.11, below). The internal diameter of all stages is 420 mm. The essential dimensions are shown in Table 3.2. Stages A and B and the three-stage group are fashioned in the reaction type of construction, while stage C was built in the chamber type with weak reaction blading. The Reynold's numbers for the turbines - obtained from the incident flow velocity and the chord length - ranged from $4 \cdot 10^4$ to $2 \cdot 10^5$ in these tests.

/41

The following parameters could be varied, during these tests:

a) the pressure coefficient, either by increasing the pressure before the stage at constant reaction and constant rate of rotation, or by varying the rotation rate at constant stage gradient;

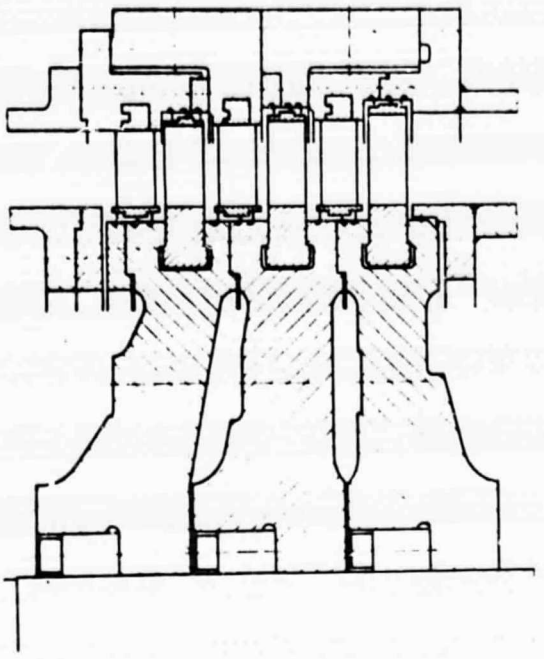

Figure 3.11 Three-stage group

TABLE 3.2 Dimensions of the test stages

Designation			Stage A	Stage B	3-stage group	Stage C
No. of blades	Stator		129	50	50	63
	Rotor		129	50	50	99
Blade length	Stator	mm	40.0	40.8	40.8	39.5/38.6
	Rotor	mm	40.0	41.3	41.2	40.0
Covering	Inner	mm	0	0	0	0.5
	Outer	mm	0	0.5	0.7	0/0.9
Exit angle	α	deg.	31.0	17.3	17.3	12.9
	β_2^1	deg.	31.0	17.3	17.3	20.1
Gap width	Stator	mm	0.7	0.48	0.48	0.5
	Rotor	mm	0.5	0.43	0.44	0.4
Shroud band width	Stator	mm	12.0	22.7	22.7	36.0
	Rotor	mm	14.0	19.0	19.0	27.0

b) the density of the working fluid, by charging the closed circuit;

c) the axial gap, which should be defined by the distance from the rotor shroud-band to the stator ring;

d) for stage C, the hub ratio, the size and number of balance holes, as well as the outer cover that marks the discontinuity of the outer limit of the meridian channel, between stator exit and rotor entrance.

/43

Naturally, it was necessary to select the most significant from among the large number of resulting parameter combinations, which are also affected by the results of the preceding measurements. We began with the determination of the excitation force for simultaneous eccentric positioning of the stator seal and the rotor seal (stage adjustment STV). To determine the effect of an eccentricity of only the stator or the rotor seal, during subsequent tests besides the stage adjustment, a separate adjustment was performed of the stator seal (stator adjustment LEV) or respectively, the rotor seal (rotor adjustment LAV).

Table 3.3, below, shows the force measurement parameters investigated. The combination outlined in a heavier line represents a reference condition, starting from which the effect of the individual parameters was investigated. The predominant portion of the measurements was devoted to the determination of the gap excitation coefficient K_2 and the simultaneously obtained moment coefficient L_1, while the less significant coefficients K_1 and L_2 usually were measured only for the reference state parameter combination. We renounced the determination of the coefficients due to rotor inclination - possible in principle on the test installation used here - since measurements performed at a different test installation [21] led us to expect relatively small values, unessential for practical stability calculations.

TABLE 3.3 Parameters for excitation force measurements

Stage A	Press.coeff.			2,0	2,5	3,0	3,5	4,0	4,5	5,0		
	Axial gap (mm)				1,6	2,0	2,5	3,1	3,6			
	Rot.rate(1/min)					2400	3000	3600				
	Load(bar)						0	0,5	1,0			
	Adjustment						STV					
Stage B	Press.coeff.			2,0	2,5	3,0	3,5	4,0	4,5	5,0		
	Axial gap(mm)						3,3					
	Rot.rate(1/min)	2830	2980	3160	3380	3650	4000	431C				
	Load(bar)						0	0,4	0,8	1,2	1,6	
	Adjustment					LEV	STV	LAV				
3-stage group	Press.coeff.			1,4	1,6	2,0	2,4	2,8	3,2			
	Axial gap(mm)						2,9					
	Rot.rate(1/min)	2000			3460	3700	4000		4500			
	Load(bar)						0					
	Adjustment						STV					
Stage C	Press.coeff.			2,0	2,5	3,0	3,5	4,0	4,5	5,0		
	Axial gap(mm)	0,5	1,0	1,5	2,0	2,5	3,0	3,5	4,0	4,5	5,0	
	Rot.rate [1/min]		3000	4000	4400	4650	5000					
	Load(bar)						0	0,15	0,35	0,50	0,75	1,1
	Adjustment					LEV	STV	LAV				
	Hub ratio						0,35	0,53	0,70			
	Outer covering						0	0,9				

/44

3.6. Force measurement results

The definition (2.5) of the flow-conditioned coefficients had assumed a linear dependence of the forces and moments on the displacement. However, the measurements showed - especially so for stage A - in part very strong non-linear dependences. For this reason, in Figure 3.12 we show the courses of the relative forces, or respectively, relative moments as a function of the relative eccentricity, for selected measurement series. According to the definition, the slope of the resulting curves then represents the corresponding coefficient. In each of the small figures, four parameters of the measurement series are recorded, besides the MR* number:

* MR = Messreihe = measurement series

- the rotation rate N (1/min)
- the isentropic tangential force US (N)
- the load PUE (bar) or hub ratio DN/DM
- the axial gap SAX (mm)

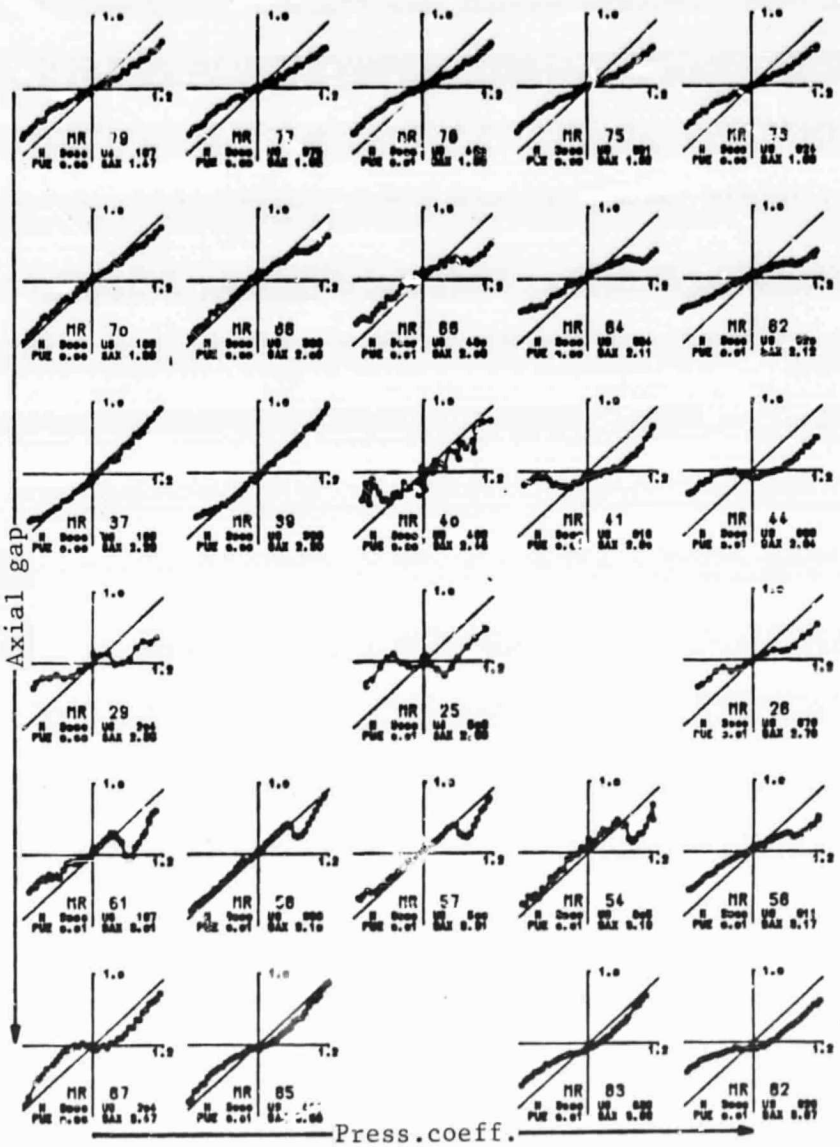

Figure 3.12 Stage A: Stage adjustment
(Relative excitation force Q2/US (%) as a function of the relative eccentricity E/LS (%))

For excitation force measurements (to determine the gap excitation coefficient K_2), a straight line was also drawn corresponding to the course expected theoretically, from equation (2.17).

Tables A6 through A26, in the Appendix, provide a survey of all the measurement series performed, with all essential parameters and results.

3.6.1. Gap excitation coefficients, stage A

Figure 3.12 above shows that in the case of the measurements on stage A, the determination of the gap excitation coefficient K_2 is not always unequivocally possible, since it is obtained from the slope of the excitation force curve. The determining influence responsible for the different deviations of the measured forces from a linear course have as yet not been clearly identified. However, the axial gap and the gradient applied to the stage should be of significant importance. For both small ($\approx$1.5 mm) and large ($\approx$3.5 mm) axial gaps, "s" shaped curves are obtained (MR 79-73, 87-82); for axial gaps between 2.0 and 2.6 mm a linear course may be assumed for /46 low tangential forces (MR 70 and 68, 37 and 39). For a value of $s_{ax} \approx 2.7$ mm an instability occurs, in a way, in that double-"s" curves are obtained (MR 29, 25 and 34) which at larger values ($\approx$ 3.1 mm) pass on to asymmetrical shapes (MR 61-54). Large gradients ($\psi > 3.5$, $U_s > 500$N) usually lead to slightly "s"-shaped curves (cf. the right half of Figure 3.12).

Besides the axial gap and the gradient, in pairs of measurement series the rotation coefficient (MR 31, 30) and the load (32, 33) were varied, by adjusting the stage's gradient in such a manner that approximately the same pressure coefficient was obtained for all measurement series. Figure 3.13, below shows the excitation forces measured under those conditions, as a

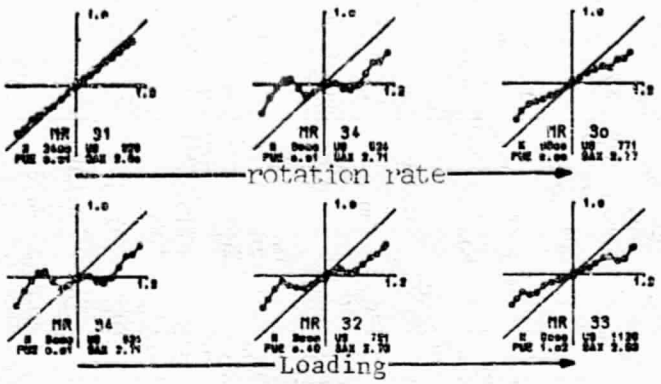

Figure 3.13 Stage A: Stage adjustment
(Relative excitation force Q2/US (%) as a function of relative eccentricity E/LS (%))

function of deflection. Changes in the rate of rotation or the load provide better linearity for the excitation force curves, whose slope and hence, gap excitation coefficient K_2, however, change only little.

The significant variation in the individual measuring points for MR 40, in Figure 3.12 - already suggested in neighboring parameter combinations (MR 66, 54) - is remarkable. The unbalance in the rotor evident in this measurement series leads one to suspect flow instabilities at the rotor shroud-band, that can occur for certain values of the axial gap, covering and /47
stator exit velocity. La Roche [23] also pointed out such effects.

To obtain the gap excitation coefficients K_2 for stage A, the slopes of the excitation force curves were taken only from approximately linear curve portions. The K_2 values thus derived are reported in Tables A6 and A7. A selection of them was plotted in Figure 3.14, below, as a function of the pressure coefficient. It can be observed that in this stage construction type somewhat smaller values of the gap excitation coefficients

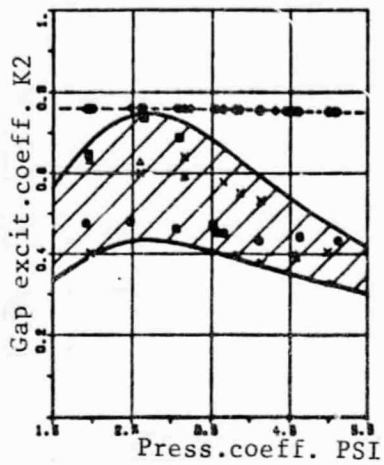

•Calc. from gap loss

Figure 3.14 Stage A: stage adjustment

can be expected, in comparison to the values obtained from the gap loss.

3.6.2. Gap excitation coefficients, stage B and three-stage group

In excitation force measurements with an added reaction stage (stage B) no such extreme non-linearities were observed, but under certain operating conditions ($\psi \approx 3.0$, $U_s \approx 400N$) certain irregularities again occurred, which were not as evident at higher or lower stage load conditions. Figure 3.15, below, shows characteristic force courses for stator, rotor and stage adjustments of stage B*. Besides changes in the gradient, in

* In the representation of the excitation forces as a function of the eccentricity, for stages B and C, as well as for the three-stage group, the opposite direction of rotation was

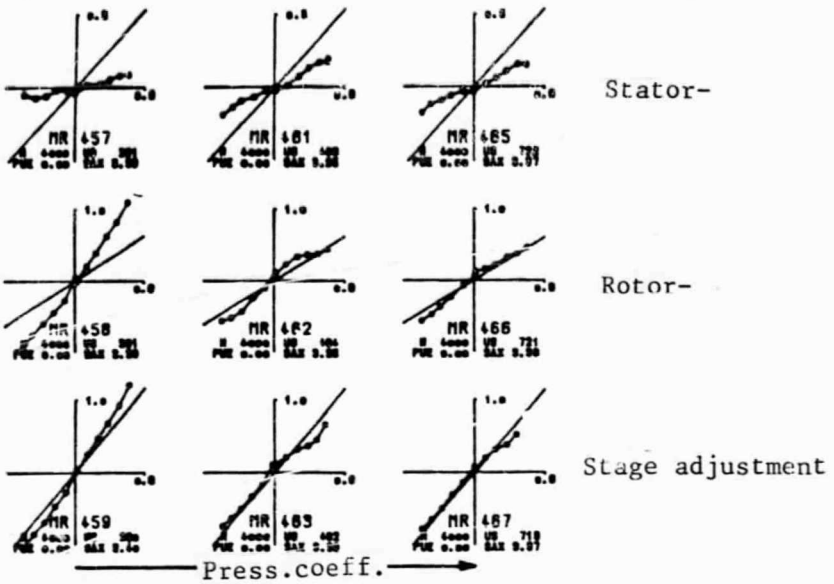

Figure 3.15 Stage B (Relative excitation force Q2/US (%) as a function of the relative eccentricity E/LS (%))

this stage the load and the rotation rate were varied over a larger range (cf. Tables A8 and A9). Based on the measurements for stages A and C, changes in the axial gap seemed unnecessary, since except for extremely small values - which hardly occur, in practice - no substantial effect was expected. Figure 3.16, /48 below, shows the K_2 values obtained from the slopes of the excitation force curves, as a function of the pressure coefficient. From the partially non-linear force curves, a global slope was always found that considered all measurement points; this led to the relatively large scatter (cf. measurement uncertainty FK2 in Tables A8 and A9). Both for the stage adjustment (STV) and for the rotor adjustment (LAV) an approximately parabolic course is obtained, with a minimum at $\psi \approx 3.5$. For the stator adjustment (LEV), relatively small values are obtained, with a maximum at approximately $\psi = 3.5$.

(cont.) considered, compared to stage A, so that here, too, a positive deflection would cause a positive force.

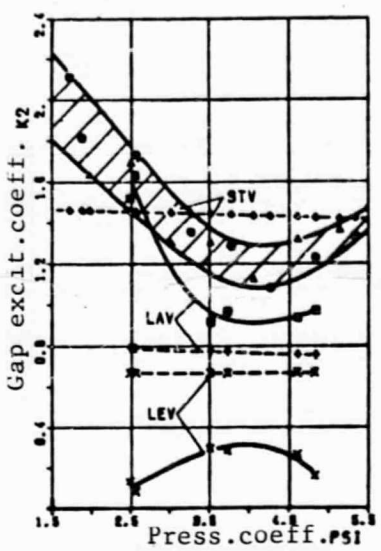

- STV 1st meas.
- STV 2nd meas.
- LAV meas.
- LEV meas.
- from SPV valc.
- from SPV calc
- from SPV calc.

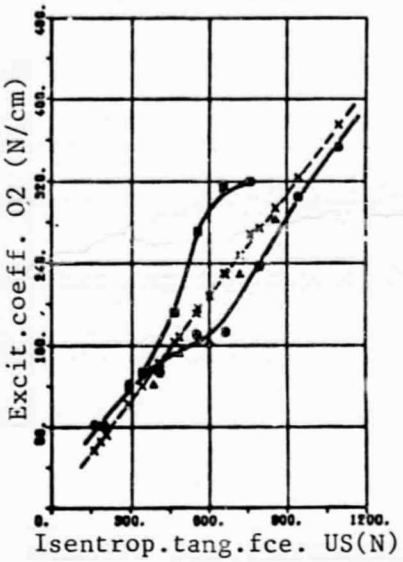

- STV var.grad. 1st meas.
- STV var. meas. 2nd meas.
- STV var. loading
- STV calc.(gap loss)

Figure 3.16 Stage B: SAX=3.3mm Figure 3.17 Stage B: SAX=3.3mm

For comparison purposes, the broken line represents values obtained by means of Traupel's [17] equations based on gap loss.

According to existing theory, the excitation coefficient q_2 is linearly dependent on the rotor's isentropic tangential force, and therefore a dimensionless plot of the measured excitation coefficients as a function of the isentropic tangential force /49 can shed more light on characteristic tendencies. For variable gradients we then obtain a non-linear course, as shown in Figure 3.17, above. For very small gradients, the curve will approach the broken line (obtained from the gap loss) from above; for very large gradients, from below. In the transition range of intermediate gradients are to be found the largest non-linearities in the measured excitation force curves (cf. Figure 3.15, page 53).

An increase in the fluid's density (load) always gives rise to

excitation coefficients that lie above existing theories, although for large tangential forces a tendency similar to that for measurements without load seems to suggest itself. This may be based on the fact that as the load is increased, the gradient across the stage - and hence, the flow geometry - hardly change at all, in contrast to measurements performed under variable gradient (cf. Table A8).

/50

In order to evaluate the effect of the rotation rate, Figure 3.18, below, shows the measured excitation coefficients and

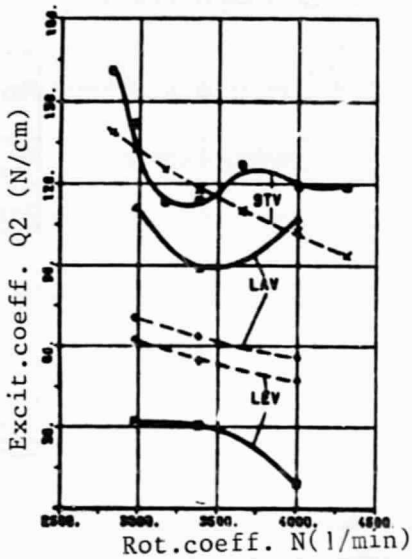

- STV meas.
- LAV meas.
- LEV meas.
- from SPV calc.
- from SPV calc.
- from SPV calc.

Figure 3.18 Stage B, SAX = 3.3 mm

those calculated from the gap loss, as a function of the rotation rate, at approximately constant stage gradient. The measurement points do not allow a generally valid statement on the effect of a variation in rotation rate, since due to the slightly "s"-shaped course, the slope of the excitation force curves appears somewhat uncertain. However, for the practical application of the test results, the effect of the rotation rate

on the gap excitation coefficient may be considered relatively small. The lower part of Figure 3.18 shows the results for separate adjustments of the stator and rotor seal, as a function of the rotation rate. The curves show that the stage excitation (stage adjustment STV) can be obtained directly as a sum of separately measured stator excitation (stator adjustment LEV) and rotor excitation (rotor adjustment LAV). While the stator excitation is always only approximately 50% of the value calculated fom the stator gap loss, the rotor excitation lies substantially above the value calculated from the rotor gap loss. It can furthermore be observed that the course of the stage excitation is characterized essentially by the excitation mechanism at the rotor shroud band. This also follows from Figure 3.19, below, which shows the course of the stator and rotor excitation as a function of the isotropic tangential force for the measurement with variable gradient and load.

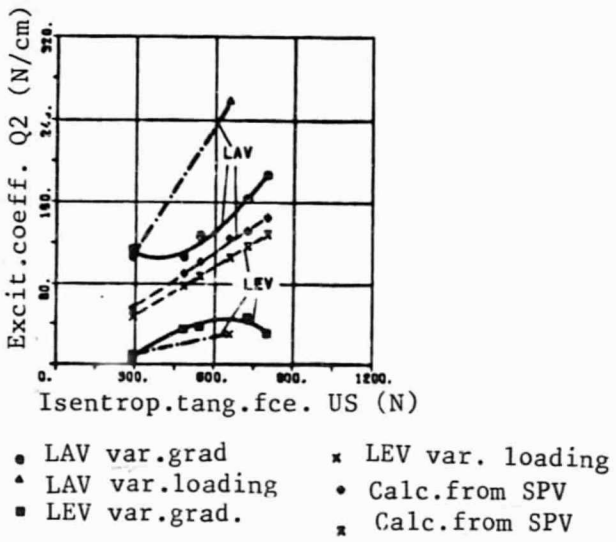

Figure 3.19 Stage B, SAX = 3.3 mm

It can be seen, once again, that the stator excitation remains substantially below and the rotor excitation - especially under load - remains above the values calculated from the gap loss /51 (cf. also Table A9).

Viewed overall, for the gap excitation coefficients corresponding to this stage one should take at least 1.5 times the values obtained to date from the linear theory. This is particularly true for high-pressure stages, since here, due to the high fluid density - as can be derived from the tests under load - relatively large excitation coefficients may occur.

Only a few measurement series were performed on the three-stage group, built by adding a stator and a rotor each before and after stage B, and in them all stator and rotor gaps were adjusted jointly (cf. Table A10).

Figure 3.20 shows a plot of the common excitation coefficient,

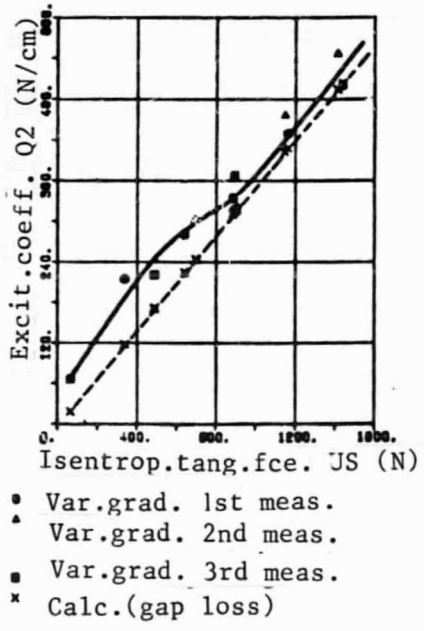

Figure 3.20 Three-stage group

as a function of the isentropic tangential force, similarly as for the single stages. Once again we can see a somewhat non-linear course, as with the measurements for the single stages. If we consider that the group's first two stages were operated under loaded conditions, in these tests, then it is

possible to explain the slightly higher excitation coefficients for the three-stage group in terms of the higher values of the individual stages under load; conversely, this also means a confirmation of the single stage results. /52

For comparison, Figure 3.21 shows the gap excitation coef-

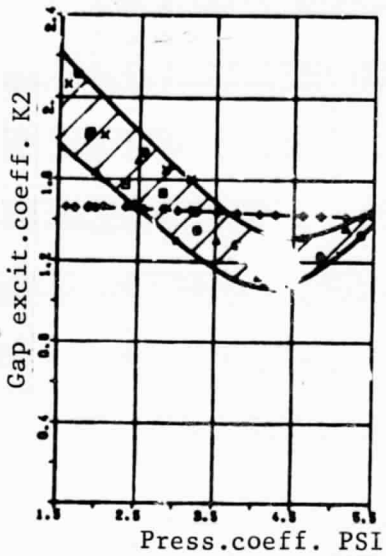

Figure 3.21 Stage construction type B

ficients K_2 for the stage adjustment of the single stage, as compared to those of the three-stage group. Within the measurement uncertainties - conditioned mainly by the partially non-linear excitation force curves - there is no noticeable difference between the gap excitation coefficients for the single stages and those for the three-stage group.

3.6.3. Gap excitation coefficient, stage C

Besides the two drum stages (A and B), we investigated a chamber

stage with weak reaction buckets (stage C).

The measurements can be subdivided into two main sections:

a) External covering or overlap $\ddot{u}_a$ = 0 mm (MR 91-253)
b) External covering or overlap $\ddot{u}_a$ = 0.9 mm (MR 254-431)*

After the first test measurements (MR 91-96), the multiple disk clutch used to that point was replaced by a membrane coupling. As Table A11 shows, there was no noticeable change. In the measurement series 91-124, the balance holes at the rotor were as large as possible (AB = 8x30 mm diameter). Later, corresponding to a calculated gap loss at the stator bottom, /53 they were reduced to 4X18 mm diameter.

Figure 3.22 shows, first and for the measurement series with AB = 8x30 mm, the gap excitation coefficients K_2 resulting from the slopes of the excitation force curves, as a function of the pressure coefficient and the axial gap (cf. also Table A11). All measured coefficients lie within a scatter band of ±7% and decrease with increasing pressure coefficient.

For stage C, the excitation forces for a given stage adjustment are always larger by a factor of 2 to 3 than those calculated from the gap loss. Hence the absolute value of the forces to be measured will also be 2 to 3 times larger than in stages A or B, respectively, which has a favorable effect on the measurement. This may also be a contributing reason to the reduced scatter in the excitation force curves, which for this stage in general follow a linear course - with the exception of the stator adjustment - as can be seen in Figure 3.23, below. (Regarding the force curve, see footnote on page 52).

---

* For external covering see page 47; u_a = UEA

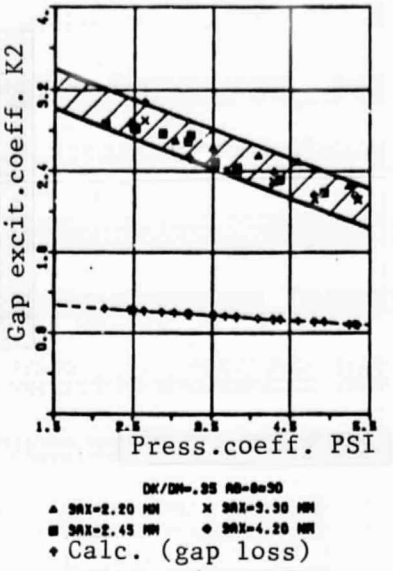

Figure 3.22 Stage C, STV UEA = 0 mm

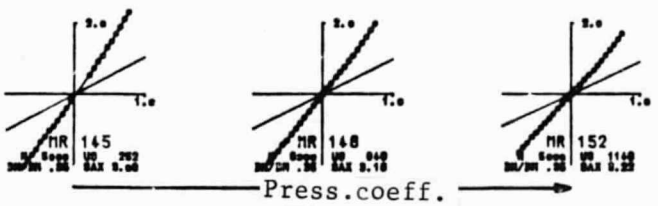

Figure 3.23 Stage adjustment UEA = 0 mm

(Relative excitation force Q2/US (%) as a function of the relative eccentricity E/LS (%))

/54

Table A12 compiles the measurements with AB = 4x18 mm diameter.

Figure 3.24, below, shows the measured K_2 values for this construction variation. If we disregard the small axial gap (1.17 mm), then all measured values lie within a scatter band of ±7%. We shall refer later to the dependence of the K_2 value on the axial gap. The K_2 values measured coincide fairly precisely with those of Figure 3.22, above; the balance holes apparently have no measurable effect on the gap excitation.

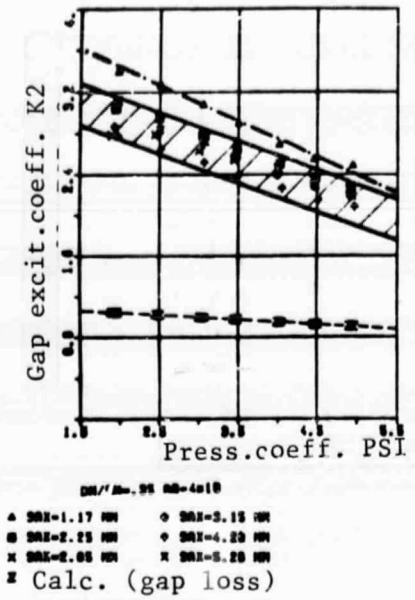

Figure 3.24 Stage C, STV UEA = 0 mm

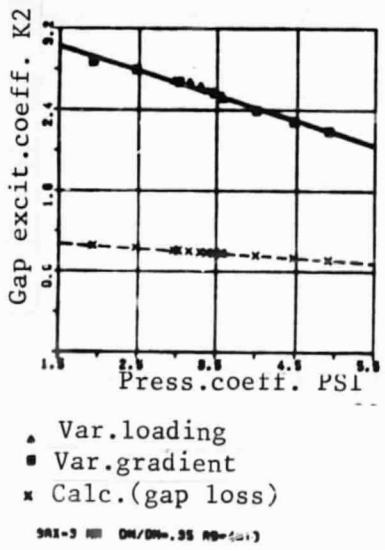

Figure 3.25 Stage C, STV UEA = 0 mm

The effect of the loading was studied for a medium axial gap of 3.25 mm, in stage C, with d_n/d_m = 0.35 and $\ddot{u}_a$ = 0 mm. For comparison, Figure 3.25 above shows the measured K_2 values as a function of the pressure coefficient, both for the loaded measurement series (MR 153-159) and for the measurement series

145-152 performed for the same axial gap. We can conclude, from the quality of the agreement, that the density of the working fluid had no effect on the gap excitation coefficient, in the range investigated for this stage (cf. Table A13).

/55

The purpose of the next measurement series was to investigate the effect of the hub ratio on the gap excitation coefficients. For medium hub ratios d_n/d_m = 0.53, the balance holes were enlarged to 4x21 mm diameter, corresponding to the higher stator gap loss. For design reasons there are no balance holes at d_n/d_m = 0.70, since the hub installed would cover the possible openings (see Figure 3.10, page 45). All tests were performed at a medium axial gap of approximately 3 mm and an external covering (UEA) of 0 mm. Figure 3.26 below shows the effect of the hub ratio on

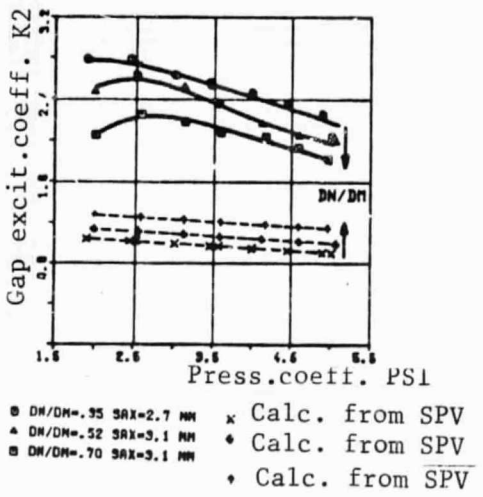

Figure 3.26 Stage C, STV UEA = 0 mm

stage excitation. For variable hub diameters, the gap excitation coefficients calculated from the gap loss also vary. for approximately constant radial gap widths, since the stator gap loss is directly proportional to the hub diameter (cf. Table A14). In contrast to the calculated values, measurements show a decrease in the gap excitation coefficient with increasing hub

diameter. The cause for this must essentially be sought in stator excitation, since no decisive changes can occur at the rotor bucket head as the hub diameter varies.

/56

This can also be seen in Figure 3.27, below, which shows the

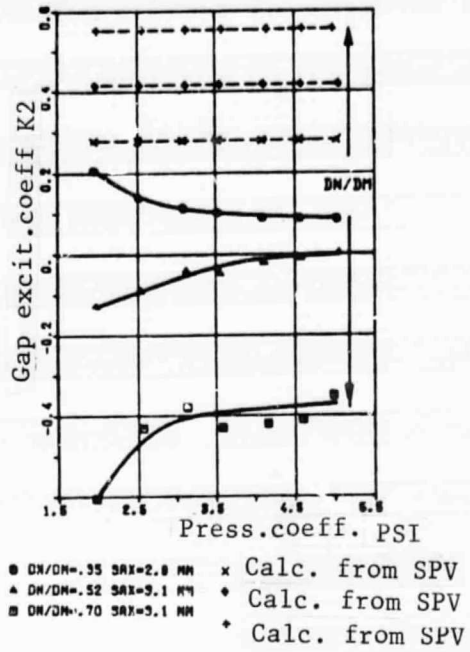

Figure 3.27 Stage C, LEV UEA = 0 mm

results of measurements at stage C with variable hub ratios, for the stator adjustment. The measured K_2 values are always below those calculated from the stator gap loss, even becoming negative for large hub ratios. As can be seen from Table A15 and in Figure 3.28, below, the forces measured are relatively small and in part, not linearly dependent on the eccentricity. For the hub ratio 0.53, the excitation coefficient can be set = 0 for practically all pressure coefficients, if for non-linear curve courses we assume that the slope of the excitation force curve near the origin is representative, similarly to what we did during the evaluation of the measurements for stage A. In addition, it can not always be assumed, in separate adjustments

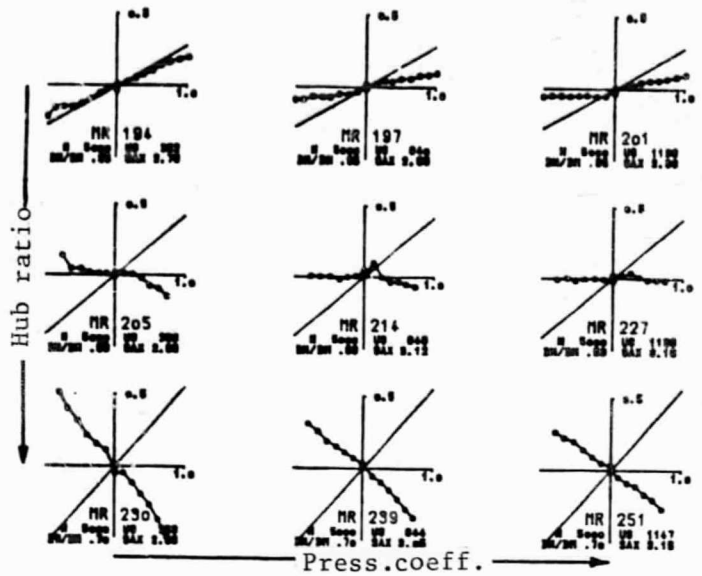

Figure 3.28 Stage C, stator adjustment UEA = 0 mm
(Relative excitation force Q2/US (%) as a function of the relative eccentricity E/LS (%))

of the stator ring, that the rotor ring does not move, minimally. Since the rotor excitation, as measured, is nearly an order of magnitude higher than the stator excitation, rotor /57
ring displacements of the order of even 1/100 of a mm already noticeably affect the measurement of the stator excitation. This becomes particularly clear when the 0-point is reset (cf. also Figure 3.37).

Figure 3.29 below shows the gap excitation coefficients for the stator, as a function of the hub ratio, for three different pressure coefficients and at nearly constant axial gap width. The reason for the course of the curve - opposite to that based on existing theory - has as yet not been identified, but it is probably conditioned by the pressure distribution at the stator hub.

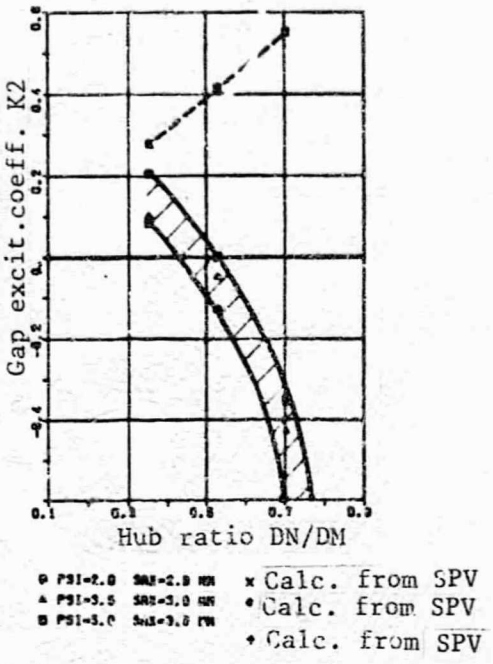

Figure 3.29 Stage C LEV
UEA = 0 mm

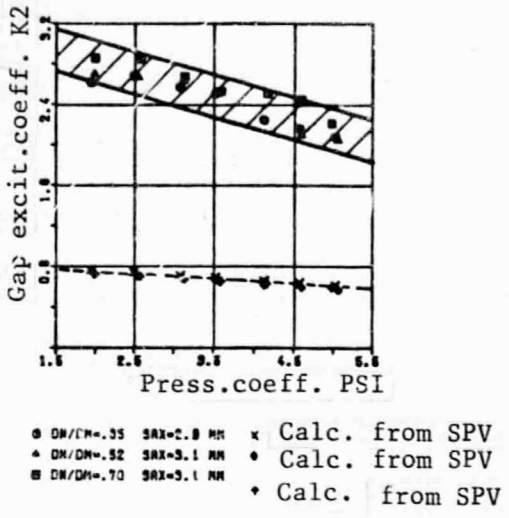

Figure 3.30 Stage C LAV
UEA = 0 mm

The measurement results for the separate rotor adjustment are shown in Figure 3.30, above, and compiled in Table A16. Disregarding negligible variations, rotor excitation per se can be considered independent of the hub ratio.

For the measurement series following, the entrance bucket was shortened, to result in an external covering by 0.9 mm. Since significant effects from the covering can be expected only in conjunction with the axial gap, a large number of measurement series were performed, at a hub ratio of 0.35, varying the /58
axial gap (see Tables A17 to A19). Here, besides the stage adjustment, separate adjustments were made for the stator and the rotor.

If we compare the results for the stage adjustment with $\ddot{u}_a = 0.9$ mm (Figure 3.31, below) with those for $\ddot{u}_a = 0$ mm (Figure 3.24, page 61), no effect of the covering seems noticeable.

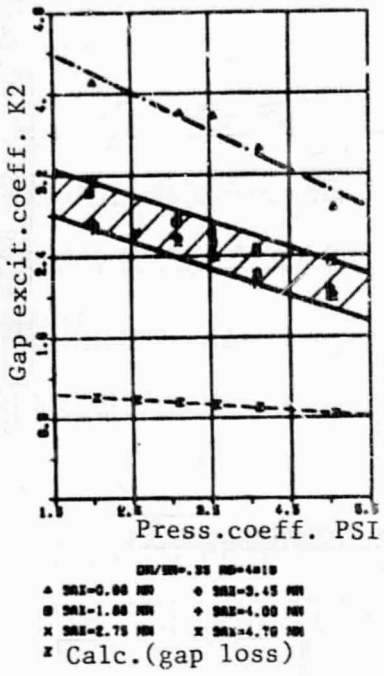

Figure 3.31 Stage C STV
UEA = 0.9 mm

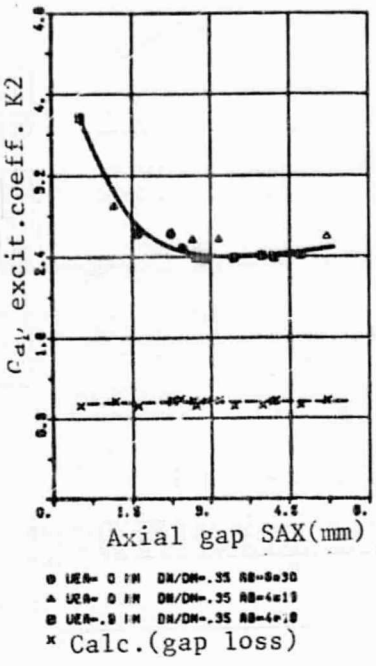

Figure 3.32 Stage C STV
PSI = 3.5

This becomes even clearer if we plot the measured gap excitation coefficients as a function of the axial gap (Figure 3.32, below), for a constant pressure coefficient. Figure 3.32 shows that for this stage, the axial gap takes on some importance only at relatively low values. For gaps below 1.5 mm one must expect a steep increase in the gap excitation coefficient; it then can increase up to a fourfold of the value calculated from the gap loss alone. The increase in the value of K_2 with decreasing axial gap can be explained in terms of increasing transverse forces arising out of the pressure distribution over the rotor /59 shroud band. As shown in section 2.2.2., the excitation forces out of the pressure distribution increase with increasing relative afflux energy at the gap entrance. Pressure measurements performed in the rotor labyrinth's first chamber, in this series, showed a decrease in the pressure gradient at the rotor shroud band, for small axial gaps. However, all other

parameters remaining equal, thereby the relative energy of the incoming flow would increase, with an increase in the forces due to the pressure distribution, as a consequence. Since the rotor excitation forms the main portion of the stage's excitation, the latter will behave similarly to the former.

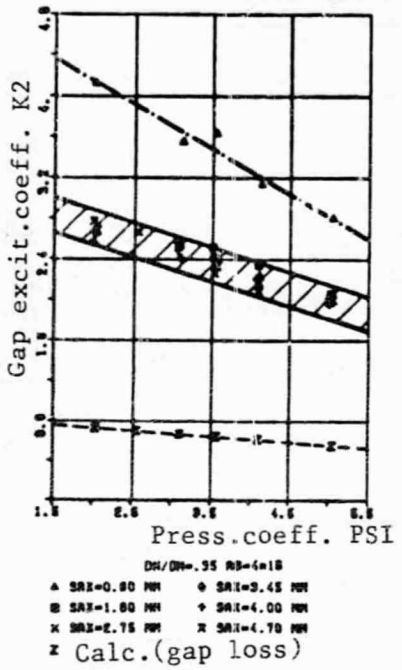

Figure 3.33 Stage C LAV
UEA = 0.9 mm

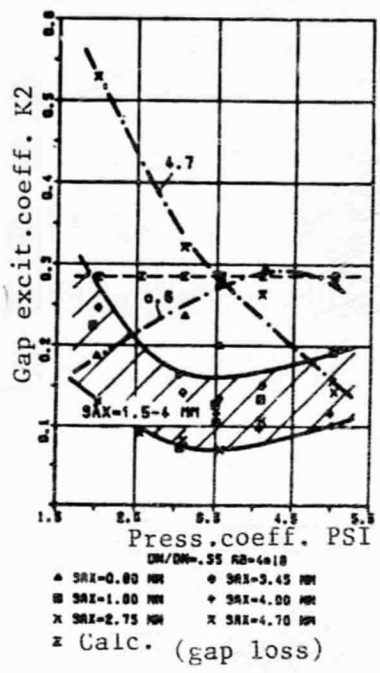

Figure 3.34 Stage C LEV
UEA = 0.9 mm

For completeness, Figure 3.33 above shows the measurement results for the rotor adjustment with outer covering $\ddot{u}_a$ = 0.9 mm. These measurement values also corresponded to those obtained for outer covering $\ddot{u}_a$ = 0 mm (see Figure 3.30, page 65).

/60

The effect of the axial gap and the pressure coefficient on the stator excitation is shown in Figure 3.34, above. For average values of the pressure coefficient and the axial gap, the gap excitation coefficient for the stator lies considerably below that calculated from the gap loss, increasing for small pressure coefficients at average axial gaps. At very small and extremely

large axial gaps, there is a tendency towards deviations that are affected by the thereby arising small gaps between stator bottom and the covering or wheel disk rotating with it.

Due to the small magnitude of the forces measured, the measurement uncertainties for the gap excitation coefficients indicated are relatively large, but even so play no significant role for practical applications, since the stator excitation is only a fraction of the stage excitation that is determining in the vibration calculation.

For an average axial gap of 2.75 mm, several measurement series were performed at different rotation rates. The corresponding data are compiled in the upper third of each of the Tables A20 to A22. The effect of the rotation rate was to be determined at a constant pressure coefficient (smaller gradient at smaller rotation rates), as well as at approximately constant tangential force (constant gradient). If, in analogy to stage B (Figure 3.18, page 55), we plot the measured excitation coefficients and those calculated from the gap loss, as a function of the rate of rotation, then we obtain a picture that states nothing, since the curves for the measured and for the calculated values are very far apart. The effect of the rotation rate is more readily seen from the ratio of measured/calculated values. As can be seen in Figure 3.35, below, both the stage and the rotor excitation increase slightly with increasing rotation rate, while that for the stator decreases. A decrease in stator excitation for increasing rate of rotation can also be seen in Figure 3.18 for stage B. The steeper slope for rotor and stage excitation with increasing rotation rate in the tests at constant gradient (dot-dash line) can be attributed to the simultaneously existing effect of the pressure coefficient, since at lower rotation rates and constant gradient the pressure coefficient increases. The preceding measurements clearly show a decrease in the ratio measurement/calculation, at increasing pressure coefficients. /61

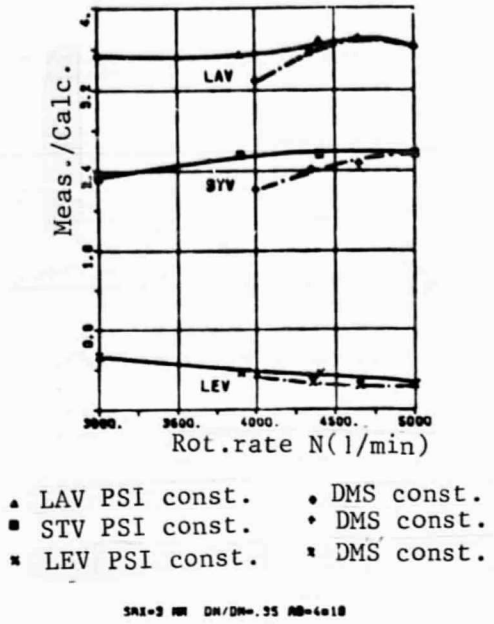

Figure 3.35 Stage C
UEA = 0.9 mm

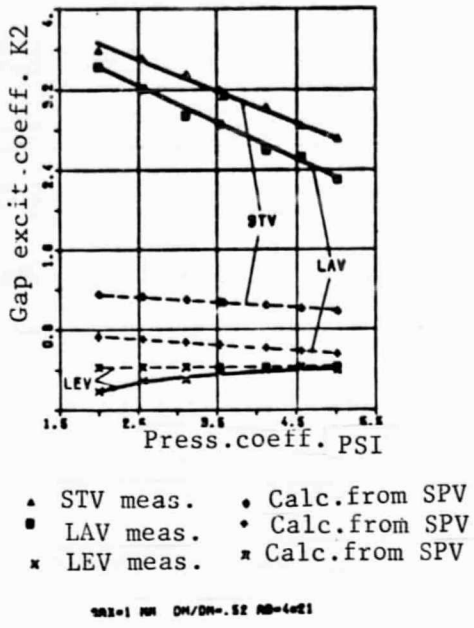

Figure 3.36 Stage C
UEA = 0.9 mm

Taking into consideration the measurement uncertainties, in these tests we can start from the premise that at least in the range investigated, the effect of the rotation rate - and hence, that of the tangential velocity of the rotor shroud band, for instance - on the gap excitation coefficient is negligibly small.

The hub ratio was also varied for the outer covering $\ddot{u}_a$ = 0.9 mm, although due to an assembly error for d_n/d_m = 0.52 the axial gap was only approximately 1.0 mm, while for d_n/d_m = 0.70 the axial gap had the usual value of 3.0 mm. The corresponding measurment data are reported in the lower halves of Tables A20 to A22. The results of the tests with the average hub ratio d_n/d_m = 0.52 are shown in Figure 3.36, above. The magnitude and the course of the rotor excitation (LAV) match earlier results quite well, taking the axial gap into account (1 mm) (cf. Figure 3.33, page 67). As to the stator excitation, especially at low pressure coefficients strongly bent excitation force curves /62

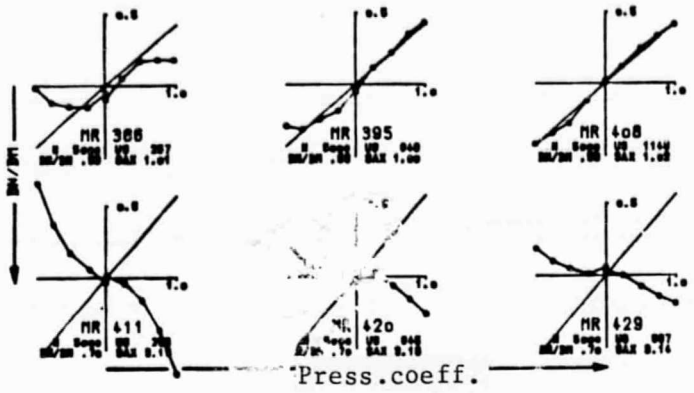

Figure 3.37 Stage C Stator adjustment UEA = 0.9 mm
(Relative excitation force Q2/US (%) as a function of the relative eccentricity E/LS (%))

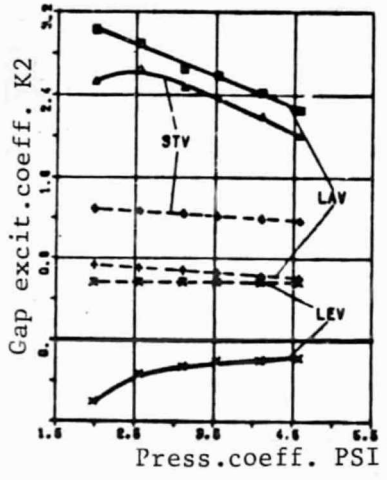

STV meas. Calc.from SPV
LAV meas. Calc.from SPV
LEV meas. Calc.from SPV

SAX=3mm DN/DM=0.7 AB=0

Figure 3.38 Stage C UEA = 0.9 mm

are obtained. Their slope near the center, however, corresponds approximately to the value calculated from the gap loss (cf. Figure 3.37, first row, below). As was true of earlier measurements, the measured stage excitation agrees fairly well

with the sum of rotor and stator excitation.

Figure 3.38 finally, shows the measurement results for d_n/d_m = 0.70 and $\ddot{u}_a$ = 0.9 mm. While the measured rotor excitation coefficients correspond approximately to those at $\ddot{u}_a$ = 0 mm (Figure 3.30, page 65) - i.e., no measurable effect from the modified covering - for the stator adjustment the excitation force curves deviate more strongly from comparable measurements (MR 230-254) (cf. also Figures 3.28 and 3.37). The cause for these differences in force course has not yet been identified, but will probably be found in the stator seal, for assembly-conditioned geometrical changes. In addition, due to shortening of the stator buckets - to modify the covering - a different percent reaction was obtained, compared to similar measurements. For the rest, a very painstaking investigation of the relatively small stator excitation forces for this stage - in comparison to the forces acting at the rotor shroud band - /63 does not seem urgent, from a practical point of view.

The stage excitation measured in this measurement sequence lies slightly above comparable measurements with $\ddot{u}_a$ = 0 mm (MR 250-254, figure 3.26), especially at the lower pressure coefficients; this is mainly due to the greater stator excitation at lower pressure coefficients, for $\ddot{u}_a$ = 0.9 mm.

/64

3.6.4. Comparison of all stages and effect of the pressure distribution

Figure 3.39 shows a comparison of the excitation force measurement results obtained for the stages investigated. Since because of design differences different calculated excitation forces result for each stage type, for comparison purposes we plotted, for each case, the ratio of the measured gap excitation coefficient for that stage ("measurement"), to the value calculated from the gap loss ("calculation"), as a function of

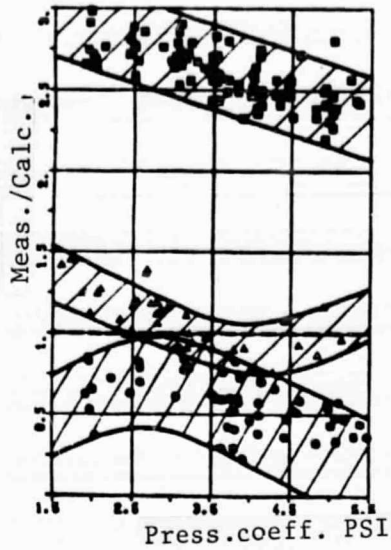

- Stage A, SAX 2-4 mm
- Stage B, SAX 3 mm
- Stage C, SAX 2-5 mm, DN/DM=0.35

Figure 3.39 Comparison of all stages

the pressure coefficient.

For stage C, we only plotted the values for $s_{ax} > 2$ mm and $d_n/d_m = 0.35$, since for the other stages no measurements exist for either very small axial gaps or variable hub ratios.

For stage A, the ratio measurement/calculation lies below 1 for all measurements; thus, for stages of this design, with relatively small buckets, we should not expect gap excitation coefficients that are significantly above the values calculated from the gap loss.

For stage B and the three-stage group the band of points is parabolical. In the usual range of application of $\psi < 3$, in such stages we can expect gap excitation coefficients that are 20-50 % higher than those calculated to date.

The excitation coefficients determined in the tests with stage C

are always higher by a factor of 2-3 than the values calculated to date from the gap loss.

/65

For a practical application of the results, we must start from the premise that flow-conditioned excitation forces are essentially composed of two parts. Besides the excitation forces that can be calculated as shown by Thomas [1] - due to a non-uniform gap loss distribution along the perimeter - there are the transverse forces, already reported in [20], which arise out of the non-uniform pressure distribution across the rotor shroud band and at the stator hub. These compressive forces can cause an increase in the excitation forces, especially at the rotor, as well as a decrease. If we start from the premise that during the tests the forces due to the gap loss, calculated by Thomas [1] with gap loss equations from Traupel [17] are fully effective, then deviating results must essentially be conditioned by varying pressure distributions over the shroud bands. For otherwise constant parameters the magnitude of the transverse forces out of the pressure distribution surely is proportional to the shroudband width, for which reason larger excitation forces ensue in stage C. In addition, the torsional effect on the flow at the gap entrance has a significant importance for the magnitude of the resulting compressive forces, as explained in section 2.2.2. In correspondence with the stator exit angle in the stages investigated, the effect of the pressure distribution on rotor excitation will be greater for stage C (α_1 = 12.9°), than for stage B (α_1 = 17.3°). In addition, stage B has no continuous shroud bands. A pressure equalization with the meridian channel is conceivable, through the gaps between blade cover-plates, which could have a decisive effect on the pressure distribution over the shroud band. In accordance with the very large stator exit angle for stage A (α_1 = 31°), we should expect relatively small excitation forces due to the pressure distribution over the rotor shroud band.

The magnitude of the excitation force Q_{2D} due only to an uneven

pressure distribution over the rotor shroud band can be expressed, in terms of the tests with rotor adjustment, approximately as the difference betwee the measured excitation force Q_2'' and the excitation force Q_{2S}'' calculated from the rotor gap loss:

$$Q_{2D} = Q_2'' - Q_{2S}'' \qquad (3.43)$$

/66

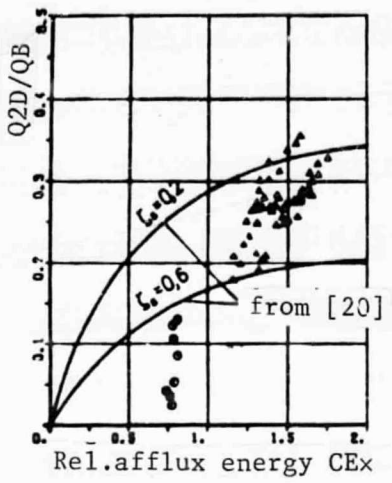

Figure 3.40 Pressure distribution forces

Figure 3.40, above, shows these compressive forces Q_{2D} - corresponding to Urlich's work [20], described in section 2.2.2. - as the relative magnitude Q_{2D}/Q_B, as a function of the relative afflux energy C_E^x. The magnitudes C_E^x and Q_B are derived from equations (2.19) and (2.20), where for stage C we used the additionally measured pressure difference at the rotor shroud band, while for stage B this pressure difference was determined from the pressure p_1, calculated for the center section and assuming a flow distribution from the potential vortex law, between the stator and the rotor.

For stage C, two curves were drawn, calculated for different loss coefficients ζ_S from [20] (cf. Figure 2.6, page 16). For the assumptions made, we obtain good agreement, here, between measurement and theory. No comparative calculations were performed for stage B, since the effect of the slits in the rotor shroud band on the pressure distribution, in this stage, is still unclear. The points plotted merely show that the $C_E^{\times}$ values obtained from the measurement data for reaction stages are considerably smaller than those obtained for constant pressure stages, as already mentioned.

To perform further comparative calculations according to [20], more precise studies are required on the flow processes in the seal gap, taking into consideration the inflow and exit flow conditions, as well as modified geometries, where applicable (for instance, for variable axial gaps).

/67

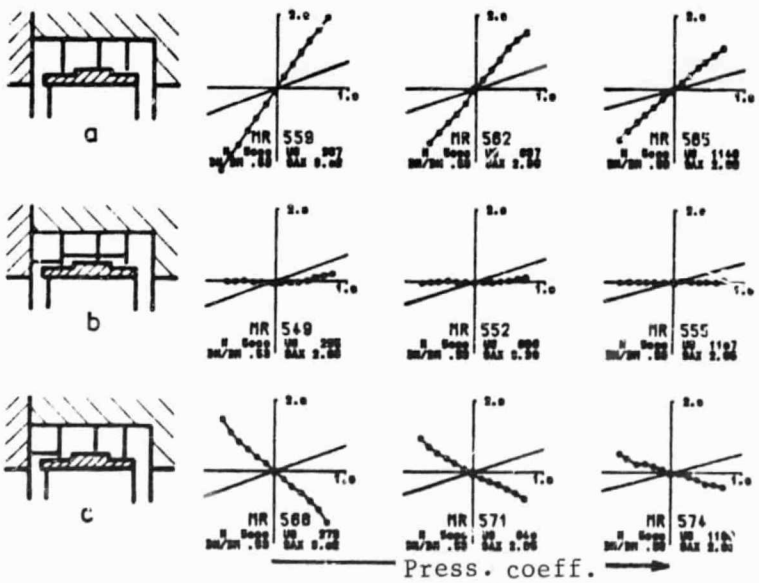

Figure 3.41 Stage C Rotor adjustment (Relative excitation excitation force Q2/US (%) as a function of the relative eccentricity E/LS (%))

/67

The large effect of the torsional incoming flow, at the rotor shroud band, can also be seen from the additional measurements for stage C, compiled in Table A23. We started from the premise that radial web plates in the rotor seal's labyrinth chambers ("strips") would reduce the torsional effect in the flow over the shroud band, which should have smaller excitation forces out of the pressure distribution, as a consequence.* As can be seen in Figure 3.41, above, in comparison to the usual construction, (a), such strips cause a substantial change in the exciting transverse forces, for eccentric rotor positioning. While for an arrangement with web plates in the first three labyrinth chambers (b) the gap excitation coefficient K_2 practically becomes 0, if the strips are used only in the first chamber (c), negative K_2 values result, which eventually could lead to a self-excited vibration running against the direction of rotation. The introduction of strips into the labyrinth chambers of the high-pressure portion of a 300 MW turboset with a tendency towards self-excited vibration brought about a cancellation or respectively, a substartial reduction in the natural-frequency disturbing vibration, such that the machine could now be operated up to maximum output perfectly undisturbed. This is shown already by a confirmation of these tests with a high-power turbine. /68

At the stator seal, the incoming and exit flow conditions at the seal gap are fundamentally different from those at the rotor shroud band; for this reason it is quite possible for opposite compressive forces to occur, that reduce the excitation. The partially strongly non-linear or respectively, asymmetrical excitation force curves observed in many measurements can essentially be conditioned by differing pressure distributions, since local pressure distributions are also very sensitive to

---

* Footnote:expansion unknown, abbreviation unintelligible; could refer to a patent application

even the smallest geometry errors (for instance, burrs at the seal peaks).

Qualitative statements about the magnitudes and dependence of the pressure distribution in the stages investigated would be possible, by means of further theoretical studies after [20], as well as corresponding pressure measurements. These should be performed at all surfaces that come in contact with the flow medium (such as hub, upper and underside of the rotor shroud band, internal cross-section of the rotor, etc.).

3.6.5. Moment coefficients L_1

In all excitation force measurements , besides the transverse force Q_2, a moment M_1 also results (equation (3.27)), from which follows the moment coefficient L_1, corresponding to the definition, equation (2.5). The effect this coefficient has on the stability behavior of real rotors is small, however, in comparison to the gap excitation coefficient K_2 and hence a less detailed description seems adequate, for the measured values of L_1. To obtain an overall view of the possible order of magnitude of this coefficient, suffice to determine its upper and lower limits and some characteristic tendencies. For more detailed statements we refer the reader to the values in the tables, in the Appendix (Tables A6 to A23). Figure 3.42 shows an overview /69 of measured L_1 coefficients for all stage types, and the usual axial gap. For the two reaction stages the values are relatively low, betwen 0 and -0.15 for stage A, while for stage B and the 3-stage group we can expect values between 0 and 0.2. Corrsponding to the negative sense of rotation of stage A, in comparison to the positive rotation of stage B, we could draw the conclusion, here, that the coefficient L_1 depends on the direction of rotation according to

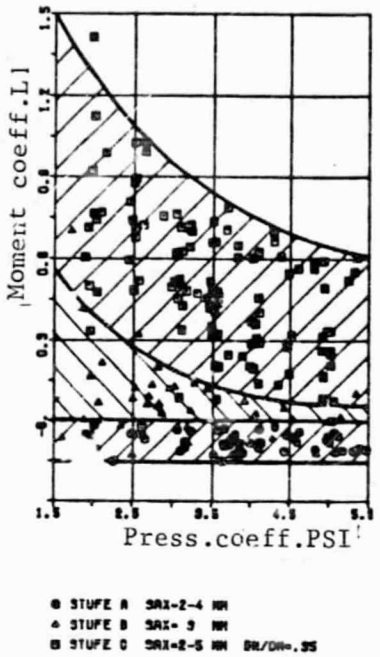

Figure 3.42 Comparison of all stages

However, this statement should be confirmed by more readily comparable measurements at two equal stages rotating in different directions, or by theoretical considerations. For stage C, the values of L_1 lie between 0 and 1, increasing steeply for small pressure coefficients. For the usual design data ($\psi \approx 3.5$), an average value of 0.5 may be assumed.

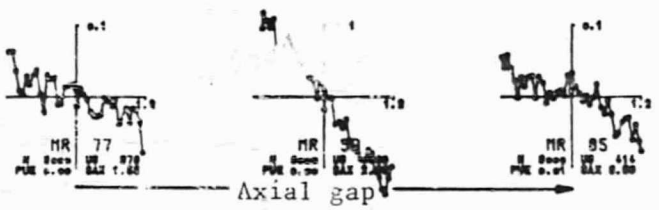

Figure 3.43 Stage A Stage adjustment (Relative moment 2·M1/DM·US (%) as a function of the relative eccentricity E/LS (%))

/70

The course of the measured moments as a function of the deflection is usually linear - within the measurement uncertainties - as shown, for example, in Figures 3.43 and 3.47. Furthermore, we can see from Figure 3.43 that for stage A the moment coefficient L_1 takes the highest absolute value for an average axial gap, and is nearly zero for very small or very large axial gaps.

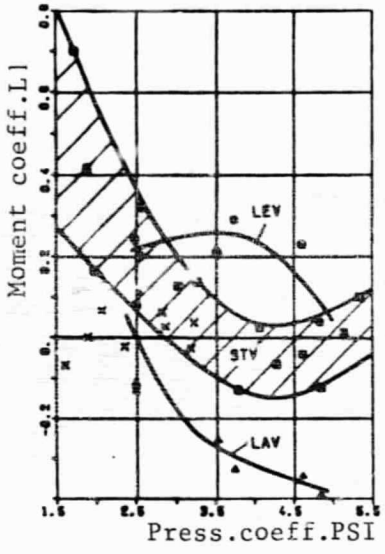

• single stage ▪ single stage
▲ single stage × triple stage

Figure 3.44 Stage B SAX = 3.3 mm

Figure 3.44, above, shows the differing effect of the stator and the rotor when they are adjusted separately, in stage B. While the stator adjustment (LEV) shows an approximately constant moment coefficient L_1 of approximately 0.2 at all pressure coefficients, the rotor adjustment (LAV) caused predominantly negative coefficients, which with increasing pressure coefficient decrease to approximately -0.4. The L_1 values obtained for stage adjustment (STV) correspond - as was the case for the K_2 values - quite well to the sum of the separately measured stator and rotor coefficients. For the three-stage group, the measured L_1 values were practically zero; the

relatively large L_1 values of the individual stages at low pressure coefficients are not observable for the stage group.

In correspondence to the force measurements, many L_1 values were measured for stage C. Because of the chamber design, it seems particularly appropriate for a fundamental insight into this stage, to study separately the effect of the various parameters on the moment coefficients. Figure 3.45, below, shows the L_1 values from the stator adjustment as a function of the hub

/71

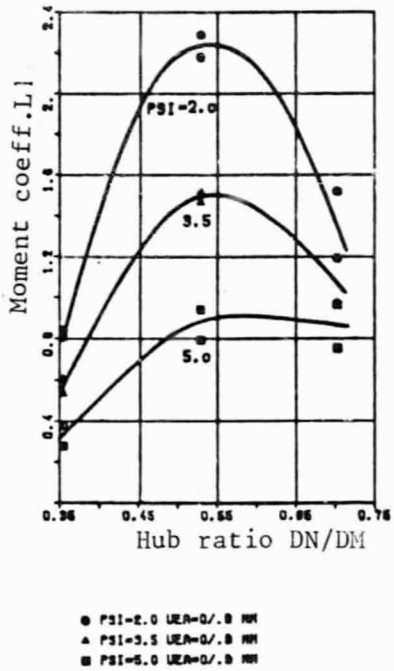

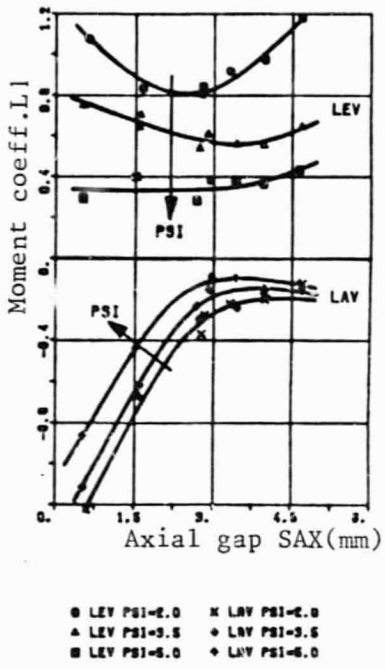

Figure 3.45 Stage C LEV
SAX = 3 mm

Figure 3.46 Stage C
DN/DM = 0.35

ratio, for different pressure coefficients and an axial gap of approximately 3 mm. In spite of the occasionally large scatter, a clear maximum can be observed for intermediate hub ratios. In addition, the L_1 value decreases steeply with increasing pressure coefficients.

The effect of the axial gap at various pressure coefficients on

the moment coefficients L_1 for the stator, or respectively, rotor can be seen in Figure 3.46, above. While for the stator adjustment (LEV) we obtain positive values of L_1, which once again decrease with increasing pressure coefficient, for the rotor adjustment (LAV) we obtain negative L_1 values which decrease steeply for low axial gap widths. The absolute value of the coefficients increases slightly with increasing pressure coefficient.

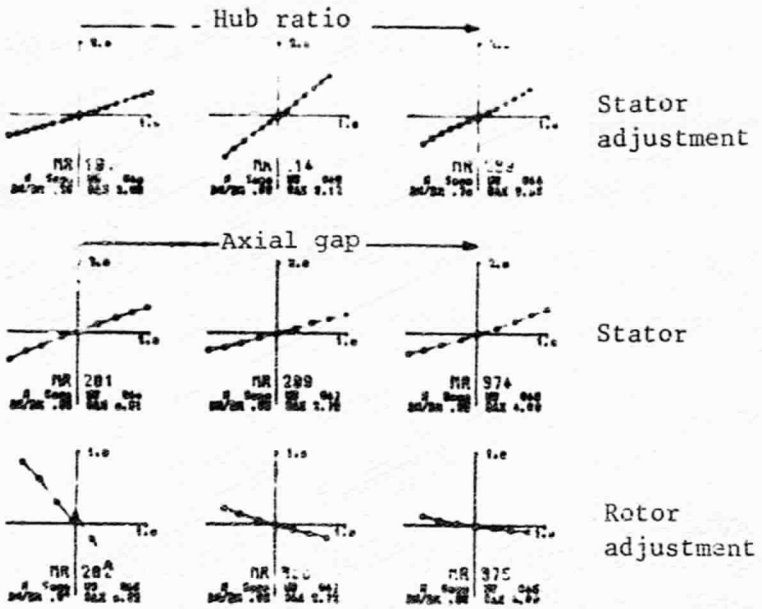

Figure 3.47 Stage C (Relative moment 2 M1/DM US (%) as a function of the relative eccentricity E/LS (%))

Figure 3.47, above, shows the generally linear course of the measured moments as a function of the displacement in dimensionless representation, for some selected measurement series. In the upper row is shown the effect of the hub ratio during stator adjustment, while the two lower rows show the /72 effect of the axial gap for stator, or respectively, rotor adjustment.

3.6.6. Deflection coefficients K_1

For selected parameter combinations (usually close to the stage's design parameters), by displacing the housing in horizontal direction, the deflection coefficient K_1 and the moment coefficient L_2 were determined, in addition to the gap excitation coefficient K_2 and the moment coefficient L_1. These measurements are compiled in Tables A24 to A26.

While the effect of the deflection coefficient K_1 on a real rotor's stability behavior is usually small, in comparison to that of the gap excitation coefficient K_2, its influence can not always be neglected. Negative coefficients K_1 act on the rotor /73 in the sense of increasing system rigidity, which is equivalent to an increase in the eigen-frequency and hence, to a stabilizing effect. Contrariwise, a positive value of K_1 has a destabilizing effect.

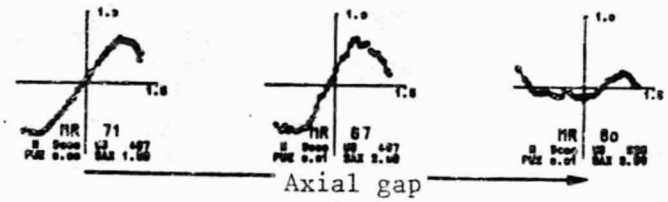

Figure 3.48 Stage A Stage Adjustment (Relative deflection force Q1/US (%) as a function of relative eccentricity E/LS (%))

For stage A only three measurement series with stage adjustment are available, which show the effect of the axial gap on the deflection force at intermediate pressure coefficients. If we disregard the non-linearities at high eccentricities, Figure 3.48 above indicates K_1 values of approximately 0.9 to 1.4, for

small and intermediate axial gaps, while for large axial gaps K_1 becomes almost zero.

For stage B, Figure 3.49, below, shows the course of the rela-

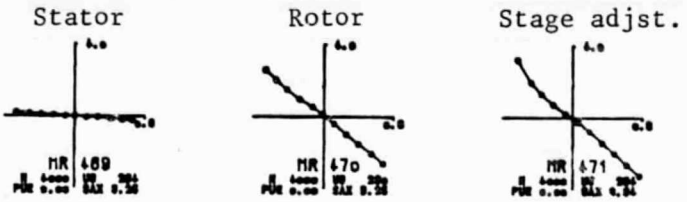

Figure 3.49 Stage B (Relative deflection force Q1/US (%) as a function of the relative eccentricity E/LS (%))

tive deflection force as a function of the eccentricity, for an intermediate tangential force. While for adjustment of the stator only we obtain a K_1 value of -0.34, for rotor and stage adjustment the K_1 values obtained are -3.6 and -3.9, respectively.

/74

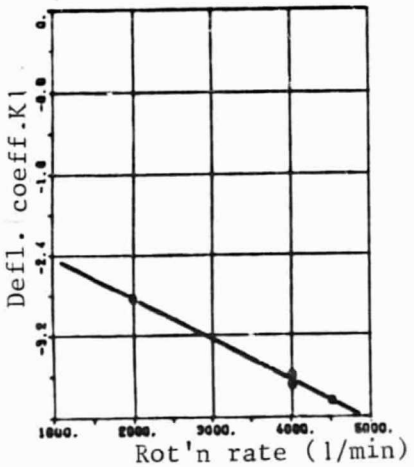

Figure 3.50 3-stage group
SAX = 3 mm, US = const.

Measurements on the three-stage group with approximately three

times the tangential force and at nominal rotation rates (4000 rpm) also yielded K_1 values of approximately -3.6 (see Figure 50, above). The figure also shows the effect of the rotation rate on the K_1 value, at nearly constant tangential force. As we can see, there is a linear increase in the value of the deflection coefficient with an increase in the rotation rate.

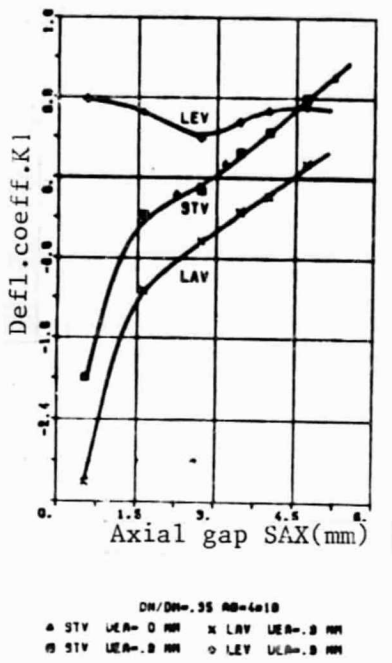

Figure 3.51 Stage C PSI=3.5

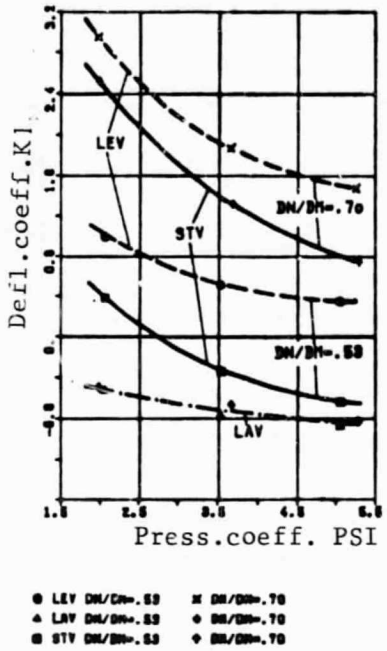

Figure 3.52 Stage C SAX=3mm

Figure 3.51, above, shows the effect of the axial gap on the deflection coefficient K_1, for stage C. For an approximately constant pressure coefficient $\psi = 3.5$ and a hub ratio of $d_n/d_m = 0.35$, the K_1 value first linearly decreases - both for rotor and for stage adjustments - with decreasing axial gap, becoming strongly negative for very small axial gaps (not customary, in practice). For stator displacements, nearly constant, throughout positive values of the deflection coefficient are obtained, which show a shallow minimum for intermediate axial gaps.

For the stator, however, the K_1 values for this stage depend strongly on the pressure coefficient and the hub ratio, as can /75

be seen in Figure 3.52, above, for a 3 mm axial gap. Corresponding to the stator coefficients, the deflection coefficient for the stage decreases approximately parabolically with increasing pressure coefficient, but with increasing hub diameter relatively large positive coefficients are obtained, caused predominantly by the stator, since as expected, the coefficients for the rotor are independent of the hub ratio.

Figures 3.51 and 3.52 once again show good agreement of the stage coefficients with the sum of the coefficients measured separately for the stator and the rotor.

3.6.7. Moment coefficients L_2

As was the case for excitation force measurements, so also in deflection force measurments do we obtain, from the two forces at the rotor's front and back end, moments M_2, from whose course over the eccentricity we can determine a moment coefficient, L_2. Figure 3.53, below, shows the measured courses of the relative /76

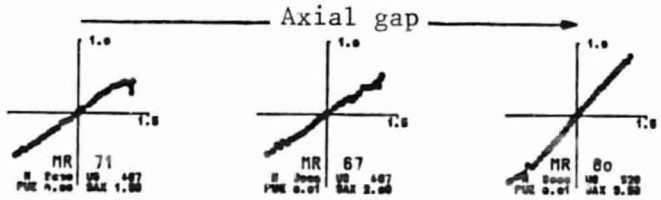

Figure 3.53 Stage A Stage adjustment (Relative moment 2·M2/DM·US (%) as a function of relative eccentricity E/LS(%))

moment $2M_2/(d_m \cdot U_s)$ as a function of the relative eccentricity e/l", both in %, for stage A. We can see from the quite linear course that for small to intermediate axial gaps (1 - 2 mm) the L_2 value is approximately 0.45, while for larger axial gaps (> 3.5 mm) the values increase to approximately 0.7.

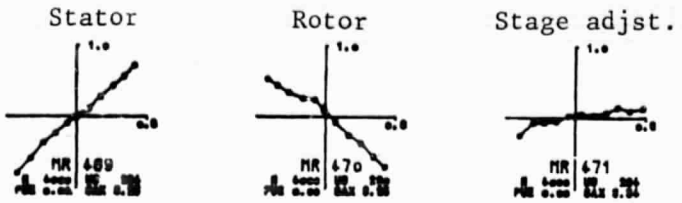

Figure 3.54 Stage B (Relative moment 2·M2/DM·US (%) as a function of relative eccentricity E/LS (%))

As Figure 3.54, above, shows, for stage B at intermediate pressure coefficients of approximately $\psi = 2.5$ and an axial gap of approximately 3.3 mm, we obtain a positive coefficient L_2 = 1.1 for stator adjustments, while for the rotor adjustments a negative value of L_2 = -0.7 is obtained. For the stage, the moment coefficient is approximately L_2 = 0.4, corresponding also to the sum of the stator and rotor values.

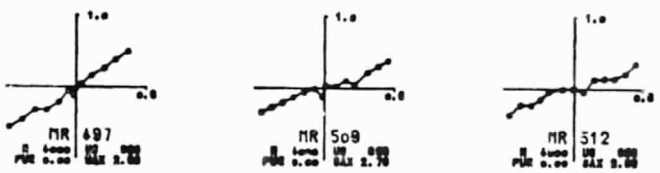

Figure 3.55 Three-stage group (Relative moment 2·M2/DM·US (%) as a function of relative eccentricity E/LS (%)

Figure 3.55, above, shows that for the three-stage group, for the same pressure coefficient and a slightly smaller axial gap, the L_2 values range from 0.3 to 0.7. We also see that the moment coefficients L_2 of multi-stage arrangements are similar in magnitude to those of single stages.

/77

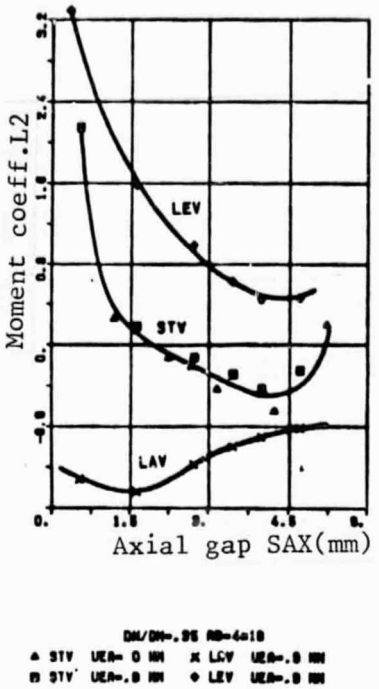

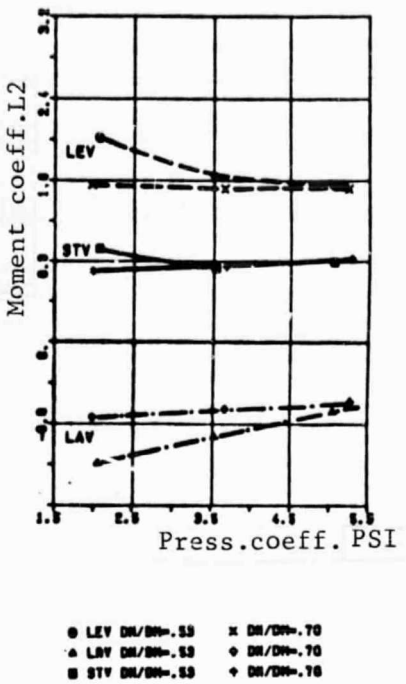

Figure 3.56 Stage C PSI=3.5

Figure 3.57 Stage C SAX=3mm

The effect of the axial gap on the moment coefficient L_2 of stage C, for a hub ratio $d_n/d_m = 0.35$ and a pressure coefficient $\psi = 3.5$, is shown in Figure 3.56, above. While the rotor's L_2 values are always negative, decreasing slightly from -0.8 to -1.4 for decreasing axial gap widths, the always positive stator values increase very steeply for small axial gaps. During stage adjustment, the two opposing momenta approximately cancel each other - except for the smaller axial gaps - so that for the stage, at the above hub ratio and pressure coefficient, the L_2 values are relatively small, between 0.2 and -0.4.

As Figure 3.57 above shows, the pressure coefficient has a relatively small effect on the L_2 values. For this stage, the stator coefficient increases with the hub diameter, resulting in somewhat higher stage coefficients, of approximately 0.8.

3.6.8. Summary of force measurements

TABLE 3.4 Review of measured coefficients from force measurements

Stator adjustment				
	K_1	K_2	L_1	L_2
Stage B	-0,3	+0,2	+0,2	+1,1
Stage C	d_n/d_m: +0,6 (+3,0 / ψ)	s_{ax}: 0 (-0,4 / +0,4; d_n/d_m)	d_n/d_m: +0,6 (+0,4 / +2,0 / ψ)	s_{ax}: +0,8 (+0,4 / +3,2 / ψ)

Rotor adjustment				
	K_1	K_2	L_1	L_2
Stage B	-3,6	+1,0 (+1,6 / ψ)	-0,2 (-0,4 / 0 / ψ)	-0,7
Stage C	s_{ax}: -0,7 (-3,0 / 0 / ψ)	s_{ax}: +2,4 (+2,0 / +4,0 / ψ)	s_{ax}: -0,3 (-1,4)	-0,8

Stage adjustment				
	K_1	K_2	L_1	L_2
Stage A	s_{ax}: +1,0 (0 / ψ)	s_{ax}: +0,7 (+0,4 / ψ)	-0,1	s_{ax}: +0,4 (+0,7)
Stage B	-3,9	+1,2 (+2,0 / ψ)	0 (+0,5 / ψ)	+0,4
3-Stage group	-3,6 (-3,8 / -2,6 / n)	+1,4 (+2,0 / ψ)	0	+0,5
Stage C	s_{ax}: 0 (-2,0 / +2,0 / ψ)	s_{ax}: 2,4 (+2,0 / +4,0 / ψ)	d_n/d_m: +0,5 (+2,0 / ψ)	s_{ax}: 0 (+2,4 / ψ)

Table 3.4, above, compiles the numerical values of the measured coefficients of flow-conditioned forces and momenta, to provide

an overview of the force measurements performed in the context of this study (approximately 500 measurement series, with 10,000 measurement points). In each case, an average value was recorded which should be representative for the individual stages of a design; where available, upper and lower limiting values that can occur during upward (Fo1) or downward (Fo2) variation of the parameter specified, are also indicated. The values of the individual parameters can be obtained from Table 3.3, as well as Tables A6 to A26; here, the design case corresponds approximately to the heavily outlined parameter combination in Table 3.3.

Based on the measurements for stage C, for adjustment of the stator only we would expect mostly positive values for the coefficient K_1, while for rotor adjustment we would expect it to be negative. For a practical application of the results, we may start from the premise that in general, for stages A and C the K_i values for the typical stage data will be close to 0, i.e., that they can be neglected for stability calculations. For stages built similarly to stage B or the three-stage group, respectively, negative K_1 of the order of -3 to -4 may occur, which however exert a stabilizing effect.

The gap excitation coefficient K_2 usually lies below the values calculated from the gap loss, for stator adjustments, even becoming negative for large hub diameters, in stage C. If - as in [1] - we take into account a possible equalizing flow in tangential direction by computing the stator gap excitation coefficient K'_{2S} with an additional factor d_n/d_m, then in many of the measurements a better agreement between experimental and calculated values could be established. However, the negative K_2 values for stator adjustment in stage C can at this point be explained only in terms of as yet unknown forces arising out of the pressure distribution at the hub, and acting in that sense. The relatively large K_2 values for rotor adjustment are essentially to be attributed to additional excitation forces /80

caused by the pressure distribution at the shroud band, as treated in more detail in earlier sections. When judging the magnitude of the K_2 value, it must be taken into consideration that for the different stages the calculated values of K_{2S} are also different, due to the differing gap losses (cf, also Tables in the Appendix).

The momenta M_1 and M_2 acting on the rotor can be explained in terms of differences in the axial pressure differences along the perimeter. Apparently the effects of the stator and rotor eccentricities on these pressure differences oppose each other, so that relatively small L_1 and L_2 values are obtained, during stage adjustments. For stage C however, at large hub diameters higher L_1 values must be expected, and in addition, extremely small axial gaps lead to large L_2 values.

4 KINETIC TESTS /81

The purpose of the kinetic tests is to measure the flow-conditioned forces on a vibrating rotor. The underlying idea is to determine the forces generated by the fluid flow, from the measured damping or stability behavior, respectively, of the system. This is accomplished by a comparison of measured damping factors with calculated values. The calculation of damping factors as a function of flow-conditioned forces presupposes the most precise possible knowledge of other system magnitudes affecting the damping behavior (mass, rigidity, damping), and for this reason the vibrating system to be studied should the simplest posible construction.

4.1. Vibration and stability behavior of a simple rotor

In order to perform the kinetic tests, first we shall investigate the effect of the individual system parameters on the damping or stability behavior, respectively, of a simple rotor. Let it consist of a mass-less shaft of rigidity c with a disk of mass m located midway between the two bearings, on which acts a flow-conditioned excitation force, summarized in the coefficients (proportional to the deflection)

$$q_2 = r_{21} = -r_{12} \qquad (4.1)$$

of the matrix $\mathfrak{R}$ (cf. section 2.2). At the two identical bearings, besides the forces from the deflection matrix $\mathfrak{R}_L$, only the uncoupled damping forces $\dot{x}d_{xx}$ and $\dot{y}d_{yy}$ are assumed to be acting. The coupling terms of the bearing damping are not taken into consideration, here, since they are not determinable in the positioning of the test rotor described below. In addition, the number of parameters remains limited to a controllable measure, thereby.

The system's damping factors u correspond - for solutions of the form

$$x = A \cdot e^{\lambda t}, \quad y = B \cdot e^{\lambda t}, \quad \lambda = u + i\omega \qquad (4.2)$$

/82

for the differential equation of vibration - to the real portions of the complex eigen-values λ.

we define as system damping

$$D_s = -\frac{u}{\omega_k} \qquad (4.3)$$

the damping factor, related to the eigen-frequency ω_k, of the system's most weakly damped eigen-vibration. The system damping is a measure of how rapidly the disturbance-stimulated eigen-vibrations decay or increase in frequency.

4.1.1. Derivation of the characteristic equation

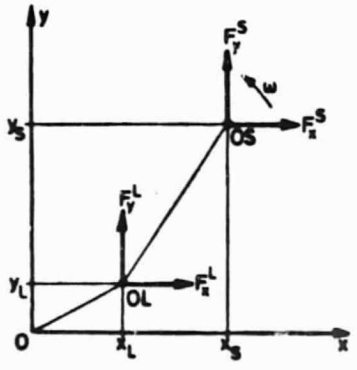

Figure 4.1 Forces at a unit mass, symmetrical rotor
0 : Trunnion center, stationary state
OL: Trunnion center, vibrating state
OS: Disk center, vibrating state

C - 2

To set up the equation of motion for the symmetrical rotor, we shall here consider only translational displacement.

In correspondence with the definitions in section 2.2. and the assumptions made above, we obtain the external forces acting on the bearing trunnion center OL and the disk center OS, as shown in Figure 4.1, above:

$$\left.\begin{aligned} F_x^S &= -m\ddot{x}_S - q_2 y_S \,, \\ F_y^S &= -m\ddot{y}_S + q_2 x_S \,, \\ F_x^L &= -d_{xx}\dot{x}_L - c_{xx}x_L - c_{xy}y_L \,, \\ F_y^L &= -d_{yy}\dot{y}_L - c_{yy}y_L - c_{yx}x_L \,. \end{aligned}\right\} \qquad (4.4)$$

/83

From the equilibrium condition for the external forces at the rotor, we obtain:

$$\left.\begin{aligned} m\ddot{x}_S + q_2 y_S + 2(d_{xx}\dot{x}_L + c_{xx}x_L + c_{xy}y_L) &= 0 \,, \\ m\ddot{y}_S - q_2 x_S + 2(d_{yy}\dot{y}_L + c_{yy}y_L + c_{yx}x_L) &= 0 \,, \end{aligned}\right\} \qquad (4.5)$$

and from the condition that the sum of the forces acting on the disk alone must be zero:

$$\left.\begin{aligned} m\ddot{x}_S + q_2 y_S + c(x_S - x_L) &= 0 \,, \\ m\ddot{y}_S - q_2 x_S + c(y_S - y_L) &= 0 \,. \end{aligned}\right\} \qquad (4.6)$$

From these we obtain

$$x_L = \frac{m}{c}\cdot\ddot{x}_S + x_S + \frac{q_2}{c}\cdot y_S \,, \quad y_L = \frac{m}{c}\cdot\ddot{y}_S + y_S - \frac{q_2}{c}\cdot x_S. \qquad (4.7)$$

If we differentiate the above equations once with respect to time, we have

$$\dot{x}_L = \frac{m}{c}\cdot\dddot{x}_S + \dot{x}_S + \frac{q_2}{c}\cdot\dot{y}_S \,, \quad \dot{y}_L = \frac{m}{c}\cdot\dddot{y}_S + \dot{y}_S - \frac{q_2}{c}\cdot\dot{x}_S. \qquad (4.8)$$

Replacing equations (4.7) and (4.8) in (4.5), we obtain two coupled linear differential equations of the third order:

$$
\left.
\begin{aligned}
&a_1\ddot{x}_S + a_2\ddot{x}_S + a_3\ddot{y}_S + a_4\dot{x}_S + a_5\dot{y}_S + a_6 x_S + a_7 y_S = 0\,,\\
&b_1\ddot{y}_S + b_2\ddot{y}_S + b_3\ddot{x}_S + b_4\dot{y}_S + b_5\dot{x}_S + b_6 y_S + b_7 x_S = 0\,,\\
&a_1 = 2d_{xx} \qquad\qquad b_1 = 2d_{yy}\\
&a_2 = 2c_{xx} + c \qquad\qquad b_2 = 2c_{yy} + c\\
&a_3 = 2c_{xy} \qquad\qquad b_3 = 2c_{yx}\\
&a_4 = 2d_{xx}\cdot\frac{c}{m} \qquad\qquad b_4 = 2d_{yy}\cdot\frac{c}{m}\\
&a_5 = 2d_{xx}\cdot\frac{q_2}{m} \qquad\qquad b_5 = -2d_{yy}\cdot\frac{q_2}{m}\\
&a_6 = 2c_{xx}\cdot\frac{c}{m} - 2c_{xy}\cdot\frac{q_2}{m} \qquad b_6 = 2c_{yy}\cdot\frac{c}{m} + 2c_{yx}\cdot\frac{q_2}{m}\\
&a_7 = 2c_{xy}\cdot\frac{c}{m} + (2c_{xx}+c)\cdot\frac{q_2}{m} \qquad b_7 = 2c_{yx}\cdot\frac{c}{m} - (2c_{yy}+c)\cdot\frac{q_2}{m}\,.
\end{aligned}
\right\} (4.9)
$$

/84

Replacing the solution (4.2) in (4.9) yields a homogeneous, linear system of equations for the unknowns A and B:

$$
\left.
\begin{aligned}
&A\cdot(a_1\lambda^3 + a_2\lambda^2 + a_4\lambda + a_6) + B\cdot(a_3\lambda^2 + a_5\lambda + a_7) = 0\,,\\
&A\cdot(b_3\lambda^2 + b_5\lambda + b_7) + B\cdot(b_1\lambda^3 + b_2\lambda^2 + b_4\lambda + b_6) = 0\,.
\end{aligned}
\right\} (4.10)
$$

This system has a non-trivial solution only when the determinant of the coefficients is zero. This condition provides the characteristic equation sought,

$$
\left.
\begin{aligned}
&A_0 + A_1\lambda + A_2\lambda^2 + A_3\lambda^3 + A_4\lambda^4 + A_5\lambda^5 + A_6\lambda^6 = 0\,,\\
&A_0 = a_6b_6 - a_7b_7\\
&A_1 = a_4b_6 + a_6b_4 - a_5b_7 - a_7b_5\\
&A_2 = a_2b_6 + a_6b_2 + a_4b_4 + a_3b_7 + a_7b_3\\
&A_3 = a_1b_6 + a_6b_1 + a_2b_4 + a_4b_2 - a_3b_5 - a_5b_3\\
&A_4 = a_1b_4 + a_4b_1 + a_2b_2 - a_3b_3\\
&A_5 = a_2b_1 + a_1b_2\\
&A_6 = a_1b_1\,.
\end{aligned}
\right\} (4.11)
$$

The real components u_i of the generally complex solutions λ_i represent the damping factors of the eigen-vibrations characterized by the imaginary component ω_i. Negative damping

factors indicate damping vibration, i.e., stability, while positive values mean instability. The stability limit is defined by the condition $u = 0$.

/85

4.1.2. Effect of the bearing's characteristic magnitudes

In this section we shall show how changes in bearing rigidity and damping, as well as the shaft rigidity, affect the course of system damping as a function of the flow-conditioned excitation acting on the system.

We defined the following reference magnitudes to obtain the most generally valid description possible of the calculation results:

system rigidity $c_s = \frac{(c_{xx}+c_{yy})\cdot c}{c_{xx}+c_{yy}+c}$,

eigen cyclic frequency $\omega_k = \sqrt{\frac{c_s}{m}}$. (4.12)

This makes it possible to describe the excitations characterized by q_2 and the damping factor u of the most weakly damped eigen-vibration as dimensionless magnitudes

System excitation $S = \frac{q_2}{c_s}$,

System damping $D_s = -\frac{u}{\omega_k}$ (4.13)

The variation of the bearing's characteristic magnitudes is described by the following parameters:

shaft/bearing rigidity ratio $F = \frac{c}{c_{xx}+c_{yy}}$

bearing rigidity anisotropy $A = \frac{c_{yy}}{c_{xx}}$

bearing rigidity coupling degree $K = \frac{c_{xy}}{c_{xx}}$

bearing coupling anisotropy $C = \frac{c_{yx}}{c_{xy}}$

bearing damping $D = \frac{2d_{xx}}{\sqrt{2c_{xx}m}}$

bearing damping anisotropy $B = \frac{d_{yy}}{d_{xx}}$. (4.14)

/86

The system parameters were so chosen, for the calculations, that they approximately correspond to those ocurring in the damping measurements to be described below (cf. Table 4.2). The following magnitudes are fixed by the test installation's design:

Mass : $m = 100$ kg
Bearing rigidity : $c_{xx} = 200$ N/mm
Shaft rigidity : $c = 70{,}000$ N/mm. (4.15)

For isotropic positioning (A=1, $c_{xx}=c_{yy}$) we then have

$$c_s = 398 \text{ N/mm}, \quad \omega_k = 63{,}1 \text{ s}^{-1}, \quad F = 1{,}5 . \quad (4.16)$$

As a start, Figure 4.2, below, shows the effect of bearing rigidity anisotropy on the course of system damping as a function of system excitation. Intermediate values are assumed for isotropic bearing damping (D = 0.10, B = 0), with the coupling rigidities equal 0 (K = 0, C = 1). Starting from a linear decrease in system damping with increasing excitation for isotropic bearing rigidity (A = 1), for anisotropic bearing positioning (A = 1) a clear increase in the limit of stability is obtained ($D_s = 0$). Over a certain range system damping remains constant, for increasing excitation, but then falls steeply.

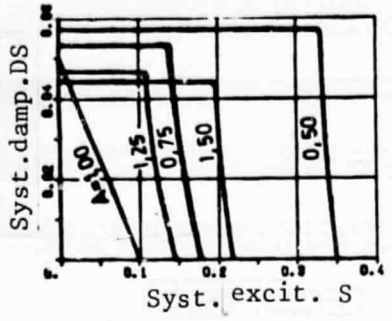

Figure 4.2 Effect of anisotropy A in the bearing rigidity without coupling (K = 0, C = 1) for isotropic bearing damping (D = 0.10)

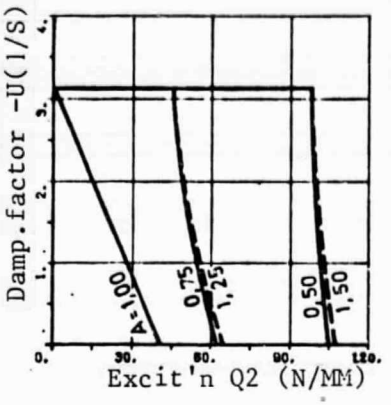

Figure 4.3 Effect of anisotropy A in the bearing rigidity without coupling (K = 0, C = 1) for isotropic bearing damping (D = 0.10)

For increased bearing rigidity in one direction (A = 1.25 or 1.50, respectively), the resulting lower limit of stability (D_s = 0) is only apparent, when compared to an equally large decrease (A = 0.75 or 0.50, respectively), since both system damping D_s and the system excitation contain system rigidity c_s in the denominator and c_s increases with A > 1, decreasing with A < 1. If we observe - as in the dimensioned representation in Figure 4.3, above - the course of the damping factor as a /87
function of the excitation coefficients, we see that the curves for A = 0.75 and A = 1.25 almost overlap, as do those for A = 0.50 and A = 1.50. There are marginally higher limits of stability for A > 1 (D_s = 0). This means that the stabilizing effect in bearing rigidity anisotropy is nearly independent of whether the rigidity is larger in one direction (A > 1) or smaller (A < 1), than in the other, provided the difference in bearing rigidities remains equally large.

The stabilizing effect of bearing rigidity anisotropy is based on the change in the mode of vibration's path - brought about by the differing rigidities - to an ellyptical shape. As can be shown, in an elliptical vibration path the energy supplied

through the excitation coefficient q_2 is smaller than for a circular path, as it occurs for isotropic bearing positioning [25].

The bearing's isotropic coupling rigidity coefficients $c_{xy} = c_{yx}$ ($K \neq 0$, $C = 1$) have an effect similar to that of bearing rigidity anisotropy, on the course of system damping, as a function of system excitation. Figure 4.4, below, shows their

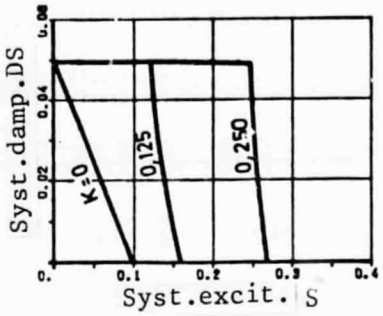

Figure 4.4 Effect of isotropic (C = 1) bearing coupling K for isotropic bearing rigidity (A = 1) and isotropic (B = 1) bearing damping D = 0.10

effect for isotropic bearing rigidity (A = 1) and an isotropic bearing damping of D = 0.10 (B = 1). We again obtain - for increasing degree of coupling K - a considerable increase in the limit of stability, as well as the characteristic sudden drop /88 in the curve. Negative values of K in the same amount result in superimposed curves.

Figure 4.5 below shows the course of system excitation as a function of anisotropy A and the degree of coupling K of the bearing rigidity, for isotropic bearing damping (D = 0.10, B = 1). The curves - which once again steeply drop off at a certain excitation - show that the stabilizing effect of anisotropy and coupling are approximately additive, if we consider the increase in the limit of stability in relation to the isotropic case (A = 1, K = 0).

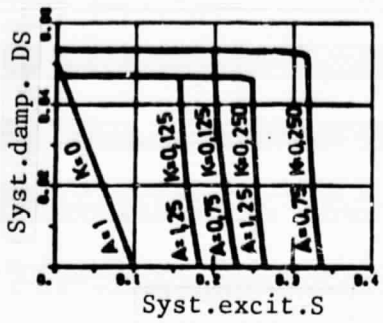

Figure 4.5 Effect of the anisotropy A of the bearing rigidity and isotropic (C=1) bearing coupling K for isotropic (B=1) bearing damping D=0.10

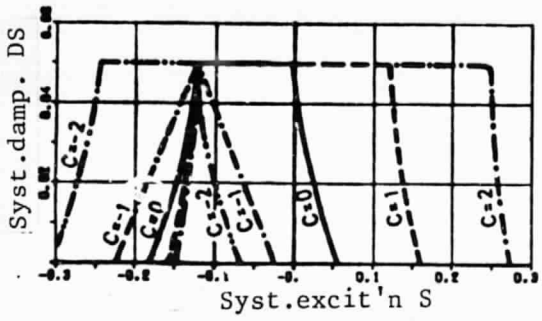

Figure 4.6 Effect of anisotropy C of bearing coupling, for a degree of coupling K=0.125 in the case of isotropic bearing rigidity (A=1) and isotropic (B=1) bearing damping D=0.10

In contrast to the dependences considered so far - which were independent of the sign of the excitation - anisotropy of the coupling rigidity ($C \neq 1$) towards the ordinate results in strongly asymmetrical curves, as can be seen in Figure 4.6, above. The dependence shown applies to isotropic bearing rigidity and damping ($A = 1$, $B = 1$, $D = 0.10$) as well as a degree of coupling of $K = 0.125$. The characteristic point is at excitation $S = -K$. Starting from it, the stable range strongly widens in the direction of positive excitation, for $C > -1$, while for increasingly negative excitation the range of stability /89
becomes smaller. For $C < -1$ we obtain curves that mirror those for $C > -1$, centered on $S = -K$ (cf. $C = -2$ and $C = 0$). For

negative degrees of coupling K in the same amount, we obtain curves that are the mirror image with respect to the ordinate of those obtained for positve K.

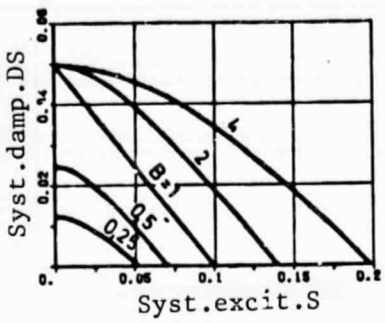

Figure 4.7 Effect of anisotropy B of the bearing damping, for bearing damping D = 0.10 and isotropic bearing rigidity (A = 1), without coupling (K = 0, C = 1)

One obvious measure to improve the operating quietness or stability, respectively, is to increase bearing damping. As can be seen from Figure 4.7, above, an increase in bearing damping in one direction (D = 0.10, B > 1) brings about - for isotropic bearing rigidity (A = 1) and vanishing coupling rigidities (K = 0, C = 1) - an increase in the limit of stability as well as a somewhat flatter course of system damping, as compared to isotropic bearing damping (B = 1). When bearing damping is decreased in one direction (B < 1), the limit of stability is correspondingly lowered and system damping - especially for small system excitation - decreases markedly, compared to B 1. Thus, for the system damping at zero excitation, the smaller damping coefficient of the bearings is determining, in the first place.

The joint effect of the anisotropy of bearing rigidity A and bearing damping B is shown in Figure 4.8, below. Bearing damping D is 0.10, the coupling rigidities are 0 (K = 0, C = 1). We can see again that the separate effects are approximately additive, viewing the change in relation to the isotropic case. According

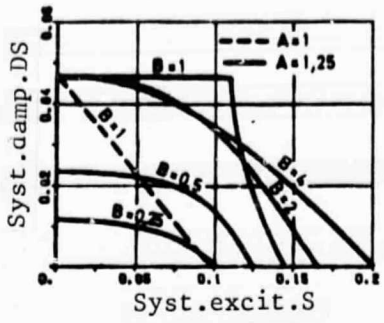

Figure 4.8 Effect of anisotropy B of bearing damping and anisotropy A of bearing rigidity, for bearing damping D=0.10, without coupling (K=0, C=1)

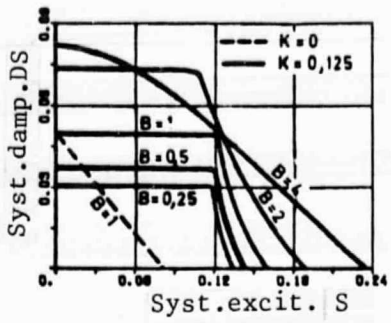

Figure 4.9 Effect of anisotropy B of bearing damping and isotropic (C=1) bearing coupling K for bearing damping D=0.10 and isotropic bearing D= rigidity (A=1)

to Figure 4.9, above, this is just as true in regard to changes in the limit of stability for anisotropic bearing damping (D = 0.10, B ≠ 1) and isotropic bearing coupling (K ≠ 0, C = 1), as well as isotropic bearing rigidity. Due to the bearing coupling however, in this case we obtain higher system damping when bearing damping increases in one direction (B > 1). For decreasing bearing damping in one direction (B < 1), we also obtain higher system damping values as when there is no coupling (cf. Figure 4.7, page 100). /90

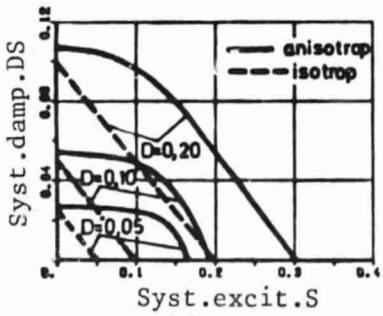

Figure 4.10 Effect of bearing damping D for isotropic bearing positioning, without coupling (A=1, K=0, C=1, B=1) and anisotropic positioning with isotropic coupling (A=1.25, K=0.125, C=1, B=2)

Finally, Figure 4.10, above, shows the effect of bearing damping

D on the course of system damping, as a function of system excitation, for isotropic bearing positioning without coupling (A = 1, K = 0, C = 1, B = 1), as well as a selected isotropic arrangement with coupling (A = 1.25, K = 0.125, C = 1, B = 2). As can be seen, for isotropic bearings, system damping and the limit of stability increase linearly with the bearing damping D, while the stabilizing effect of anisotropy and coupling - compared to the isotropic case - becomes smaller with increasing D. /91

The dependence relationships shown to this point are valid throughout for arrangements with very rigid shafts (F = 175). As the rigidity ratio F decreases, the magnitude of system damping and the limit of stability also decrease markedly. Figure 4.11 shows the course of the curves for selected parameters, for four different F values. For isotropic coupling (C = 1), curves symmetrical with respect to the ordinate are obtained, which drop ever more steeply towards the limit of stability (D_s = 0) with decreasing shaft rigidity. The stabilizing effect of anisotropy or the coupling of bearing rigidity, respectively, is much stronger at smaller F values, although system damping for S = 0 decreases slightly, in comparison to the isotropic case (cf. curves d, e, f, g with b). In contrast, for larger bearing damping, system damping and the limit of stability are raised nearly linearly for all rigidity ratios (curves a, b and c). For anisotropic coupling rigidities (C ≠ 1), asymmetrical courses occur, which for a positive degree of coupling K showed an increased stability range for positive excitation, which for negative degrees of coupling can be found mirrored with respect to the ordinate, for negative excitation (curves f and g). The same symmetry condition also applies to a selected anisotropic positioning (curves h and i).

Figures 4.2 to 4.11 show that the limit of stability of the vibration model under consideration can be increased relatively simply by changing the anisotropy or the coupling of bearing rigidities. However, increased system damping and hence faster

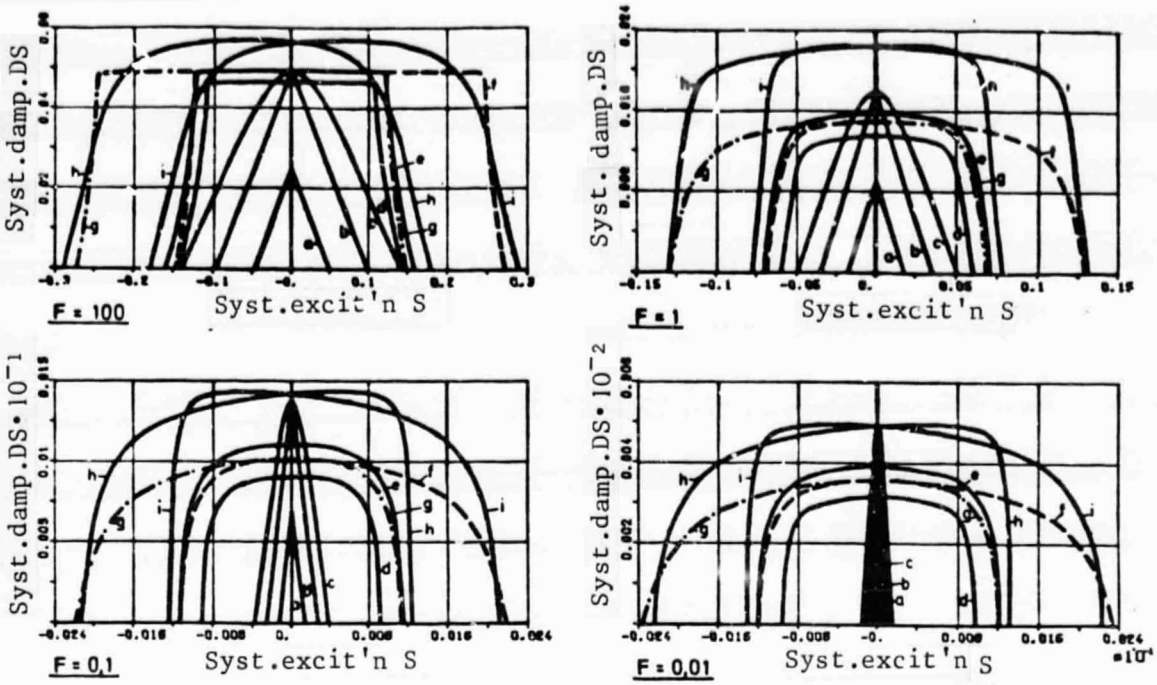

Figure 4.11 Effect of the rigidity ratio F for various bearing parameters

Curve		a	b	c	d	e	f	g	h	i
Bearing rigidity anisotropy	A	1,00	1,00	1,00	1,25	1,00	1,00	1,00	1,25	1,25
Bearing rigidity deg. of coupling	K	0	0	0	0	0,125	0,125	-0,125	0,125	-0,125
Bearing coupling anisotropy	C	1	1	1	1	1	2	2	2	2
Bearing damping	D	0,05	0,10	0,10	0,10	0,10	0,10	0,10	0,10	0,10
Bearing damping anisotropy	B	1	1	2	1	1	1	1	2	2

damping of stochastic disturbances can be achieved only by means of increased damping in both directions.

For tests from which the excitation is to be determined from the measured damping factor, an isotropic system is best suited, since there the damping factor depends linearly on the excitation.

/93

4.1.3. Effect of the flow-conditioned forces and momenta

The coefficients of the characteristic equation (4.11) can in principle be determined also by taking into consideration the matrices $\mathfrak{a}_S$ and $\mathfrak{k}_S$, as well as all characteristic magnitudes of the bearing. If we generalize the problem by removing the assumption of a symmetrical arrangement, the calculations procedure becomes very clear. It is appropriate, in that case, to use Landzberg's [7] procedure, for instance, enlarged by Vogel [10] to include the general case of anisotropic positioning and consideration of all flow-conditioned forces and momenta. However, this method of calculation of the frequency equation by means of transfer matrices, provides satisfactory results only as long as the number $\underline{n}$ of subdivisions of the rotor remains within bounds, since the maximum degree of the resulting end polynomial is 8n.

In view of the kinetic tests to be discussed later, by means of which the combined destabilizing effect of all flow-conditioned forces and momenta is determined, we shall now calculate the effect of the individual coefficients on the stability behavior of a symmetrical Laval shaft, using the procedures indicated by Landzberg or Vogel, respectively. The system parameters selected approximately correspond to those of the test installation (cf. Table 4.2):

Mass	m	= 111 kg	
Shaft rigidity	c	= 70,000 N/mm	(4.16)
Bearing rigidity	c_{xx}	= 200 N/mm	
Shaft/bearing rigidity ratio	F	= 175	
Anisotropy of the bearing rigidity	A	= 1.00	
Bearing rigidity degree of coupling	K	= -0.04	
Anisotropy of bearing coupling	C	= 1.25	
Bearing damping	D	= 0.10	
Anisotropy of bearing damping	B	= 1.00	

For the previously described calculation procedures for the effect of the bearing parameters on the damping behavior, only translational vibration motion was considered; when external momenta exist, because of the coefficients L_i and also to include the gyrostatic effect, it is necessary to take into account the moment of inertia J_i, when the characteristic equation is set up. For the rotor under study, we have the following values /94

$$J_x = J_y = 1{,}85 \text{ kg m}^2 , \quad J_z = 1{,}23 \text{ kg m}^2. \qquad (4.17)$$

Furthermore, in order to calculate the coefficients r_{ik} or k_{ik}, respectively, of the matrices $\mathfrak{R}$ or $\mathfrak{K}$, respectively, from the coefficients K_i and L_i, or A_i and B_i, respectively, we must still establish the following magnitudes:

Rotor blade length	$l'' = 40$ mm	(4.18)
Average rotor diameter	$d_m = 460$ mm	
Operating rotation rate	$n = 5000/\text{min}$	

At constant coefficients, the changes occurring in the flow-conditioned forces acting on the system take place through variations in the isentropic tangential force U_s, which for constant rotation rate is directly proportional to the output. For a dimensionless description we introduce the tangential force or output ratio, respectively,

$$\chi = \frac{U_s}{U_s^{\times}} \qquad (4.19)$$

where the reference magnitude $U_s^{\times} = 800$ N is selected in such a manner that for the calculations performed the limit of stability ($D_s = 0$) lies at approximately $\chi = 1$.

For a systematic investigation of the destabilizing or stabilizing effects, respectively, of the individual coefficients of the forces proportional to the deflection, we shall assume - based on the results of the force measurements -

an average gap excitation coefficient value of K = 2, which is representative of the usual turbine stages. On the base of the measurements performed in the context of this and Urlich's [20] studies, as well as in accordance with Piltz's theoretical considerations, we may start from the assumption that the remaining coefficients of the flow-conditioned forces proportional to the deflection lie within the range -2 to +2.

/95

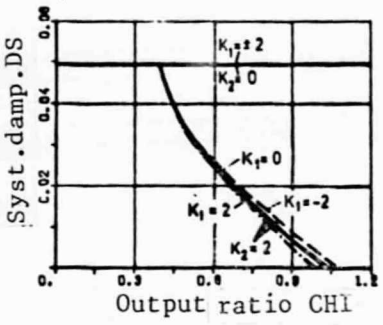

Figure 4.12 Effect of the deflection coefficient K_1 and the gap excitation coefficient K_2 on the damping behavior of the test rotor

In the first place, Figure 4.12, above, shows the effect of the deflection coefficient K_1 and the gap excitation coefficient K_2 on the course of system damping, as a function of the output ratio χ (CHI). While for $K_1 = \pm 2$ there is no change in system damping with increasing output, for $K_2 = 2$ we obtain the characteristic course, with a sudden, steep drop at a certain output. This feature is retained even when we take K_1 into account, in addition to K_2. Positive K_1 values have a slightly destabilizing effect, while that of negative K_1 is stabilizing. However, changes in system damping are relatively minor, in comparison to the effect of K_2. If the coefficient K_2 only is to be considered, we could also use the system excitation S, defined earlier, for the output ratio χ; with the parameters chosen here, $S \approx 0.1 \cdot \chi$.

The effect of the inclination coefficients K_3 and K_4 - as well as the gap excitation coefficient K_2 - on the damping behavior of the test rotor is shown in Figure 4.13, below. It can be seen

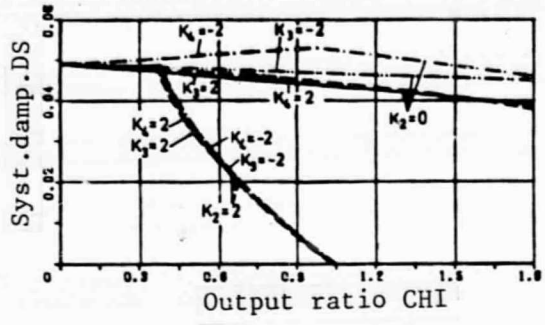

Figure 4.13 Effect of the inclination coefficients K_3 and K_4 and the gap excitation coefficient K_2 on the damping behavior of the test rotor

that despite the assumption of a symmetrical rotor, the inclination coefficients cause minor changes in system damping, even though compared to the gap excitation coefficient their effect is very small. /96

Calculations that take into account the moment coefficients L_1 through L_4 show that these coefficients cause no changes in the most weakly damped eigen-frequency, as long as the values for K_3 and K_4 are equal to zero. This fact is understandable, since the L-values have momenta acting on the rotor, as a consequence, that in the case considered here can excite only the higher-frequency and more strongly damped eigen-vibrations, with predominating inclination movements of the disk. If the inclination coefficients K_3 or K_4, respectively, are not null, then the moment coefficients L_i affect also the most weakly damped, mainly translational eigen-vibrations, since external momenta cause small rotor inclinations; due to the K_3 or K_4 values, respectively, these inclinations give rise to small transverse forces. To estimate the effect of the L-values in conjunction with K_3 or K_4 values, respectively, we started by calculating the course of system damping as a function of the output ratio for a gap excitation coefficient $K_2 = 2$, with

simultaneous effect of an L and either a K_3 or a K_4 value. Since the curves run very close together, a tabular presentation of the results is to be preferred to a graphical one, for the calculated numerical values. Table 4.1, below, shows, for each

TABLE 4.1 Percentage change in the test rotor's limit of stability for additional consideration, in each case, of an L and a K_3 or K_4 value, respectively, compared to the effect of $K_2 = 2$ alone

	$L_1 = 2$	$L_2 = 2$	$L_3 = 2$	$L_4 = 2$	$L_1 = -2$	$L_2 = -2$	$L_3 = -2$	$L_4 = -2$
$K_3 = 2$	-0,88	+2,0	-0,2	+0,29	-0,06	+1,33	-0,72	-0,88
$K_4 = 2$	+1,04	-1,05	-0,32	-1,11	-2,44	-0,58	-1,27	-0,20
$K_3 = -2$	+0,80	+1,46	+0,67	+0,44	+0,82	-0,42	+1,43	+1,27
$K_4 = -2$	-0,64	+1,15	+0,34	-1,83	+2,19	+0,03	+1,21	+0,35

case, the percentage of change in the test rotor's limit of stability, in relation to the effect of K_2 alone. The maximum change to be expected is ±2.5%. In reality, it is not only either a K_3 or a K_4 that occur together with an L value, besides K_2, but rather, the rotor's damping behavior is determined by the simultaneous effect of all K_i and L_i. Table 4.1 shows that in comparison to the single effect of $K_2 = 2$, the combination

$$K_2 = +2 \quad K_3 = K_4 = -2 \quad L_1 = L_3 = L_4 = -2 \quad L_2 = +2 \qquad (4.20)$$

leads us to expect the highest stabilizing effect, while

$$K_2 = +2 \quad K_3 = K_4 = +2 \quad L_1 = L_3 = L_4 = -2 \quad L_2 = +2 \qquad (4.21)$$

would have the most unfavorable, destabilizing effect.

Figure 4.14, below, shows the system damping curves as a function of the output ratio for the value combinations (4.20) and (4.21), in comparison to the curve obtained considering only

K_2 = 2 (curves a and c). In addition are shown curves b and d, indicating the maximum possible additional effect of K_1.

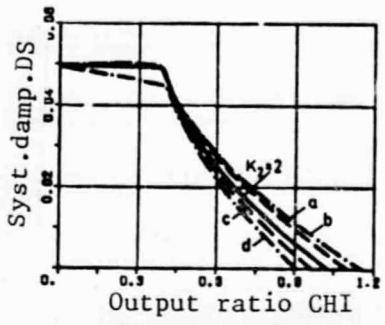

	K_1	K_2	K_3	K_4	L_1	L_2	L_3	L_4
a	0	+2	-2	-2	-2	+2	-2	-2
b	-2	+2	-2	-2	-2	+2	-2	-2
c	0	+2	+2	+2	-2	+2	-2	-2
d	+2	+2	+2	+2	-2	+2	-2	-2

Figure 4.14 Effect of the coefficients K_i and L_i - proportional to the deflection - on the test rotor's damping behavior

If we start from the premise that for K_2 = 2 the coefficients for the other forces and momenta proportional to the deflection lie between +2 and -2, then we can establish, with the aid of Figure 4.14 above, that the test rotor's stability behavior is essentially determined by the gap excitation coefficient K_2 alone, with the other coefficients able to affect the limit of stability by a maximum of 10%, upwards or downwards.

/98

For the coefficients A_i and B_i of the flow-conditioned forces and momenta that are proportional to the velocity, there are only theoretical studies [3, 4, 6] available, to date. According to them, these coefficients also lie between +2 and -2, for the usual steam turbine stages. Based on the definition (2.5), we can estimate the magnitude A_i and B_i would have to have to give rise to forces and momenta approximately equal to those generated by the coefficients K_i and L_i, proportional to the deflection. Assuming a circumpolar vibrational movement of angular frequency ω_s we obtain, from the condition of equally large maximum forces or momenta, respectively, the following

relationships:

$$\left.\begin{aligned} A_i = p \cdot K_i \;,\quad B_i = p \cdot L_i \;,\quad i = 1,2,3,4 \\ p = \frac{1}{2} \cdot \frac{d_m}{l''} \cdot \frac{\omega}{\omega_n} \;. \end{aligned}\right\} \qquad (4.22)$$

Here ω designates the operating angular frequency, d_m the average diameter and l" the stage's rotor blade length. The factor p has a value - for instance, for the kinetic measurements described below - of approximately 50, while it lies near approximately 10 for the usual high-pressure stages of power plant turbines. Thus, we may expect substantial effects of the forces and momenta proportional to the velocity, on the stability behavior of rotors built in actual practice, when their coefficients A_i and B_i lie within the order of magnitude between 10 and 100.

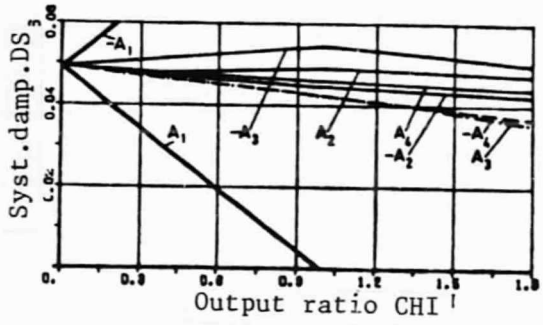

Figure 4.15 Effect of only the coefficient A_i = 100, of the forces proportional to the velocity, on the test rotor's damping behavior

To investigate the effect of the forces and momenta proportional to the velocity, on the test rotor's stability behavior, we shall assume extreme values of ±100 for the coefficients A_i and B_i, respectively. Figure 4.15, above, shows the course of system damping as a function of the output ratio, taking into account one A_i coefficient each time. The resulting curves are similar to those for the K-values, except that here the coefficient A_1 has

the decisive effect. It describes a damping force that for circumpolar motion lies along the same line of application as the excitation force characterized by the coefficient K_2. Negative K_1 values have a stabilizing effect, while those with a positive value of A_1 of corresponding magnitude can cause instability.

/99

Calculations with $B_i = \pm 100$ show - as was the case with the L-values - no effect on the most weakly damped eigen-vibrations. We shall not here engage in a detailed investigation of the effect of different combinations of A and B values, since as was the case for the coefficients proportional to the deflection, the effect of the remaining A_i or B_i values, respectively, should not exceed the order of ±10%, in comparison to the effect of coefficient A_1 alone.

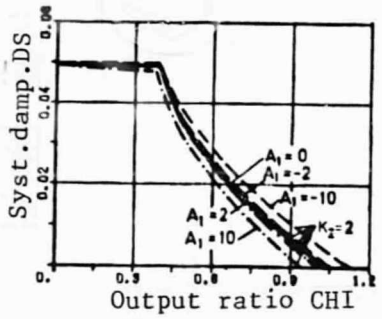

Figure 4.16 Effect of the force coefficient A_1 - proportional to the velocity - and of the gap excitation coefficient K_2 on the test rotor's stability behavior

Figure 4.16, above, shows the effect of various A_1 values on the course of the test rotor's system damping, in comparison to the effect of $K_2 = 2$. Even at relatively large A_1 values of ±10, the resulting changes in the limit of stability are only ±7.5%, with negative values of K_1 having a stabilizing effect, while that of positive values is destabilizing. The effect of the remaining A_i and B_i coefficients - in comparison to K_2 - is hence very small, in agreement with the statements above.

/100

4.2. Test arrangement, equipment and measurement procedures

In order to perform the damping measurements, the bearing suspension of the test turbine described in section 3.1 was modified. Figure 4.17, below, shows the attachment of the

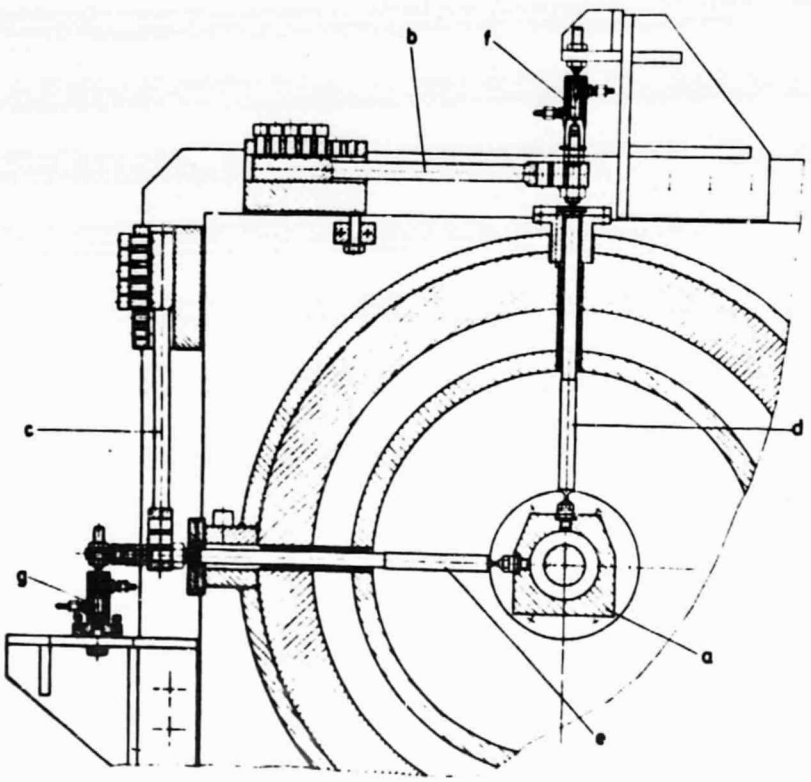

Figure 4.17 Bearing suspension for kinetic tests

bearing's external ring a at two mutually perpendicular spring-bars b and c. The rigidity can be modified by displacing the load application point. The bearing suspension's coupling rigidity can be reduced by indenting the lead-in rods d and e; in addition, the taperings offer a good possibility for non-contact sealing with small leak-losses. The dampers f /101 and g are filled with a viscous liquid (a mixture of Oppanol B

10 and Oppanol B 3), in which the rod dips. The arrangement of the dampers shown has been the best for the tests performed to date, since it precludes the liquid from running out. The damper liquid's temperature is maintaned constant by means of water circuit regulated by a thermostat. The damping coefficient can be adjusted by varying the liquid's temperature, the rod's depth of immersion, or the rod diameter. The same bearing suspension is used for both front and back bearings, so that with a runner centrally located on the shaft we can assume that the rotor is symmetrical. The test-turbine construction just described makes it possible to vary the following vibration system parameters:

a) the bearing rigidity, in either $\underline{x}$ or $\underline{y}$ direction, and hence the system's eigen-frequency or positioning anisotropy, respectively;

b) bearing damping, in the $\underline{x}$ or $\underline{y}$ direction, respectively;

c) the excitation acting on the system, by changing the turbine output.

By means of two cables, whose ends are attached to the front or back lead-in rods, respectively, the rotor may be deflected in either the horizontal or vertical direction, as needed. By scraping the tense cable against an edge, a shock-like excitation can be imparted to the runner, to translational vibration. The resulting shaft movement is sensed by two non-contact displacement pick-ups displaced by 90 with respect to each other at the front and rear bearings; after amplification, the signals are stored on magnetic tape.

Normally, the course of a measurement series is as follows:

As was the case with the force measurements, first the housing is adjusted centrally to the rotor. Then the bearing suspension's force constant is determined. To this end the

runner is deflected in horizontal direction with the tensioning device for the pressure gauge (see Figure 3.2, page 23), by applying weights at the front and back bearings; the ensueing /102 displacement is recorded by means of the pick-ups. For the vertical direction, weights are placed on a bridge connecting the two vertically placed damper containers.

Next, the damping constant for each direction is determined, by striking in the x or y direction, respectively, and evaluating the resulting damping curves. It is desirable to obtain damping values as similar as possible for both directions, which is accomplished by varying the immersion depth of the damping rods (isotropic damping). The different immersion depth for the same temperature of the liquid is a result of the rod motion, which is different in the two directions. With the method indicated, anisotropic damping can be measured precisely only with vanishing coupling of the two directions. The small coupling rigidity present during the tests will occasion only small measurement errors, for small anisotropy of the damping values, which will not be significant in comparison to the remaining measurement uncertainties.

The determination of the force and damping constants of the bearing suspension is repeated at very low output, once the turbine has been started and has attained operating regime. Next, the output is increased stepwise, at constant rotation rate, by increasing the inlet pressure. The runner is deflected and released three times in each direction, for each operating point. As was the case for the force measurements, besides recording the displacement paths, all pressures and temperatures as well as the position of the inner rings and the tangential force, are measured.

4.3. Evaluation of damping tests

The calculation of all turbine or stage data, respectively, for each measurement point, is performed as described in section 3.3 (page 30). Excluded are the pressure gauge calibration and the evaluation of the transverse forces.

/103

To determine the excitation acting at the individual measurement points, it is necessary first to determine the damping factors for the individual vibration curves. The envelope of the amplitude maxima after the sudden release of the shaft corresponds - at linear force, damping and excitation constants - to the equation

$$A = c_0 e^{-ut}, \qquad (4.23)$$

where the damping factor u is a measure of damping. The evaluation of the damping factors is shown in Figure 4.18, below. After shaping in the corresponding amplifiers, the signals from the four vibration receivers are stored on magnetic tape. A two-beam, X-Y oscillograph is provided for visual control of the runner movements during the tests. The reproduction and recording of the vibrations by means of a liquid-jet oscillograph is performed separately for the front and back measurement points. Since the analog components used (band-pass filter, amplitude computer, logarithmator) yield more precise results at operating tensions of approximately 5 volt, the sensor signals are amplified by a factor of 20. The purpose of the band passes is to filter out vibration signals due to unbalance and stochastic disturbances not essential to the problem. An analog component forms the vibration amplitude from both directions. With a subsequent analog calculator, a logarithmic recording of the vibrational motion can be obtained. The initial tension U_a of the logarithmator is given by the equation

$$U_a = -2\lg(10U_e) \qquad (4.24)$$

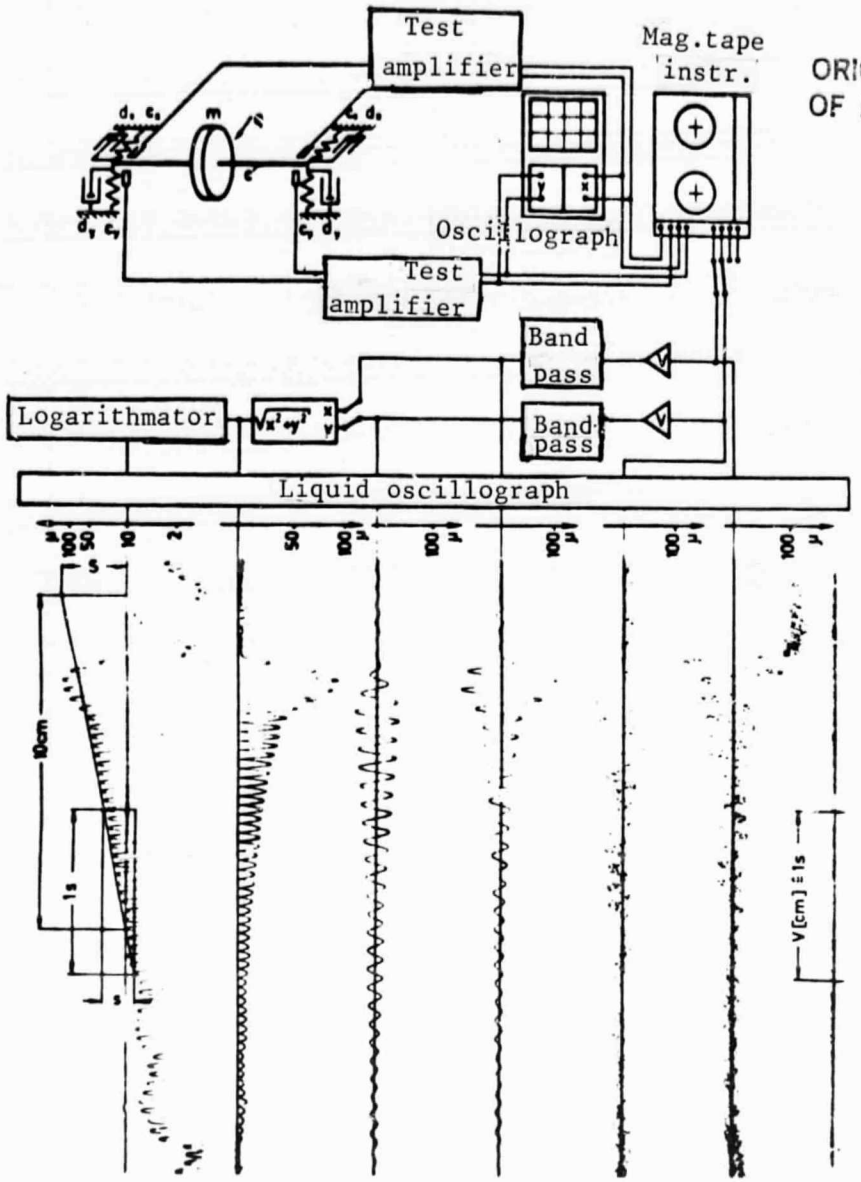

Figure 4.18 Recording and evaluation of damping curves

where U_e is the input tension. For the displacement pick-up used, that voltage is a linear function of the runner's amplitude. We thus obtain, with (4.23)

$$U_a = -2\lg(10C_1 e^{-ut}) = C_2 - \frac{2}{\ln 10}\cdot(-ut) , \qquad (4.25)$$

i.e., the course of the logarithmated amplitude maxima is a linear function of time. The damping factor u of the vibration

is thus given by the slope s of the straight-line envelope of the amplitudes

/105

$$u = -\frac{\ln 10}{2} \cdot s = -1,1513 \cdot s \,, \qquad (4.26)$$

where s is defined as a positive quantity for a damping vibration, as seen in Figure 4.18. During the evaluation, the slope S of the straight line was measured in mm per 10 cm paper advance and therefore equation (4.26) takes the form

$$u = -0,011513 \cdot S \cdot V \qquad (4.27)$$

where V is the paper advance in cm/s. The initially very steep decrease in amplitude must be considered a building-up process and hence not taken into consideration for the determination of the damping factor. In this manner, 12 slope values are obtained per measurement point, to be formed from the six damping curves each at the front and back bearing, for triplicate stimulation each in horizontal and vertical direction. Table A27 shows the determination of the damping constant for a measurement series. The measurement points 7200 and 7214 were taken for the standing rotor, point 7201 under rotation but at very low output. The first line contains - besides the paper advance V selected - the slopes of the damping curve determined for the front bearing, in columns SX1 to SY3. From the average for a given direction we obtain, using equation (4.27), a damping factor UX or UY, respectively. Correspondingly the same applies also to the values for the rear bearing, in the second line. Omitted slope values characterize damping curves that because of interfering external influences did not provide unequivocal values. For an uncoupled linear vibration system we obtain, from the damping factor u, the damping constant

$$d = -2mu \,, \qquad (4.28)$$

where m is the vibrator's mass. For an arrangement with one

damper each at both bearings we obtain, for the individual damping constants,

$$d_{xV} = -mu_{xV}\,, \quad d_{xH} = -mu_{xH}\,, \quad d_x = \frac{d_{xV} + d_{xH}}{2}\,, \qquad (4.29)$$
$$d_{yV} = -mu_{yV}\,, \quad d_{yH} = -mu_{yH}\,, \quad d_y = \frac{d_{yV} + d_{yH}}{2}\,.$$

/106

The three measurments are used to form an average for each direction, expressed with the 95% confidence range resulting from the various slopes.

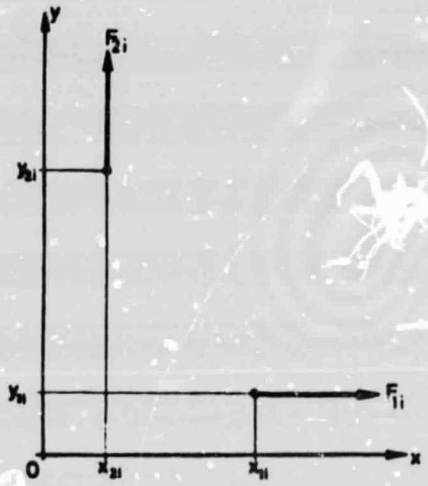

Figure 4.19 Measurement of the force constant

The determination of the force constants for the four bearings is accomplished by the stepwise application of weights. During the first measurement series with n different forces F_{1i} in the x direction, we do not only get deflections x_{1i} in the x direction, but because of the coupling members, also displacements y_{1i} in the y direction (see Figure 4.19, above). From the equilibrium of forces between the applied forces F_{1i} and the restoring forces of the bearing suspension we obtain, keeping in mind definition (2.6) of the bearing rigidity,

$$\left.\begin{aligned} F_{1i} &= -(c_{xx}x_{1i} + c_{xy}y_{1i}) \,, \\ 0 &= -(c_{yx}x_{1i} + c_{yy}y_{1i}) \,. \end{aligned}\right\} \qquad (4.30)$$

Correspondingly, in a second measurement series also with n forces F_{2i} in the $\underline{y}$ direction, we obtain the deflections x_{2i} and y_{2i} shown in Figure 4.19 and from them, because of the equilibrium of forces,

$$\left.\begin{aligned} 0 &= -(c_{xx}x_{2i} + c_{xy}y_{2i}) \,, \\ F_{2i} &= -(c_{yx}x_{2i} + c_{yy}y_{2i}) \,. \end{aligned}\right\} \qquad (4.31)$$

For the same number $\underline{n}$ of measurement points in both measurement series we obtain, from the forces applied and the displacement measured, the relationships

/107

$$\left.\begin{aligned} F_{1i} &= -c_{xx}x_{1i}\cdot(1 - k_i) \,, \quad F_{1i} = c_{xy}y_{1i}\cdot(1 + \tfrac{1}{k_i}) \,, \\ F_{2i} &= -c_{yy}y_{2i}\cdot(1 - k_i) \,, \quad F_{2i} = c_{yx}x_{2i}\cdot(1 + \tfrac{1}{k_i}) \,, \\ k_i &= \frac{x_{2i}y_{1i}}{x_{1i}y_{2i}} \,, \quad i = 1, 2, \ldots, n \,. \end{aligned}\right\} \qquad (4.32)$$

By fitting a straight line to the $\underline{n}$ measurement points by the least squares method, the four force constants of the bearing suspension can be determined, from these equations. In conjunction with the masses of all vibrating parts determined by weighing, prior to assembly, following section 4.1 we can now calculate the course of the damping factor as a function of the excitation. From this relation of dependence we obtain an excitation constant $\underline{q}$ with the damping factor $\underline{u}$ determined for each measurement point, which contains all flow-conditioned excitation and damping magnitudes. The determination can be performed graphically - as shown in Figure 4.20, below - or by iterative calculation from the vibration differential equations

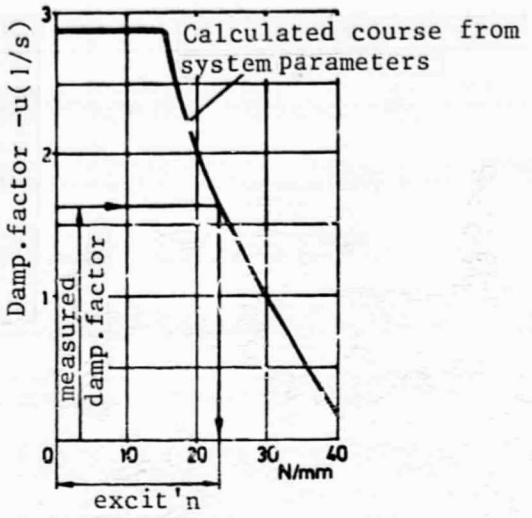

Figure 4.20 Determination of the excitation from the measured damping factor

(see section 4.1) - as performed during the evaluation of the measurements. To this end, the excitation must be varied until the damping factor obtained from the solution of the characteristic equation agrees with the measured value. Table A28 compiles the results of the evaluation for one measurement series. At the top are listed the parameters of the test series, to be considered constant during the measurement. The designations corresponded to the definitions in section 4.1.2. /108 The slopes (SX1 to SY3) determined from the damping curves are indicated, for each measurement point. From the average of the slopes and the corresponding paper advance V we obtain the damping factor U from equation (4.27), as well as a 95% confidence range FU, as measurement uncertainty. From the damping factor and the remaining system parameters we calculate the excitation coefficient or constant q, with the aid of which we form a K-value, for comparison with the results from the force measurements:

$$K = \frac{q}{U_s} \cdot l'' , \qquad (4.33)$$

Here, l" is the rotor blade length and U_s the isentropoic tangential force, calculated from the data recorded at each measurement point, as during the force measurements. For each measurement point, system damping (DS) and system excitation (S) are indicated, besides the pressure coefficient (PSI).

4.4. Results

Damping measurements yield gap excitation coefficients K that must be thought of as containing the effects of all the coefficients of the defelection matrix $\mathfrak{R}_s$ and of the velocity matrix $\mathfrak{C}_s$ (see equation (2.5)). As we have shown in section 4.1., the effect of the remaining coefficients is relatively small, when compared to that of the gap excitation coefficient K_2. Numerical values are already available for most of the coefficients proportional to the deflection, from the force measurements (cf. Table 3.4, as well as [21]). With the exception of K_2, for the design parameters of the stages investigated, their numerical values are essentially smaller than 2, so that we can disregard their effect on the damping behavior, during the tests performed here.

Since again with the exception of A_1 tne effect of the coefficients proportional to the velocity can be regarded as vanishingly small, by comparison to the force measurements, the kinetic tests can provide some insight into the magnitude of A_1. /109

Table 4.2, below, provides an overview of the system parameters for the kinetic test series performed in the context of this

TABLE 4.2 Parameters for kinetic tests series
(Designations as in section 4.1.2.)

KINETIC TESTS SHAFT RIGIDITY C = 71000 N/M

NR	TYPE	MASS KG	CXX N/MM	CYY N/MM	CXY N/MM	CYX N/MM	DX NS/MM	DY NS/MM	F	DMK 1/S	A	K	C	D	B
1	A	67.4	196.1	196.1	-2.0	-2.0	0.076	0.075	179	78.3	1.00	-0.01	1.00	0.0295	1.00
24	C	111.0	196.8	194.0	-7.7	-9.8	0.401	0.382	178	89.6	0.99	-0.04	1.27	0.1215	0.95
20	C	111.0	196.8	194.0	-7.7	-9.8	0.395	0.386	178	89.6	0.99	-0.04	1.27	0.1194	0.98
23	C	111.0	196.8	194.0	-7.7	-9.8	0.340	0.342	178	89.6	0.99	-0.04	1.27	0.0969	1.01
22	C	111.0	196.8	194.0	-7.7	-9.8	0.298	0.319	178	89.6	0.99	-0.04	1.27	0.0902	1.07
21	C	111.0	196.8	194.0	-7.7	-9.8	0.293	0.244	178	89.6	0.99	-0.04	1.27	0.0737	1.00
25	C	111.0	196.8	194.0	-7.7	-9.8	0.206	0.216	178	89.6	0.99	-0.04	1.27	0.0623	1.05
26	C	111.0	163.9	194.0	-7.7	-12.0	0.426	0.389	214	94.3	1.18	-0.05	1.54	0.1414	0.91
27	C	111.0	163.9	194.0	-7.7	-12.0	0.331	0.301	214	94.3	1.18	-0.05	1.54	0.1098	0.91
28	C	111.0	163.9	154.5	-8.0	-12.0	0.380	0.387	214	94.3	0.94	-0.05	1.49	0.1280	1.00
30	35T	185.0	197.1	208.9	-10.8	-10.8	0.307	0.460	178	96.2	1.06	-0.05	1.00	0.0719	1.50
31	35T	185.0	205.9	210.4	-11.8	-11.8	0.259	0.411	170	97.2	1.02	-0.06	1.00	0.0594	1.59

A N=3000 1/MIN SAX=2,25 MM

35T N=4000 1/MIN SAX=3,10 MM

C N=3000 1/MIN SAX=3,00 MM DK/DM=0,70 UEA=,9 MM

study. At this point a more detailed investigation of the stage parameters - as was done for the force measurements - seems unnecessary, since damping measurements provide only the overall destabilizing effect of all flow-conditioned forces. In addition, due to the relatively large measurement uncertainties for these measurements, the mostly small effects of parameter variations are hard to identify.

Figure 4.21, below, shows the results of the measurements with stage A. The individual measurement points of the damping curve are significantly scattered, in parts; however, viewed overall, the K-values determined kinetically correspond - within measurement uncertainties - to those from the force measurements, shown for comparison (solid curve or solid triangular points, respectively).

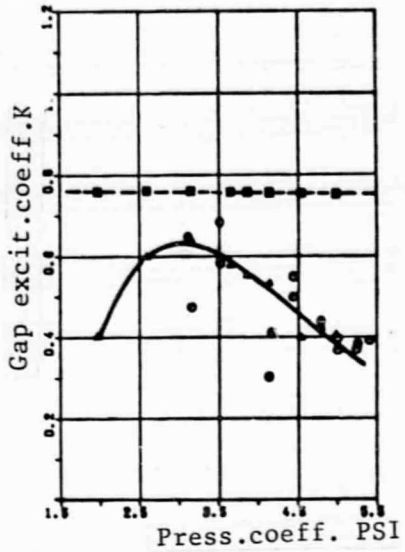

Figure 4.21 Stage C SAX = 3 mm

The broken line represents the values obtained from the gap loss.

The increase in bearing damping made possible by the greater excitation forces in the three-stage group and stage C, allowed a considerable improvement in measurement precision, since the portion of uncontrollable structure damping became correspondingly smaller.

In the damping tests with stage C, besides changes in bearing damping (MR 20-25), there were also variations in bearing /111
rigidity and the anisotropy of bearing rigidity (MR 26-28). Figures 4.22 and 4.23, below, show the K-values determined, as a function of the pressure coefficient ψ. In comparison to the corresponding values from the force measurements (solid line, corresponding to Figure 3.38 (page 70)), the resulting values of the excitation coefficients are 10 to 20% lower, for this stage. It must be taken into consideration, here, that the

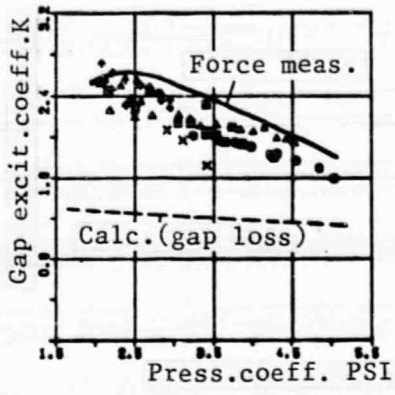

- Meas. series 24
- Meas.series 20
- Meas.series 23
- Meas.series 22

Figure 4.22 Stage C kinetic measurements

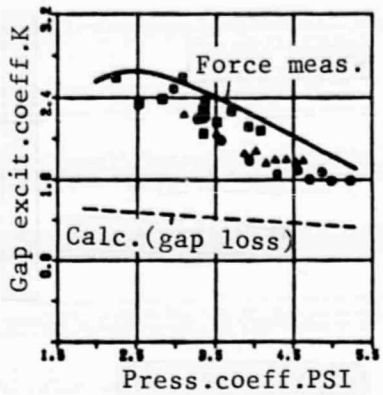

- Meas.series 21
- Meas.series 25

- Meas.series 26
- Meas.series 27
- Meas.series 28

Figure 4.23 Stage C kinetic measurements

determination of the bearing suspension's spring rigidity was performed only in measurement series 20 and 28. The measurement uncertainties for this measurement have the same effect for all intermediate measurement series; for this reason, for an unequivocal statement about the trend of the kinetic test results, only the values of measurement series 20 and 28 should be considered. The values of the other measurement series can show only the satisfactory reproducibility of the results, as well as the effect of variable bearing damping.

The results of the kinetic tests with the three-stage group are shown in Figures 4.24 and 4.25, below. In analogy to the force measurements (cf. Figure 3.21, page 58), with decreasing pressure coefficients and starting at $\psi = 2.3$, increasing gap excitation coefficients are obtained, that for $\psi = 1.5$ have a value that is nearly 1.5-fold that calculated from the gap loss (Figure 4.24). For variable rotation rates and approximately constant tangential velocity, the kinetic tests /112

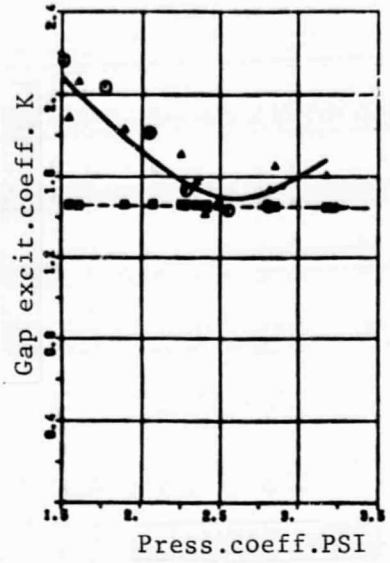

Figure 4.24 3-stage group
SAX = 3 mm

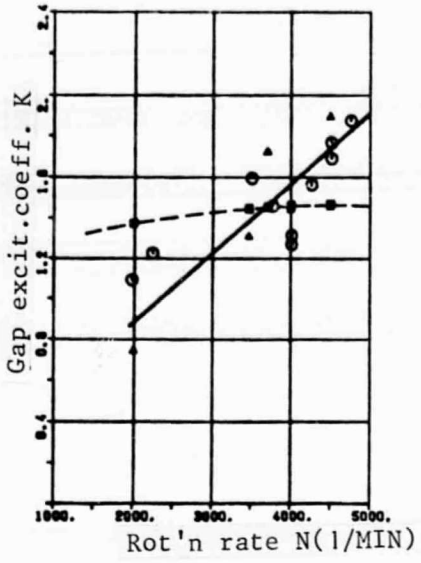

Figure 4.25 3-stage group
SAX = 3 mm

show (Figure 4.25) - in agreement with the force measurements (cf. Table A10) - a slight increase in the gap excitation coefficient for increasing rotation rates, as well as a decrease at lower rotation rates, each case compared to the values calculated from the gap loss.

Taking into consideration the measurement uncertainties - especially in the determination of the force constants - for the kinetic tests performed we can start from the premise that the effect of fluid forces proportional to the velocity, on the stability behavior of thermal turborotors is very small, when compared to that of the forces proportional to the deflection.

4.5. Considerations on error in damping tests /113

It is the purpose of these considerations to estimate the magnitude of the system parameter errors, as well as their effect on the excitation constant determined. The latter is expressed as a function of all system parameters:

$$q = q(m, c, c_{xx}, c_{yy}, c_{xy}, c_{yx}, d_x, d_y, u) \quad . \qquad (4.34)$$

According to the law of error propagation, the total error f_q will be

$$f_q = \sqrt{\left(\frac{\partial q}{\partial m} f_m\right)^2 + \left(\frac{\partial q}{\partial c} f_c\right)^2 + \left(\frac{\partial q}{\partial c_{xx}} f_{c_{xx}}\right)^2 + \ldots + \left(\frac{\partial q}{\partial u} f_u\right)^2} \quad , \qquad (4.35)$$

where f_m, f_c, $f_{c,xx}$ ... f_u are the measurement uncertainties for the individual system magnitudes, and the expressions

$$\frac{\partial q}{\partial m}, \frac{\partial q}{\partial c}, \frac{\partial q}{\partial c_{xx}}, \ldots, \frac{\partial q}{\partial u} \qquad (4.36)$$

describe the effect of the individual measurement uncertainties on the measured variable q. These weighting factors can be determined by sequentially varying the individual system parameters by the estimated measurement uncertainty, and then calculating the variation caused in q using the evaluation program. From the individual weighting factors and measurement uncertainties, and using equation (4.35) we then obtain the total error expected.

The measurement uncertainties to be expected from the measurements performed are:

- the weighing error for all vibrating parts is certainly less than 1%;

- the shaft rigidity is calculated from the shaft diameter and the distance between bearings. The maximum deviation from the actual value will be less than 1%;

- in the determination of spring rigidities in the bearing suspension by fitting a straight line to the measurement points, 95% confidence bands are obtained for the calculated slope, which correspond to the rigidity measurement uncertainty. For the rigidities c_{xx} or c_{yy}, respectively, /114
those uncertainties are of the order of 2%, while for the coupling magnitudes c_{xy} and c_{yx} - due to the very small displacement to be measured - relatively large measurement errors, of the order of 20%, can occur;

- the damping values as well as the damping factor are formed as averages of several measurements. The 95% confidence range of the average corresponds to the measurement uncertainty, here. The measurement uncertainty obtained for the damping constant, in the evaluation, was of approximately 5% (see Table A27), while for the damping factors the 95% confidence ranges lie between 3% and 25% (cf. column FU in Table A28). However, if the measurement uncertainties are expressed as percentages, it must be taken into consideration that for deviations of the same magnitude, the numbers for small values of the measured variable will appear relatively large.

To estimate the effect of the measurement uncertainties, an error calculation was performed for each measurement series, whose results are partially shown in Table A29. As an example, we selected in each case the average of the measured damping factors, and as measurement uncertainty, the average of the 95% confidence ranges. As a control, we investigated both upward and downward deviations of the measurement parameters, in all calculations; approximately equal changes were obtained for the excitation constant.

The error calculation shows that the measurement uncertainties of mass and shaft rigidity have a very small effect, while deviations in bearing rigidity - which substantially affect the course of the damping factor as a function of the excitation - cause relatively large errors in the determination of the excitation. The measurement uncertainties in bearing damping and the damping factors, in contrast, have a less significant effect.

In spite of the relatively large measurement uncertainties (10 - 20%) in the determination of the bearing rigidities and damping factors, the overall error for the kinetic tests is no larger than approximately 10%, on the average.

5 EFFECT OF GAP FLOW-CONDITIONED FORCES ON THE STABILITY BEHAVIOR OF FRICTION-BEARING SUSPENDED ROTORS

/115

Building on Thomas' fundamental work [1], several publications formulate theortical considerations on the effect of external forces on the stability behavior of simple rotor models. While in analogy to Thomas, Gasch [2] investigates only the single effect of the excitation constants q_2 - derived from the gap excitation coefficient K_2 by means of equation (3.23), for rigid bearing suspension - Piltz [13] considers - also for rigid suspension - all the coefficients of the matrices R_s and R_s, whose magnitude was estimated by him from theory [6]. Kraemer [8], Pollmann [9] and Vogel [10] have calculated the limit of stability for a singly fitted Laval shaft with friction bearings, taking into consideration the gap excitation constant or coefficient q_2.

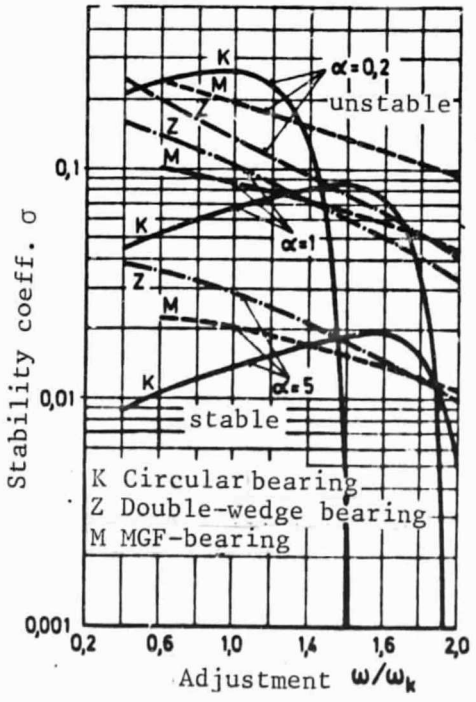

Figure 5.1
Stability chart for a symmetrical, single-mass vibrator with friction bearings (So_k=0.2, b/d=0.5)

As an example of such calculations, Figure 5.1, above, shows the Sommerfeld coefficient of the bearings related to the critical rotation rate

$$So_k = \frac{mg}{2bd} \cdot \frac{\psi^2}{\eta\omega_k} \quad (5.1)$$

and a width ratio b/d of the stability coefficient $\sigma = q_2/c$, /116 as a function of the adjustment ω/ω_k of the shaft, for various types of friction bearing, for various values of a magnitudes designated "relative shaft elasticity",

$$\alpha = \frac{mg}{c} \cdot \frac{1}{2\psi R} = \frac{g}{\omega_k^2} \cdot \frac{1}{2\psi R} . \quad (5.2)$$

It indicates the statistical bending of the shaft under its weight, in relation to the bearings' diameter clearance. It can be seen that the circular bearing often has lower stability coefficients than other kinds of bearings. The σ-values sharply decrease with increasing shaft elasticity α. The abrupt drop of for increasing ω/ω_k characterizes the instability due to the so-called "oil whip".

In all previous publications, to date, regarding the stability behavior of friction bearing-supported rotors, only the gap excitation constant or gap excitation coefficient K_2, respectively, were taken into consideration. Here, using some examples, we shall also illustrate the effect of other coefficients - measured within the context of this study - on the damping and stability behavior of friction bearing supported rotors. The calculations were performed using the method indicated by Landzberg [7] as expanded by Vogel [10], without considering here internal damping and the gyrostatic effect.

The rotor model investigated, in similarity to the high-pressure part of a 300 MW turbine set, had the following data:

bearing distance	l = 5000 mm	} (5.3)
Mass (centered between bearings)	m = 5000 kg	
Shaft rigidity	c = 300,000 N/mm	
Operating rotation rate	n = 3000/min	

The turborotor's individual stages shall be summarized into a representative stage located midway between the bearings, with the following data:

isentropic nominal output	p_s = 100 MW	} (5.4)
average rotor diameter	d_m = 800 mm	
rotor blade length	l" = 50 mm	

/117

A characterization of the bearing's characteristic magnitudes as in (4.13) seems inappropriate for the typical friction bearings, since the individual dimensionless quantities - such as the anisotropies of the rigidity, damping and coupling - can not be varied independently of each other. In addition, the values of the dimensionless quantities for the various types of friction bearings are usually well beyond numerical values applicable to the test installation, as described in section 4.1.2. Since the friction bearings' force and damping constants depend essentially only on the bearing shape and the Sommerfeld coefficient

$$So = \frac{mg}{2bd} \cdot \frac{\psi^2}{\eta\omega} \qquad (5.5)$$

it should suffice here to investigate the effect of the bearings' characteristic quantities on the basis of three types of bearings (circular, double-wedge and MGF-triple-wedge bearings), with a width ratio b/d = 0.8 and two Sommerfeld coefficients each (So = 0.2 and 0.5). The required bearing constants are taken from the tables given by Glienicke in [16].

The following values shall be considered representative, in correspondence with the measurement results (cf. Table 3.4, as well as [20]), of the coefficients of flow-conditioned forces and momenta:

$$\left.\begin{array}{ll} \text{deflection coefficient} & K_1 = 2 \\ \text{gap excitation coefficient} & K_2 = 2.5 \\ \text{inclination coefficient} & K_3 = 0.5 \\ \text{inclination coefficient} & K_4 = -0.5 \\ \text{moment coefficient} & L_1 = 2 \\ \text{moment coefficient} & L_2 = 2 \end{array}\right\} \qquad (5.6)$$

The moment coefficients L_3 and L_4 are also disregarded, as were coefficients proportional to the velocity, A_i and B_i, since reliable indications are lacking as to the magnitude of these coefficients.

In order to describe the calculation results, we shall plot, for each case, the system damping

$$D_s = -\frac{u}{\omega_k} \qquad (5.7)$$

/118

as a function of the output ratio

$$\chi = \frac{P}{P_s} \qquad (5.8)$$

The rigid angular eigen-frequency of the rotor,

$$\omega_k = \sqrt{\frac{c}{m}} \qquad (5.9)$$

shall be used here as a reference angular frequency.

In general, the solutions to the frequency equation consist of two conjugated, complex eigen-values, which change with increasing χ while the remaining eigen-values remain nearly constant. If we consider the real portion of the two conjugated

complex eigen-values, dependent on χ and determining for system damping, then we will observe that as χ increases, one of them decreases, while the other increases. It may occur that the increasing solution shows a smaller real part, for $\chi = 0$, that the solution decreasing with χ.

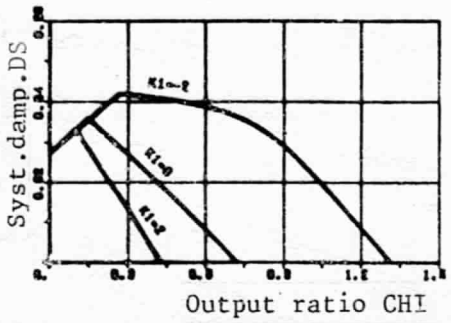

Figure 5.2 Circular bearing So=0.2 Effect of deflection coefficient K for a gap excitation coefficient k =2.5

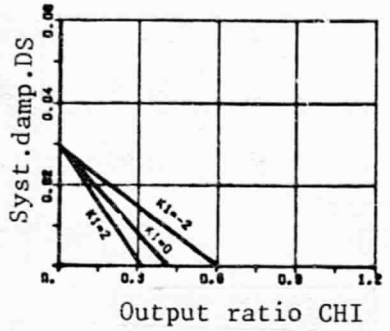

Figure 5.3 Circular bearing, So=0.5 Effect of deflection coefficient K for a gap excitation coefficient K =2.5

Figure 5.2, above, shows the course of system damping D_s as a function of the output ratio χ, for a rotor suspension in circular bearings with an So coefficient of 0.2. According to the definition, system damping shall be the relative real portion of the most weakly damped eigen-vibration; for this reason, curves with a bend occur since for small outputs the solution increasing with χ is determining. The great influence of the deflection coefficient K_1 continues to be remarkable. Taking this coefficient into consideration, in addition to the gap excitation coefficient, in this case, for a negative K_1 = -2, causes a substantial increase in the limit of stability by a good 80%, in comparison to the effect of K_2 = 2.5 alone; in contrast, a positive K_1 = 2 lowers the limit of stability by 40%. /119

Changes in system damping due to the remaining coefficients - K_3 = 0.5, K_4 = -0.5, L_1 = L_2 = 2 - in comparison to the effect of K_2 and K_1 lies always below 0.1%, here and for all other bearing

variations investigated.

In a circular bearing, an increase in the Sommerfeld coefficient to 0.5 causes a considerable decrease in the system damping value and in the limit of stability. Figure 5.3, above, shows the resulting curves for the effect of K_2 = 2.5 alone, as well as also considering K_1. The increase in the limit of stability due to a negative deflection coefficient K_1 = -2 is almost 50% here, while for a positive K_1 = 2 the limit of stability is lowered by 25%.

In the suspension of the rotor in double-wedge bearings with an So = 0.2, for no gap excitation (χ = 0) we obtain relatively high system damping values (see Figure 5.4, below), which decrease with increasing output, however. The effect of the deflection coefficient K_1 is not as strong, in this case, as it was in a suspension in circular bearings. The increase in the /120 limit of stability, compared to the efect of K_2 = 2.5 alone, was almost 30% for a negative K_1 = -2, while for a positive K_1 = 2 a 20% decrease occurred.

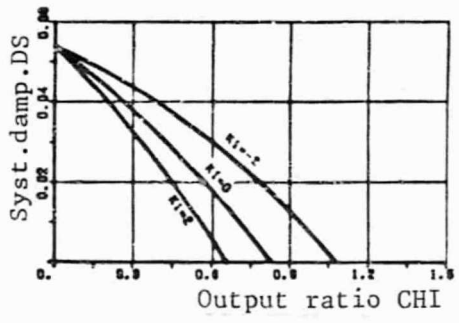

Figure 5.4 Double-wedge bearing, So=0.2 Effect of deflection coefficient K for a gap excitation coefficient K =2.5

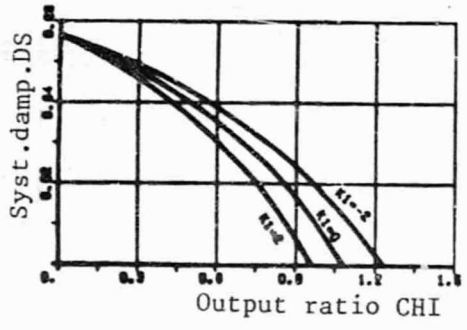

Figure 5.5 Double-wedge bearing, So=0.5 Effect of deflection coefficient K for a gap excitation coefficient K =2.5

An increase in the So coefficient to 0.5 also results in greater system damping in the double-wedge bearing, as well as increased limit of stability (Figure 5.5, above). Here, the influence on the limit of stability by the deflection coefficient K_1 = -2 or

k_1 = 2, respectively, is reduced to approximately ±10%.

Finally, Figure 5.6 below, shows the course of system damping as a function of the output ratio for a suspension of the rotor in MGF-bearings. Relatively small system damping values are obtained, here, which increase slightly with increasing output, however and then drop rapidly, once a certain output has been reached. Although system damping decreases slightly as the So coefficient increases, the limit of stability increases considerably. In this type of bearing the effect of the deflection coefficient K_1 is very small, affecting the limit of stability by a maximum of ±2.5%

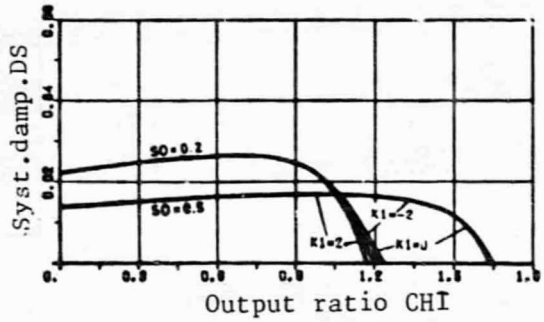

Figure 5.6 MGF-three-wedge bearing Effect of the deflection coefficient K_1 and the So coefficient for a gap excitation coefficient K_2=2.5

/12*

The calculations performed show that in practical stability considerations the significance of the deflection coefficient K_1 - in addition to that of the gap excitation coefficient K_2 - must not be underestimated. Measurements at the three turbine stages in part yielded positive K_1-values, which have a destabilizing effect. In turbomachines, for eccentric rotor positions, considerable transverse forces - generated in non-uniform pressure distributions at shaft seals - can occur [18, 24], which in general act against the direction of deflection and hence have a stabilizing effect.

The effect of the remaining coefficients of flow-conditioned forces and momenta on the stability behavior of thermal turborotors can be considered small, in comparison, judging from the information here presented regarding their magnitude.

6 SUMMARY

Flow-conditioned forces can stimulate thermal turbo-machines to self-excited vibrations. Since these forces increase in proportion to the turbine's output, their consequence can be severe operational limitations to the affected power plant. Thus, in order to predetermine the vibration and stability behavior of turborotors to be constructed, besides the characteristic quantities of the bearings we need reliable information on the magnitude and effect of flow-conditioned forces. Dimensionless coefficients are introduced to describe the forces caused by the fluid flow, as a function of the displacement. The so-called gap excitation coefficient K_2 is of decisive significance to the stability behavior; it describes a vibration-causing transverse force acting perpendicularly to the deflection. In part, this excitation force can be explained as the resultant of the variable tangential force of a turbine stage, caused by non-uniform gap losses at eccentrically positioned rotors; also in part, as resulting from a non-uniform pressure distribution along the perimeter, in the seal gap, caused by a torsional effect on the flow.

/122

A test installation was built for the experimental determination of the flow-conditioned forces, which made it possible to measure the forces and momenta acting on a turborotor, as a function of its eccentric positioning with respect to the housing. Force measurements were performed on two 50% reaction stages in drum design, with recessed shroud bands over stator and rotor blading, as well as on a three-stage group of this design. These measurements resulted in gap excitation coefficients of a magnitude that is the same as that derived theoretically from gap losses at the stator and the rotor blading. In contrast, significantly higher excitation forces occurred during force measurements on a weak reaction stage in chamber construction.

The separate determination of the stator and rotor portions in stage excitation made possible by the test installation's design, yielded relatively small excitation forces in all stages for an eccentric stator seal, whose values were below those calculated from stator gap loss. In contrast, significantly higher excitation forces were generated by an eccentricity of only the rotor seal, than those calculated to date from gap losses. As we have shown, this may be attributed to the additional effect of compressive forces produced during torsional flow through the rotor gap.

To a smaller extent, experimentally determined deflection and moment coefficients are reported for the stages investigated, besides the gap excitation coefficient.

The coefficients measured always represent an average of many individual measurements. Possible measurement uncertainties are analyzed and estimated.

By modifying the rotor's bearing suspension in the test installation, it became possible to measure the overall effect of all flow-conditioned forces on the vibrating rotor, during kinetic tests. To perform and evaluate such tests, we carried out calculations of the effect of the bearing's characteristic magnitudes, as well as that of the flow-conditioned forces, on the damping and stability behavior of the test rotor. It was discovered that the anisotropy of the bearing rigidity exerted /123 a particularly stabilizing effect. In addition, the test rotor's stability behavior is determined essentially by the gap excitation coefficient K_2, for fixed bearing characateristics, with the effect of the remaining coefficients - to the extent that they are of the order of magnitude of K_2 - being small, in comparison.

The kinetic measurements were performed for one of the two 50%

reaction stages, the three-stage group and the weak reaction stage; there was good agreement with the force measurements. Thus - at least for the relatively low vibration frequencies investigated - the effect of coefficients proportional to the velocity on the stability behavior may be considered negligibly small.

To conclude, the stability behavior of turborotors suspended in friction bearings is investigated, taking into consideration the measured coefficients for flow-conditioned forces. It was discovered that for certain types of friction bearing the effect of the deflection coefficient, compared to that of the gap excitation coefficient, is not always negligible, while the remaining coefficients practically have no stabilizing or destabilizing effect.

7 REFERENCES /124

1 Thomas, H. J., Instabile Eigenschwingungen von Turbinenlaeufern, angefacht durch die Spaltstroemung in Stopfbuechsen und Beschauflungen [Unstable eigen-vibrations of turbine rotors, excited by the gap flow in glands and blading], Bull. de l'AIM, No. 11/12, 1039-1063 (1958).

2 Gasch, R., Stabiler Lauf von Turbinenrotoren [Stable running of turbine rotors], Konstruktion 17, No. 11, 447-452 (1965).

3 Alford, J. S., Protecting turbomachinery from self-excited rotor whirl, Transactions ASME, J. of Eng.f.Power 87, No. 10, 333-344 (1965)

4 Spurk, J. H. and Keiper, R., Selbsterregte Schwingungen bei Turbomaschinen infolge der Labyrinthstroemung [Self-excited vibrations in turbomachines due to labyrinth flow], Ingenieur-Archiv 43, No. 2/3, 127-135 (1974)

5 Kostyuk, A. G., A theoretical analysis of the aerodynamic forces in the labyrinth glands of turbomachines, Teploenergetika (Thermal Engineering) 19, No. 11, 29-33 (1972)

6 Piltz, E., Belastung von Dampfturbinenlaufraedern bei Auslenkungen der Welle [Stressing of steam turbine rotors due to shaft deflection], Konstruktion 24, No. 4, 141-148 (1972)

7 Landzberg, A. H., Stability of a turbine-generator rotor including the effects of certain types of steam and bearing excitations, Transactions ASME, J. Appl.Mech. 27, No. 3, 410-416 (1960)

8 Kraemer, E., Selbsterregte Schwingungen von Wellen infolge von Querkraeften [Self-excited vibrations in shafts due to transverse forces], BWK 20, No. 7, 307-213 (1968)

9 Pollmann, E., Stabilitaet einer in Gleitlagern rotierenden Welle mit Spalterregung [Stability of a shaft rotating in friction bearings, under gap excitation], Fortschrittsberichte VDI, Zeitschriftsreihe 1*, No. 15 (1969)

10 Vogel, D. H., Die Stabilitaet gleitgelagerter Rotoren von Turbomaschinen unter besonderer Beruecksichtigung einer Erregung durch Spaltstroeme [The stability of turbomachine rotors suspended in friction bearings, with special consideration of gap flow excitation], Dissertation, Munich Institute of Technology (1969)

11 Schirmer, G. F., Zur Stabilitaet der Schwingungen von Turbinenwellen [The stability of turbine shaft vibrations], Dissertation, Darmstadt Institute of Technology (1969)

12 Gasch, R., Unwucht-erzwungene Schwingungen und Stabilitaet von Turbinenlaeufern [Unbalance-forced vibrations and the stability of turbine runners], Konstruktion 25, No. 5, 161-168 (1973)

13 Piltz, E., Einfluss von Dampfbelastungen auf die Stabilitaetsgrenze einer einstuefigen Modellturbine [Effect of steam load on the limit of stability of a single-stage model turbine], Konstruktion 25, No. 5, 161-168 (1973)

14 Kostyuk, A. G., Shatokhin, V. F. and Ivanov, N. M., Calculation of the threshold capacity of large turbine

* Progress Reports of the VDI [Verein Deutscher Ingenieure = Association of German Engineers] Journal Series 1

generators, Teploenergetika (Thermal Engineering) 21, No. 3, 15-19 (1974)

15 Winter, C. J., Lastabhaengige instabile Bewegungen von Turbinenlaeufern [Load-dependent, unstable movements of turbine runners], Dissertation, Darmstadt Institute of Technology (1968)

16 Glienicke, J., Experimentelle Ermittlung der statischen und dynamischen Eigenschaften von Gleitlagern fuer schnellaufende Wellen. Einfluss der Schmierspaltgeometrie und der Lagerbreite [Experimental determination of the static and dynamic characteristics of friction bearings for high-speed shafts. Effect of the lubrication gap geometry and the bearing width], Fortschrittsberichte VDI- Zeitschriftreihe 1, No. 22 (1970)

17 Traupel, W., "Thermische Turbomaschinen" ["Thermal turbomachines"], Vol. 1, 1st. Edition, Springer, Berlin - Goettingen - Heidelberg 1958

18 Lomakin, A. A., Die Berechnung der kritischen Drehzahl und der Bedingung fuer Sicherung der dynamischen Stabilitaet des Laeufers von hydraulischen Hochdruck-Maschinen unter Beruecksichtigung der Kraefte, die in den Dichtungen entstehen [The calculation of the critical rotation rate and the condition for insuring the dynamic stability of the rotor of hydraulic high-pressure machines, taking into consideration the forces generated in the seals], Energomaschinostrojenie, No. 4, 1-5 (1958)

19 Rosenberg, S. Sch., Orlik, V. G. and Martschenko, Ju. A., Untersuchungen aerodynamischer Querkraefte bei einer Wellenexzentrizitaet [[nvestigation of the aerodynamic transverse forces in cases of shaft eccentricity], Energomaschinostrojenie, No. 8, 15-17 (1974)

20 Urlichs, K., Durch Spaltstroemung hervorgerufene Querkraefte and

den Laeufern thermischer Turbomaschinen [Clearance flow-generated transverse forces at the rotors of thermal turbomachines], Dissertation, Technical University Munich (1975)

21 Thomas, H.-J., Urlichs, K. and Wohlrab, R., Laeuferinstabilitaet infolge Spalterregung [Rotor instability due to gap excitation], Forschungsvereinigung Verbrennungskraftmaschinen [Research Association "Internal Combustion Engines"], Frankfurt, Forschungsbericht [Research Report] No. 167 (1974)

22 Sachs, L., "Statistische Auswertungsmethoden" ["Statistical Evaluation Methods"], Springer, Berlin - Goettingen - Heidelberg (1969)

23 La Roche, U., Untersuchung der Stroemung ueber einen Absatz im Zusammenhang mit den Injektionsverlusten bei Dampf- und Gasturbinen [Investigation of the flow over a step in connection with injection losses in steam and gas turbines], Communications from the Institute for Thermal Turbomachines, Swiss Institute of Technology at Zurich, No. 10 (1965)

24 Hochreuther, W., Kraefte bei axial durchstroemten Spalten [Forces in gaps with axial flow], Dissertation, Stuttgart University (1975)

25 Gasch, R. and Pfuetzner, H., "Rotordynamik" ["Rotor Dynamics"], Springer, Berlin - Heidelberg - New York 1975

8 DESIGNATIONS /126

A	Anisotropy in bearing rigidity
A_i	Force coefficients proportional to the velocity
B	Anisotropy in bearing damping
B_i	Moment coefficients proportional to the velocity
C	Anisotropy in bearing coupling
C_E^x	relative incident flow energy
D	relative bearing damping
D_s	system damping
F	Force; shaft/bearing rigidity ratio
J	Moment of inertia
K_1	Deflection coefficient
K_2	Gap excitation coefficient
K_3, K_4	Inclination coefficients
K'_{II}, K''_{II}	Gap loss coefficients
L_i	Moment coefficients
M	Moment
MR	Measurement series
P	Output
Q	Transverse force
Q_2	Gap excitation force
R	Gas constant
S	System excitation
T	Kelvin (absolute) temperature
U	Tangential force; tension
V	Paper advance
a	specific work
b	shroud band width
c	absolute flow velocity; shaft rigidity
c_{ik}	spring rigidity
d	diameter
d_{ik}	damping constants
e	eccentricity

f	measurement uncertainty
g	acceleration of gravity
Δh_s	isotropic gradient
l	blade length
m	mass
$\dot{m}$	throughput
n	rotation rate
p	pressure
g_2	gap excitation constant
r	percentage reaction
r_{ik}	coefficients of the load matrix, proportional to the velocity
s	standard deviation
s_{ax}	axial gap
t	time; temperature
u	damping factor; tangential velocity
w	relative flow velocity
x, y, z	spatial coordinates
z', z''	number of seal peaks
Δ	Difference
χ	output or tangential force ratio, resp.
α	flow angle at turbine blading; throughput coeff.
β	flow angle at turbine blading
ε	expansion coefficient
ζ_{sp}	gap loss
η	efficiency; dynamic viscosity
κ	isentropic exponent
λ	complex frequency
ρ	density
τ	tolerance or measurement uncertainty, resp.
ϕ	bending or tangential angle; throughput coeff.
ψ	pressure coefficient
ω	angular frequency
$\mathfrak{b}$	load vector

A	load matrix, proportional to the velocity
R	load matrix, proportional to the deflection
w	movement vector

/128

Subscripts and superscripts:

D	out of the pressure distribution
L	stemming from the bearing
S	stemming from flow medium; calculated from the gap loss
a	exit
e	entrance
i	inner; internal; variable counter
k	critical; variable counter
m	intermediate, average
s	isentropic
x, y	in x or y direction, respectively
0	before the stator
1	between stator and rotor; in the direction of deflection
2	after rotor; perpendicular to the direction of deflection
'	stator
"	rotor

/129

A P P E N D I X

/130

Clarification of designations used in the computer printouts, in alphabetical order:

AB	equalizing drill-hole in the rotor
AL2	flow angle $_2$ from (3.16)
BE1	flow angle $_1$ from (3.16)
COAX	flow velocity c_o from (3.11)
C1	flow velocity c_1 from (3.10 to 3.13)
C2	flow velocity c_2 from (3.16)
DHSST	isentropic gradient of the stage, from (3.8)
DN/DM	hub ratio
DPB1	Pressure differencials (Figure 3.4)
DPB12	" " "
DPB2	" " "
DPBT	" " "
DPT	" " "
ETAE	effective efficiency of the stage group, from (3.6)
ETAI	internal efficiency of the stage group, from (3.7)
ETAU	Tangential efficiency of the stage, from (3.17)
FDP	Measurement uncertainty for the measurement orifice pressure differential p_B
FK1, FK2, FL1, FL2	Measurement uncertainties of the measured coefficients K_1, K_2, L_1 and L_2, from (3.42)
FM	Measurement uncertainty for the throughput, from (3.32) and (3.33)
FP	Measurement uncertainty for the pressure before the

	measurement orifice, from (3.37)
FRHO	Measurement uncertainty for the density before the measurement orifice, from (3.38)
FT	Measurement uncertainty for the temperature before the measurement orifice
HSG	isentropic gradient for the stage group, from (3.3)
KH	force at the rear bearing
KV	force at the front bearing
K1	measured deflection coefficient K_1
K2	measured gap excitation coefficient K_2, from (3.23)
K2S	gap excitation coefficient K_{2S} calculated from the gap loss; from (2.18)
LS	rotor blade length l"
L1	measured moment coefficient L_1 from (3.24) /131
L2	measured moment coefficient L_2
M	throughput, from (3.1)
MNR	measurement point number
MP	indicates a measurement point
MR	measurement series number
MW	average value
M1	measurement moment M_1 from (3.27)
M1 - M2	deviation of the measured throughputs at measurement orifices 1 and 2
N	turbine rotation rate
P	turbine output, from (3.5)
PA	pressure at turbine exit
PE	pressure at turbine entrance
PE/PA	pressure ratio for stage group
PHI	throughput coefficient , from (3.19)
PSI	pressure coefficient , from (3.18)
PO	pressure before stage stator
P1	pressure after stage stator, from (3.10 to 3.13)
Q2	measured excitation force Q_2, from (3.27)
Q2S	stage excitation force calculated from the gap loss, from (3.26)
Q2SLA	rotor excitation force calculated from the gap loss,

	from (3.26)
Q2SLE	stator excitation force calculated from the gap loss, from (3.26)
REAK	percentage reaction $\underline{r}$ in the central section, from (3.14)
SAX	axial gap s_{ax}
STAB	standard deviation of the mean, from (3.25)
STREUUNG	standard deviation of the coefficients of the fitted straight line, from (3.29)
TA	temperature at turbine exit
TAUA	measurement uncertainty for throughput coefficient , from (3.34)
TAUE	measurement uncertainty for the expansion coefficient , from (3.35)
TE	temperature at turbine entrance
TO	temperature before the stator
U	measured stage group tangential velocity
US	isentropic tangential force U_s, from (3.4)
ÜEA	external covering or overlap /132
W1	flow velocity w_1, from (3.16)
W2	flow velocity w_2, from (3.16)
XLA, YLA	rotor displacement with regard to housing in the $\underline{x}$ or $\underline{y}$ direction, respectively
XLE, YLE	stator hub displacement with respect to the stator in the $\underline{x}$ or $\underline{y}$ direction, respectively

The designations used in Tables A27 to A29 have been explained in the corresponding chapters 4.3 (page 114) and 4.5 (page 126)

TABLE A1 Protocol for pressure sensor calibration

Illegible

CALIBRATION IN MILLIMETER

MM	H2 1 1	I2 1 2	I2 1 3	H2O 4	H2O 5	H2O 6	H2O 7	H2O 8	HG A	HG B	HG C
3713	1113.0	977.0	972.0	1034.0	1122.0	892.0	1008.0	1000.0	1175.0	912.0	911.0
3735	1131.0	990.0	986.0	1040.0	1147.0	868.0	1008.0	999.0	1222.0	889.0	888.0
3752	1162.0	1025.0	957.0	1040.0	1171.0	844.0	1009.0	998.0	1267.0	866.0	855.0
3769	1183.0	1033.0	955.0	1052.0	1193.0	824.0	1010.0	997.0	1309.0	844.0	843.5

MM DR	I P T BAR	I P T VOLT	P E BAR	P E VOLT	D P R T BAR	D P R T VOLT	D P R 2 BAR	D P R 2 VOLT
A 3718	-1.3505	-213771-6	0.3520	563761-6	-0.0008	-203841-5	-0.0226	364261-6
B 3735	-1.4441	-116101-5	0.4493	717411-6	-0.0009	-238741-5	-0.0274	468331-6
C 3752	-1.5146	-140591-5	0.5340	865461-6	-0.0011	-272381-5	-0.0321	571041-6
D 3769	-1.6193	-163981-5	0.6206	1008411-5	-0.0013	-272491-5	-0.0362	663921-6

					D P R 1 2 BAR	D P R 1 2 VOLT	C P R 1 BAR	C P R 1 VOLT
IPT =	-0.011	3452337	+3.7220276401	* VOLT				
STREUUNG	0.011	7791504	0.013605999	6				
PE =	0.011	2105586	+0.9503390001	* VOLT	0.0061	-390141-5	-0.0231	617221-5
STREUUNG	0.012	3410411	0.0290465092		0.0073	-449121-5	-0.0282	739871-5
					0.0084	-564271-5	-0.0330	866801-5
DPRT =	0.011	7476329	+0.0059775970	* VOLT	0.0095	-695851-5	-0.0373	966191-5
STREUUNG	0.010	5046589	0.0023317069					
DPR2 =	-0.015	8274365	-0.6585813875	* VOLT				
STREUUNG	0.010	2672415	0.0050521605					
DPR12 =	0.011	4721582	-0.0146246912	* VOLT				
STREUUNG	0.010	8867427	0.0017013351					
DPR1 =	0.010	9011145	-0.2401572828	* VOLT				
STREUUNG	0.011	4817769	0.0059960556					

TABLE A2 Protocol for stage group calculation and pressure gauge calibration for measurement series 293

			TE	TA	PE	PA	PE/PA	ISG	J	P	JS	ETAE	ETAI
			C	C	BAR	BAR	-	KJ/KG	N	K W	N	--	--
1291	2.1		33.6	21.1	1.1402	0.9612	1.1862	14.673	203.13	24.402	255.86	0.794	0.862
1292	2.1		33.6	21.1	1.1407	0.9617	1.1860	14.642	203.98	24.505	256.14	0.796	0.865
1293	2.1		33.6	21.1	1.1413	0.9620	1.1863	14.679	204.23	24.535	256.59	0.796	0.865
1294	2.1		33.6	21.1	1.1409	0.9617	1.1864	14.668	204.05	24.513	256.21	0.796	0.865
1295	2.1		33.6	21.1	1.1409	0.9615	1.1865	14.676	204.38	24.613	256.77	0.796	0.866
1296	2.1		33.6	21.1	1.1411	0.9617	1.1862	14.675	204.84	24.668	256.26	0.799	0.867
1297	2.1		33.6	21.1	1.1412	0.9610	1.1875	14.770	206.20	24.832	258.66	0.797	0.867
1298	2.1		33.7	21.1	1.1421	0.9618	1.1874	14.762	207.06	24.936	259.75	0.800	0.868
	2.1		33.6	21.1	1.1411	0.9617	1.1866	14.700	204.73	24.656	256.90	0.797	0.866
			0.01	0.01	0.00	0.00	0.00	0.01	0.05	0.05	0.04	0.00	0.00
			0.03	0.04	0.02	0.01	0.02	0.10	0.22	0.22	0.16	0.00	0.07

FORCE MEASUREMENT CALIBRATION

			KV	KVG	KH	KHI	KHG
			VOLT	N	N	VOLT	N
1291		-	0.0350	-1.0573	0.0000	0.0010	0.0288
1292		-	-0.3742	1.9192	1.9613	-0.3472	1.9308
1294		-	0.7806	3.8804	3.9227	-0.7079	3.9006
1296		-	0.3536	-2.0204	-1.9613	0.3561	-1.9103
1298		-	0.7156	-3.9417	-3.9227	0.7353	-3.9815
1291		-	0.0120	0.0145	0.0000	0.0166	-0.0562
1293		-	0.0276	0.0587	0.0000	-0.0046	0.0604
1297		-	0.0432	0.1427	0.0000	0.0213	0.0274

FORCE MEASUREMENT FORCE [N] = -0,0896369536 -5,3342167035 * VOLT +-0,075 N
SCATTER 0,0267077254 0,1655394473

FORCE MEASUREMENT FORCE [N] = 0,0343823095 -5,4616831308 * VOLT +-0,051 N
SCATTER 0,0181861543 0,0452938031

TABLE A3 Protocol for stage group and individual stage calculation for measurement series 490

STAGE GROUP MEASUREMENT SERIES 490 (EXCITATION FORCE)

(Illegible) ROTATION RATE 4000RPM

			TE C	TA C	PE BAR	PA BAR	PE/PA -	HSG KJ/KG	J N	P KW	HS N	ETAE --	ETA --
		+1.73	46.4	15.4	1.4042	0.9636	1.4573	32.750	756.37	73.076	881.98	0.859	0.939
		+2.01	46.9	15.2	1.4038	0.9624	1.4576	32.816	756.84	73.122	881.38	0.859	0.939
		+1.61	47.2	15.4	1.4052	0.9643	1.4573	32.829	758.37	73.270	882.52	0.859	0.941
		+1.63	47.4	15.4	1.4038	0.9655	1.4561	32.785	756.59	73.098	880.95	0.859	0.943
		+1.63	47.6	15.3	1.4048	0.9641	1.4570	32.857	757.72	73.207	882.13	0.859	0.942
		+1.63	47.8	15.3	1.4062	0.9656	1.4563	32.842	757.99	73.233	882.09	0.859	0.943
		+1.74	48.0	15.2	1.4035	0.9632	1.4572	32.910	757.53	73.188	883.13	0.858	0.941
		+1.83	48.5	15.2	1.4025	0.9625	1.4571	32.952	756.92	73.120	882.06	0.858	0.940
		+1.54	46.7	15.3	1.4033	0.9634	1.4566	32.946	757.85	73.219	882.24	0.859	0.942
		+1.81	48.9	15.3	1.4042	0.9641	1.4564	32.952	757.38	73.174	882.21	0.859	0.942
		+1.69	47.7	15.3	1.4042	0.9639	1.4569	32.864	757.35	73.171	882.06	0.859	0.941
			1.26	0.21	0.10	0.00	0.00	0.02	0.02	0.02	0.02	0.00	0.00
			1.24	1.34	0.13	0.04	0.01	0.07	0.03	0.03	0.02	0.02	0.05

(Illegible) STAGE

	STATOR	ROTOR	
BEARING WIDTH	22.70	19.00	MM
(Illegible) ANGLE	17.30	17.30	GRAD
(Illegible)	0.90	0.90	
NO. OF SEAL PEAKS	3	3	

STAGE		PI BAR	DISST KJ/KG	PI BAR	REAK	PSI	PHI	COAX M/S	C1 M/S	C2 M/S	AL2 GRD	M1 M/S	BE1 GRD	M2 M/S	ETAD
1		1.4042	10.833	1.3147	0.445	2.34	0.31	31.1	108.2	29.3	94.2	33.0	77.1	98.4	0.895
2		1.3953	10.944	1.1918	0.436	2.34	0.31	31.4	109.5	29.3	95.8	33.5	76.1	98.1	0.876
3		1.3838	11.087	1.1191	0.415	2.34	0.30	32.0	112.2	29.2	99.2	34.9	73.2	97.0	0.897
		1.3944	10.955	1.1952	0.432	2.34	0.31	31.5	110.0	29.3	96.4	33.8	75.5	97.6	0.896

TABLE A4 Protocol for force measurements evaluation for a measurement series with stator adjustment

Illegible

	STATOR			ROTOR				MEASUREMENT					
								KV	KH	QZ	QZ/QS	YV/LS	
								%	%	%	o/o	o/o	%
A	1835				.002	-0.01	-0.02	0.01	-0.05	-0.044	-0.017	0.01	-0.019
B	1837				-.006	0.03	-0.14	-0.22	0.19	-0.026	-0.010	0.23	0.114
C	1838				-.009	0.08	-0.37	-0.56	0.32	-0.239	-0.093	0.50	0.243
D	1839				-.011	0.08	-0.54	-0.82	0.55	-0.272	-0.105	0.74	0.378
E	1840				.000	-0.00	-0.71	-1.16	0.69	-0.470	-0.182	0.97	0.510
F	1841				-.009	0.04	0.24	0.33	-0.16	0.163	0.063	-0.27	-0.135
G	1842				-.006	0.03	0.41	0.49	-0.36	0.139	0.054	-0.52	-0.245
H	1843				-.004	0.04	0.60	0.76	-0.55	0.207	0.080	-0.77	-0.352
I	1844				-.003	0.02	0.76	0.94	-0.68	0.263	0.102	-1.01	-0.447
J	1845				-.003	0.02	0.02	0.06	0.06	0.119	0.046	-0.01	-0.050

	LE	LA	STIFE	
(Illegible) CONSTANT	1834		1834	N/M
(Illegible) CONSTANT	142		842	N/M
Illegible	.285	.000	.285	
Illegible	.131	.000	.131	
Illegible	.459	.000	.459	

TABLE A5 Error computation for mass flow measurements

(Illegible)
ERROR COMPUTATION [illegible] MEASUREMENT SERIES
293 FF

MEAS.ORIFICE 1, MEASUREMENT UNCERTAINTY

TEMPERATURE 0.5 K
PRESSURE BEFORE ORIFICE 138 PA
PRESSURE DIFFERENTIAL 29 PA

HR	M	ET D/D	EP D/D	ER(1) D/D	ER2 D/D	EM D/D	TAUA D/D	TAUE D/D	EM KG/S
1231	293	0.16	0.23	0.33	1.14	0.82	0.43	0.07	.0172
1255	295	0.16	0.24	0.33	0.85	0.53	0.42	0.10	.0174
1317	299	0.16	0.25	0.29	0.75	0.59	0.42	0.11	.0178
1351	305	0.16	0.26	0.31	0.91	0.65	0.42	0.10	.0177
1414	308	0.16	0.27	0.32	1.05	0.79	0.42	0.09	.0179
1439	311	0.16	0.29	0.33	1.21	0.76	0.42	0.08	.0159
1455	315	0.16	0.31	0.35	1.85	1.04	0.43	0.06	.0180
1517	317	0.16	0.26	0.30	0.32	0.61	0.42	0.11	.0173
1535	320	0.16	0.25	0.30	0.79	0.60	0.42	0.11	.0175
1559	325	0.16	0.24	0.29	0.65	0.56	0.41	0.12	.0184
1617	329	0.16	0.22	0.27	0.53	0.53	0.41	0.14	.0189

MEAS.ORIFICE 2, MEASUREMENT UNCERTAINTIES

TEMPERATURE 0.5 K
PRESSURE BEFORE ORIFICE 274 PA
PRESSURE DIFFERENTIAL 85 PA

HR	M	ET D/D	EP D/D	ER(1) D/D	ER2 D/D	EM D/D	TAUA D/D	TAUE D/D	EM KG/S
1231	293	0.16	0.24	0.29	1.54	0.94	0.43	0.07	.0195
1255	295	0.16	0.21	0.27	1.02	0.58	0.42	0.11	.0189
1317	299	0.16	0.20	0.25	0.88	0.53	0.42	0.12	.0191
1351	305	0.16	0.22	0.27	1.08	0.71	0.42	0.10	.0186
1414	308	0.16	0.22	0.28	1.25	0.73	0.42	0.09	.0188
1439	311	0.16	0.23	0.28	1.45	0.85	0.42	0.08	.0189
1455	315	0.16	0.25	0.30	2.22	1.23	0.43	0.06	.0208
1517	317	0.16	0.21	0.27	0.37	0.56	0.42	0.11	.0187
1535	320	0.16	0.21	0.25	0.93	0.65	0.42	0.12	.0188
1559	325	0.16	0.20	0.25	0.78	0.59	0.41	0.13	.0195
1617	329	0.16	0.18	0.24	0.63	0.55	0.41	0.15	.0207

TABLE A6 STAGE A VARIATION OF DIFFERENT PARAMETERS

FORCE MEASUREMENT PERPENDICULAR TO DEFLECTION DIRECTION
(EXCITATION FORCE MEASUREMENT)

STAGE ADJUSTMENT VARIATION PRESSURE COEFFICIENT

MR	PSI	SAX	N UPM	TE C	PE BAR	M KG/S	DPT BAR	US N	K2S	K2	FK2 O/O	L1	FL1 O/O
29	2.0	2.3	3000	24	1.0146	2.78	.0616	204	0.76	0.28	18	-0.11	22
49	2.2	2.5	3000	23	1.0298	2.98	.0692	242	0.76	0.55	11	-0.15	7
25	3.6	2.7	3000	26	1.0738	3.85	.1136	503	0.76	0.22	46	-0.15	20
27	3.9	2.7	3000	37	1.0705	3.77	.1175	531	0.76	0.17	54	-0.12	19
43	4.8	2.6	3000	23	1.1192	4.54	.1570	792	0.75	0.25	19	-0.11	5
26	5.2	2.8	3000	26	1.1278	4.69	.1675	876	0.75	0.35	[illegible]	-0.11	15
45	5.3	2.7	3000	24	1.1306	4.79	.1741	919	0.75	0.28		-0.11	5
28	5.4	2.6	3000	28	1.1257	4.66	.1724	906	0.75	0.33		-0.10	9
46	5.8	2.7	3000	24	1.1500	5.06	.1935	1067	0.75	0.34	8	-0.09	8

STAGE ADJUSTMENT VARIATION AXIAL GAP

30	3.7	2.1	3000	27	1.0832	3.87	.1181	524	0.76	0.46	7	-0.07	12
34	3.8	2.7	3000	31	1.0834	3.84	.1176	524	0.76	0.22	39	-0.13	16
35	3.7	3.1	3000	26	1.0843	3.89	.1186	526	0.76	0.39	11	-0.06	27
52	3.8	3.1	3000	28	1.0828	3.92	.1204	543	0.76	0.46	8	-0.14	11
51	5.0	3.2	3000	29	1.1225	4.55	.1592	816	0.75	0.43	6	-0.07	11

STAGE ADJUSTMENT VARIATION ROTATION RATE

31	3.7	2.6	2900	28	1.0286	3.02	.0718	323	0.75	0.65	2	-0.09	18
34	3.8	2.7	3000	31	1.0834	3.84	.1176	524	0.76	0.22	39	-0.13	16
30	3.9	2.8	3000	31	1.1293	4.62	.1765	771	0.76	0.44	8	-0.12	14

STAGE ADJUSTMENT VARIATION LOADING

34	3.8	2.7	3000	31	1.0834	3.84	.1176	524	0.76	0.22	39	-0.13	16
32	3.7	2.8	3000	37	1.5823	5.46	.1653	731	0.76	0.32	15	-0.08	24
33	4.0	2.9	3000	45	2.1872	7.83	.2392	1128	0.75	0.35	8	-0.08	17

TABLE A7 STAGE A VARIATION OF THE PRESSURE COEFFICIENT AND THE AXIAL GAP

/139

FORCE MEASUREMENT PERPENDICULAR TO DEFLECTION DIRECTION
(EXCITATION FORCE MEASUREMENT)

STAGE ADJUSTMENT

MR	PSI	SAX	N UPM	TE C	PE BAR	M KG/S	DPT BAR	US M	K2S	K2	FK2 O/O	L1	FL1 O/O
79	1.9	1.5	3000	27	1.0224	2.70	.0581	187	0.76	0.48	4	-0.05	15
78	2.5	1.5	3000	28	1.0409	3.09	.0756	276	0.76	0.48	3	-0.05	16
77	3.0	1.5	3000	31	1.0599	3.44	.0936	379	0.76	0.48	4	-0.03	25
76	3.6	1.6	3000	33	1.0771	3.74	.1097	480	0.76	0.45	4	-0.03	18
72	3.7	1.6	3000	35	1.0771	3.69	.1118	487	0.76	0.45	3	-0.03	24
75	4.1	1.6	3000	36	1.0931	3.99	.1262	591	0.75	0.43	3	-0.03	23
74	4.6	1.6	3000	40	1.1036	4.22	.1420	705	0.75	0.44	4	-0.04	13
73	5.1	1.7	3000	40	1.1248	4.46	.1583	824	0.75	0.43	3	-0.06	8
70	2.0	2.0	3000	29	1.0213	2.73	.0589	193	0.76	0.63	3	-0.06	12
69	2.6	2.0	3000	32	1.0412	3.13	.0784	293	0.76	0.63	5	-0.05	24
68	3.2	2.1	3000	33	1.0598	3.48	.0960	396	0.76	0.59	5	-0.08	17
66	3.6	2.1	3000	35	1.0752	3.74	.1109	490	0.76	0.45	9	-0.08	10
65	3.8	2.1	3000	35	1.0803	3.83	.1160	525	0.76	0.39	7	-0.07	11
64	4.1	2.1	3000	33	1.0901	4.01	.1270	594	0.76	0.38	7	-0.08	9
63	4.6	2.1	3000	33	1.1077	4.29	.1439	711	0.75	0.39	6	-0.08	8
62	5.0	2.1	3000	31	1.1238	4.53	.1592	820	0.75	0.33	6	-0.08	9
37	1.9	2.3	3000	19	1.0190	2.79	.0604	196	0.76	0.65	10	-0.07	17
38	2.6	2.4	3000	20	1.0436	3.29	.0832	314	0.76	0.74	4	-0.07	14
39	3.1	2.4	3000	20	1.0589	3.57	.0979	399	0.76	0.69	4	-0.11	6
40	3.5	2.4	3000	21	1.0736	3.83	.1120	486	0.76	0.47	15	-0.13	18
48	3.8	2.6	3000	24	1.0830	3.97	.1208	545	0.76	0.31	22	-0.13	7
41	4.1	2.6	3000	22	1.0940	4.17	.1319	616	0.76	0.29	21	-0.10	8
42	4.4	2.6	3000	23	1.1056	4.34	.1433	695	0.75	0.27	20	-0.11	5
44	5.1	2.6	3000	24	1.1287	4.68	.1660	858	0.75	0.25	17	-0.12	8
61	2.0	3.0	3000	27	1.0244	2.77	.0599	197	0.76	0.40	12	-0.06	27
59	2.6	3.1	3000	27	1.0439	3.17	.0799	298	0.76	0.60	8	-0.05	15
58	3.1	3.1	3000	29	1.0623	3.51	.0973	399	0.76	0.64	6	-0.10	10
57	3.6	3.3	3000	30	1.0795	3.80	.1135	500	0.76	0.58	6	-0.09	7
53	3.9	3.1	3000	31	1.0843	3.89	.1202	543	0.76	0.55	7	-0.08	9
54	4.1	3.2	3000	31	1.0943	4.06	.1294	605	0.76	0.53	12	-0.08	17
55	4.5	3.2	3000	33	1.1076	4.26	.1425	699	0.75	0.40	6	-0.06	9
56	5.0	3.2	3000	32	1.1239	4.51	.1580	811	0.75	0.41	6	-0.06	7
87	2.0	3.5	3000	27	1.0325	2.80	.0617	204	0.76	0.50	11	-0.02	112
86	2.6	3.5	3000	29	1.0527	3.20	.0802	301	0.76	0.53	8	-0.02	71
85	3.2	3.6	3000	31	1.0727	3.55	.0999	414	0.76	0.60	5	-0.04	19
81	3.8	3.6	3000	31	1.0911	3.88	.1190	532	0.76	0.63	6	-0.05	10
83	4.2	3.6	3000	36	1.1065	4.00	.1338	636	0.76	0.50	7	-0.02	35
88	4.5	3.6	3000	30	1.1178	4.33	.1426	697	0.75	0.36	9	-0.05	12
82	5.1	3.7	3000	36	1.1339	4.53	.1601	828	0.75	0.36	10	-0.04	14

TABLE A8 STAGE B VARIATION OF THE PRESSURE COEFFICIENT, THE ROTATION RATE AND THE LOADING

FORCE MEASUREMENT PERPENDICULAR TO DEFLECTION DIRECTION
(EXCITATION FORCE MEASUREMENT)

STAGE ADJUSTMENT

NR	PSI	SAX	F UPM	TE C	PE BAR	M KG/S	DPT BAR	US N	K2S	K2	FK2 0/0	L1	FL1 0/0
441	1.7	3.3	4000	40	1.0809	1.94	.0918	161	1.46	2.19	5	0.70	18
442	1.9	3.4	4000	30	1.0870	2.05	.1036	186	1.46	1.81	7	0.42	35
445	2.6	3.4	4000	40	1.1091	2.35	.1403	290	1.46	1.73	4	0.32	35
446	3.3	3.4	4000	50	1.1423	2.80	.1770	408	1.44	1.35	10	0.14	149
449	3.8	3.3	4000	31	1.1877	3.02	.2230	550	1.44	1.28	29	-0.13	369
450	4.3	3.3	4000	33	1.2109	3.21	.2528	662	1.43	1.08	8	-0.07	222
453	4.8	3.2	4000	40	1.2302	3.41	.2866	795	1.42	1.23	4	-0.12	84
454	5.3	3.4	4000	38	1.2877	3.66	.3250	944	1.42	1.33	12	0.10	122
455	5.9	3.3	4000	37	1.3234	3.88	.3632	1097	1.41	1.33	6	0.05	63
456	2.0	3.3	4000	27	1.0860	2.16	.1116	206	1.46	1.63	7	0.16	52
459	2.5	3.4	4000	31	1.1108	2.41	.1420	290	1.46	1.69	7	0.08	78
460	3.0	3.4	4000	35	1.1475	2.65	.1727	386	1.45	1.30	9	0.13	46
463	3.5	3.4	4000	40	1.1751	2.85	.2006	482	1.44	1.30	10	0.00	999
464	4.1	3.3	4000	43	1.2069	3.07	.2339	601	1.43	1.12	8	0.03	108
467	4.6	3.4	4000	49	1.2353	3.23	.2640	719	1.42	1.31	7	-0.04	93
468	5.1	3.3	4000	51	1.2684	3.44	.2981	855	1.42	1.36	7	0.01	439
472	2.1	3.3	4311	26	1.1162	2.42	.1414	265	1.46	1.85	6	0.21	10
459	2.5	3.4	4000	31	1.1108	2.41	.1420	290	1.46	1.69	7	0.08	78
473	2.9	3.4	3850	27	1.1159	2.42	.1412	313	1.45	1.67	9	0.12	26
476	3.4	3.4	3381	28	1.1139	2.41	.1406	338	1.44	1.39	9	0.12	41
477	3.9	3.3	3182	28	1.1128	2.41	.1403	361	1.43	1.29	6	0.07	29
480	4.4	3.3	2981	28	1.1120	2.42	.1405	385	1.42	1.52	5	0.05	116
481	4.9	3.3	2828	28	1.1109	2.42	.1404	406	1.41	1.64	4	0.07	42
488	2.8	3.4	4000	39	1.1365	2.53	.1574	343	1.45	1.61	6	0.20	52
487	2.7	3.4	4000	43	1.6090	3.51	.2146	464	1.45	1.71	4	0.13	65
486	2.7	3.3	4000	51	2.0172	4.28	.2595	557	1.45	2.01	7	0.09	64
485	2.7	3.3	4000	61	2.4727	5.06	.3069	654	1.45	1.98	7	0.06	120
482	2.9	3.4	4000	49	3.0209	6.25	.3679	760	1.46	1.74	6	0.12	88

TABLE A9 STAGE B VARIATION OF THE PRESSURE COEFFICIENT, THE ROTATION RATE AND THE LOADING

FORCE MEASUREMENT PERPENDICULAR TO DEFLECTION DIRECTION
(EXCITATION FORCE MEASUREMENT)

STATOR AJUSTMENT

HR	PSI	SAX	N UPM	TE C	PE BAR	M KG/S	DPT BAR	US N	KZS	KZ	FR2 0/0	L1	PL1 0/0
442	2.6	3.4	4000	37	1.1000	2.37	.1417	292	0.67	0.08	48	0.20	17
447	3.7	3.4	4000	30	1.1849	3.02	.2204	544	0.67	0.29	41	0.29	26
451	4.8	3.2	4000	39	1.2504	3.41	.2870	795	0.67	0.16	14	0.04	51
457	2.5	3.4	4000	30	1.1168	2.42	.1422	291	0.67	0.13	25	0.24	9
461	3.5	3.3	4000	39	1.1739	2.86	.2012	483	0.67	0.30	10	0.21	10
465	4.6	3.4	4000	47	1.2367	3.25	.2653	727	0.67	0.27	12	0.23	13
457	2.5	3.4	4000	30	1.1168	2.42	.1422	291	0.67	0.13	25	0.24	9
474	3.4	3.4	3381	28	1.1139	2.41	.1404	337	0.67	0.38	5	0.23	9
478	4.4	3.3	2981	28	1.1119	2.42	.1402	384	0.67	0.35	7	0.26	6
483	2.7	3.3	4000	58	2.4689	5.10	.3079	696	0.67	0.19	19	0.26	6

ROTOR ADJUSTMENT

444	2.6	3.4	4000	38	1.1051	2.35	.1405	290	0.79	1.63	6	0.11	82
448	3.7	5.4	4000	29	1.1863	3.03	.2215	546	0.77	0.97	26	-0.33	105
452	4.8	3.2	4000	40	1.2500	3.41	.2870	796	0.75	0.97	6	-0.39	20
458	2.5	3.4	4000	31	1.1170	2.42	.1421	291	0.79	1.52	9	-0.11	58
462	3.5	3.4	4000	39	1.1757	2.85	.2013	484	0.77	0.91	21	-0.25	13
466	4.6	3.4	4000	49	1.2382	3.24	.2647	721	0.76	0.94	8	-0.34	13
458	2.5	3.4	4000	31	1.1170	2.42	.1421	291	0.79	1.52	9	-0.11	58
475	3.4	3.4	3381	28	1.1140	2.41	.1406	337	0.77	1.09	11	-0.17	17
479	4.4	3.3	2981	28	1.1120	2.42	.1404	385	0.75	1.19	4	-0.21	16
484	2.7	3.3	4000	59	2.4726	5.09	.3076	655	0.79	1.63	11	-0.28	19

TABLE A10 THREE-STAGE GROUP VARIATION OF THE PRESSURE COEFFICIENT AND THE ROTATION RATE

FORCE MEASUREMENT PERPENDICULAR TO DEFLECTION DIRECTION
(EXCITATION FORCE MEASUREMENT)

STAGE ADJUSTMENT ALL STAGES

MR	PSI	SAX	F UPM	TE C	PE DAR	M KG/S	OPT BAR	US N	K2S	K2	FK2 O/O	L1	FL1 O/O
493	1.3	2.8	4000	57	1.1842	1.77	.2157	339	1.45	2.64	3	-0.21	94
489	1.9	2.9	4000	36	1.3106	2.32	.3515	637	1.47	1.83	5	0.00	676
490	2.3	2.9	4000	40	1.4042	2.59	.4404	882	1.46	1.57	2	-0.02	104
491	2.8	2.9	4000	61	1.4916	2.84	.5289	1162	1.46	1.53	6	0.06	118
492	3.2	3.0	4000	67	1.5799	3.08	.6173	1440	1.45	1.44	6	0.04	51
494	1.6	2.9	4000	35	1.2489	2.10	.2903	489	1.46	2.06	4	-0.07	107
495	2.1	2.9	4000	53	1.3262	2.31	.3668	692	1.46	1.82	5	0.07	200
496	2.5	2.8	4000	67	1.3978	2.50	.4385	902	1.46	1.48	6	-0.13	67
498	2.9	2.8	4000	68	1.4819	2.77	.5219	1148	1.45	1.65	4	0.03	332
499	3.2	2.8	4000	64	1.5755	3.07	.6128	1414	1.45	1.60	8	-0.03	263
503	1.5	3.0	4000	21	1.2427	2.17	.2908	487	1.46	1.89	17	0.19	116
504	2.2	2.9	4000	25	1.4086	2.74	.4542	893	1.46	1.71	23	0.46	147
509	2.3	2.8	4000	39	1.3968	2.61	.4364	859	1.46	1.54	21	0.05	352
512	2.4	2.8	4000	50	1.3995	2.58	.4451	898	1.46	1.41	26	0.24	97
511	6.9	2.8	2000	42	1.2541	2.17	.3026	1078	1.37	0.74	44	0.17	104
502	3.2	2.8	3464	50	1.4107	2.61	.4477	1047	1.45	1.31	11	-0.08	105
501	2.8	2.8	3702	52	1.4092	2.59	.4463	975	1.46	1.72	5	0.05	89
500	2.4	2.8	4000	55	1.4073	2.57	.4449	901	1.46	1.44	3	-0.57	19
513	2.0	2.8	4500	52	1.4337	2.69	.4787	886	1.47	1.89	39	-0.11	242

TABLE A11 STAGE C VARIATION OF THE PRESSURE COEFFICIENT, THE AXIAL GAP AND THE CLUTCH

FORCE MEASUREMENT PERPENDICULAR TO DEFLECTION DIRECTION
(EXCITATION FORCE MEASUREMENT)

STAGE ADJUSTMENT UEA=.0 MM DN/DM=.35 AB=8*30 MULTIPLE DISK CLUTCH

MR	PSI	SAX	F UPM	TE C	PE BAR	M KG/S	DPT BAR	US N	K2S	K2	FK2 O/O	L1	FL1 O/O
94	2.1	2.4	5000	30	1.1566	2.25	.1940	291	1.04	2.87	2	0.99	2
90	2.5	2.4	5000	29	1.2118	2.59	.2336	3[illegible]	1.03	2.93	2	0.83	7
92	2.9	2.5	5000	31	1.2301	2.69	.2686	465	1.00	2.77	1	0.75	2
91	3.2	2.4	5000	32	1.2689	2.90	.3081	564	0.99	2.75	1	0.70	2
95	3.5	2.5	5000	32	1.3063	3.09	.3434	658	0.97	2.48	1	0.66	1
96	3.8	2.5	5000	34	1.3384	3.24	.3749	745	0.96	2.43	1	0.65	1

STAGE ADJUSTMENT UEA=.0 MM DN/DM=.35 AB=8*30 MEMBRANE CLUTCH

98	2.5	2.4	5000	27	1.2089	2.54	.2356	382	1.02	2.83	1	0.88	3
99	3.2	2.4	5000	33	1.2798	2.92	.3060	560	0.99	2.69	1	0.71	3
100	3.8	2.5	5000	33	1.3538	3.30	.3798	757	0.96	2.38	1	0.61	2
101	4.4	2.5	5000	35	1.4227	3.61	.4488	951	0.93	2.31	1	0.61	2
102	4.9	2.5	5000	37	1.4896	3.89	.5102	1153	0.91	2.18	1	0.57	2
104	2.5	2.2	5000	24	1.1877	2.51	.2297	372	1.03	2.88	1	0.81	4
105	3.0	2.2	5000	27	1.2429	2.84	.2888	517	1.00	2.69	1	0.76	2
106	3.5	2.2	5000	29	1.2836	3.09	.3390	651	0.97	2.62	1	0.74	2
108	4.1	2.3	5000	32	1.3430	3.38	.4021	832	0.96	2.54	0	0.63	3
109	4.6	2.3	5000	46	1.3706	3.47	.4389	962	0.91	2.48	1	0.57	5
110	5.2	2.3	5000	54	1.4274	3.68	.4987	1142	0.88	2.25	1	0.52	4
111	2.6	3.1	5000	29	1.1908	2.56	.2426	406	1.02	2.90	3	0.99	5
115	4.3	3.3	5000	53	1.3268	3.22	.3904	829	0.93	2.30	2	0.70	6
116	4.8	3.3	5000	56	1.3750	3.42	.4433	990	0.91	2.18	2	0.57	4
117	5.3	3.4	5000	59	1.4301	3.66	.5014	1178	0.88	2.12	3	0.60	8
118	2.6	4.2	5000	36	1.1884	3.48	.2870	394	1.02	3.09	7	1.03	19
119	3.2	4.2	5000	42	1.2313	2.75	.2890	532	0.99	2.53	7	0.72	4
120	3.7	4.2	5000	45	1.2712	2.96	.3335	654	0.96	2.40	2	0.71	4
122	4.3	4.2	5000	49	1.3297	3.25	.3959	839	0.93	2.39	4	0.66	8
123	4.8	4.2	5000	52	1.3767	3.46	.4480	1000	0.91	2.16	3	0.59	10
124	5.3	4.2	5000	56	1.4247	3.65	.5016	1169	0.88	2.15	5	0.55	20

TABLE A12 STAGE C VARIATION OF THE PRESSURE COEFFICIENT AND THE AXIAL GAP

FORCE MEASUREMENT PERPENDICULAR TO DEFLECTION DIRECTION
(EXCITATION FORCE MEASUREMENT)

STAGE ADJUSTMENT UEA=.0 MM DM/DM=.35 AB=4*18

MR	PSI	SAX	F UPM	TE C	PE BAR	M KG/S	DPT BAR	US N	K2S	K2	FK2 O/O	L1	FL1 O/O
129	2.0	1.1	5000	24	1.1546	2.23	.1823	264	1.05	3.39	1	0.20	27
130	2.5	1.2	5000	28	1.2090	2.55	.2361	385	1.02	3.26	1	0.17	17
131	3.1	1.2	5000	31	1.2649	2.85	.2927	525	1.00	3.07	1	0.15	18
132	3.5	1.2	5000	34	1.3130	3.10	.3410	652	0.97	2.89	1	0.21	21
134	4.0	1.2	5000	36	1.3744	3.39	.4014	821	0.95	2.68	1	0.22	29
135	4.5	1.2	5000	37	1.4273	3.64	.4551	977	0.93	2.54	1	0.25	20
136	4.9	1.2	5000	39	1.4876	3.88	.5154	1154	0.91	2.48	1	0.28	17
137	1.9	2.2	5000	28	1.1519	2.17	.1772	254	1.05	3.04	1	0.50	6
138	2.5	2.2	5000	30	1.2080	2.52	.2332	379	1.02	2.95	1	0.48	6
139	3.0	2.2	5000	32	1.2630	2.84	.2911	520	1.00	2.78	1	0.45	5
140	3.5	2.3	5000	33	1.3141	3.10	.3407	651	0.97	2.63	0	0.35	7
142	4.0	2.3	5000	34	1.3768	3.41	.4040	828	0.95	2.50	1	0.20	13
143	4.5	2.3	5000	36	1.4302	3.66	.4586	987	0.92	2.36	1	0.18	15
144	4.9	2.2	5000	38	1.4830	3.87	.5122	1145	0.91	2.28	1	0.17	9
145	1.9	3.1	5000	25	1.1484	2.17	.1769	252	1.05	2.87	2	0.71	8
146	2.5	3.1	5000	28	1.2051	2.52	.2323	376	1.02	2.79	1	0.74	3
147	3.0	3.1	5000	30	1.2623	2.84	.2903	517	1.00	2.67	1	0.62	3
148	3.5	3.2	5000	31	1.3124	3.11	.3403	648	0.97	2.56	1	0.52	5
150	4.0	3.2	5000	33	1.3754	3.41	.4028	821	0.95	2.39	1	0.37	8
151	4.5	3.2	5000	34	1.4305	3.67	.4594	986	0.92	2.28	1	0.29	11
152	4.9	3.2	5000	37	1.4842	3.88	.5136	1146	0.91	2.18	1	0.31	9
160	2.0	4.2	5000	28	1.1460	2.17	.1789	258	1.04	2.77	2	0.92	3
161	2.5	4.2	5000	30	1.2034	2.52	.2341	382	1.02	2.65	1	0.71	3
162	3.1	4.2	5000	32	1.2596	2.84	.2923	525	0.99	2.52	1	0.52	4
163	3.5	4.2	5000	32	1.3095	3.10	.3399	649	0.97	2.37	1	0.47	6
165	4.0	4.2	5000	34	1.3779	3.43	.4071	835	0.95	2.26	1	0.36	9
166	4.5	4.2	5000	36	1.4310	3.68	.4621	1000	0.92	2.15	1	0.32	9
167	4.9	4.2	5000	38	1.4864	3.89	.5172	1162	0.90	2.08	1	0.33	8
168	2.0	5.2	5000	26	1.1432	2.19	.1799	260	1.05	3.12	2	1.41	2
169	2.5	5.2	5000	29	1.1994	2.52	.2334	381	1.02	2.84	2	1.02	2
170	3.1	5.2	5000	32	1.2581	2.84	.2922	526	0.99	2.71	2	0.72	3
171	3.5	5.2	5000	35	1.3026	3.05	.3357	640	0.97	2.59	2	0.66	4
173	4.0	5.2	5000	35	1.3676	3.37	.3991	815	0.95	2.44	2	0.60	6
174	4.5	5.2	5000	37	1.4216	3.62	.4536	977	0.92	2.29	2	0.55	9
175	4.9	5.2	5000	40	1.4760	3.83	.5088	1137	0.91	2.19	2	0.49	8

TABLE A13 STAGE C VARIATION OF THE LOADING

FORCE MEASUREMENT PERPENDICULAR TO DEFLECTION CORRECTION
(EXCITATION FORCE MEASUREMENT)

STAGE ADJUSTMENT UEA=.0 MM DN/DM=.35 AB=4*18 VARIATION GRADIENT

MR	PSI	SAX	N UPM	TE C	PE BAR	M KG/S	DPT BAR	US M	K2S	K2	FK2 O/O	L1	FL1 O/O
148	3.5	3.2	5000	31	1.3124	3.11	.3403	648	0.97	2.56	1	0.52	5
150	4.0	3.2	5000	33	1.3754	3.41	.4028	821	0.95	2.39	1	0.37	8
151	4.5	3.2	5000	34	1.4305	3.67	.4594	986	0.92	2.28	1	0.29	11
152	4.9	3.2	5000	37	1.4842	3.88	.5136	1146	0.91	2.18	1	0.31	9

STAGE ADJUSTMENT UEA=.0 MM DN/DM=.35 AB=4*18 VARIATION LOADING

153	3.6	3.2	5000	31	1.3056	3.11	.3464	666	0.97	2.53	1	0.48	5
159	3.6	3.2	5000	35	1.3228	3.14	.3486	675	0.97	2.50	1	0.46	4
158	3.5	3.2	5000	37	1.5181	3.55	.3890	743	0.97	2.54	1	0.48	4
157	3.4	3.2	5000	38	1.7457	4.03	.4339	821	0.98	2.58	1	0.46	4
156	3.3	3.3	5000	39	1.9483	4.43	.4716	879	0.98	2.63	1	0.47	5
155	3.2	3.3	5000	40	2.3006	5.12	.5340	973	0.99	2.66	1	0.48	5
154	3.0	3.3	5000	40	2.7927	6.06	.6138	1082	1.00	2.68	1	0.50	4

TABLE A14 STAGE C VARIATION OF THE PRESSURE COEFFICIENT AND THE HUB RATIO

FORCE MEASUREMENT PERPENDICULAR TO DEFLECTION DIRECTION
(EXCITATION FORCE MEASUREMENT)

STAGE ADJUSTMENT UEA=.0 MM DN/DM=.35 AB=4*18

MR	PSI	SAX	I UPM	TE C	PE BAR	M KG/S	DPT BAR	US N	K2S	K2	FK2 O/O	L1	FL1 O/O
176	1.9	2.6	5000	22	1.1449	2.17	.1754	268	1.05	2.78	2	0.61	11
177	2.4	2.6	5000	26	1.2005	2.51	.2302	370	1.03	2.79	2	0.59	10
178	3.0	2.6	5000	28	1.2582	2.84	.2894	514	1.00	2.63	1	0.52	8
179	3.4	2.6	5000	31	1.3055	3.08	.3365	639	0.98	2.54	2	0.44	9
182	4.0	2.7	5000	36	1.3649	3.36	.3961	809	0.95	2.46	1	0.29	9
183	4.5	2.7	5000	38	1.4192	3.61	.4505	968	0.92	2.35	2	0.28	10
184	4.9	2.7	5000	42	1.4680	3.80	.5002	1120	0.90	2.25	2	0.26	11
181	3.5	2.7	5000	34	1.3031	3.06	.3341	636	0.98	2.56	2	0.42	9
204	2.5	2.9	5000	40	1.1747	2.39	.2215	362	1.02	2.63	1	0.68	4
203	3.6	2.9	5000	44	1.2794	2.96	.3278	634	0.97	2.36	2	0.44	3
202	5.0	2.9	5000	46	1.4484	3.73	.4977	1127	0.90	2.04	3	0.26	8

STAGE ADJUSTMENT UEA=.0 MM DN/DM=.53 AB=4*21

207	2.0	3.0	5000	31	1.1355	2.14	.1771	257	1.14	2.47	4	1.83	2
210	2.5	3.1	5000	36	1.1878	2.46	.2291	377	1.12	2.74	2	1.55	3
213	3.1	3.1	5000	39	1.2440	2.77	.2862	520	1.09	2.51	2	1.33	1
216	3.6	3.1	5000	41	1.2935	3.03	.3357	653	1.07	2.35	2	1.25	2
223	4.1	3.1	5000	44	1.3495	3.30	.3940	819	1.04	2.16	1	1.07	3
226	4.6	3.2	5000	47	1.4009	3.52	.4460	975	1.02	2.04	2	0.96	2
229	5.1	3.2	5000	50	1.4538	3.73	.4985	1139	0.99	1.98	2	0.86	3

STAGE ADJUSTMENT UEA=.0 MM DN/DM=.70 AB=0

232	2.0	2.9	5000	35	1.1337	2.11	.1755	254	1.27	2.06	4	0.74	4
235	2.6	2.9	5000	38	1.1915	2.45	.2311	380	1.25	2.25	1	0.63	7
238	3.1	3.0	5000	42	1.2465	2.74	.2849	515	1.23	2.18	2	0.47	4
241	3.6	3.1	5000	45	1.2946	2.99	.3325	645	1.21	2.08	2	0.50	3
247	4.2	3.1	5000	53	1.3515	3.23	.3887	810	1.18	2.04	1	0.59	10
250	4.6	3.1	5000	40	1.4236	3.62	.4610	1000	1.16	1.93	2	0.50	3
253	5.0	3.1	5000	40	1.4711	3.82	.5089	1142	1.15	1.81	3	0.47	5

TABLE A15 STAGE C VARIATION OF THE PRESSURE COEFFICIENT AND THE HUB RATIO

FORCE MEASUREMENT PERPENDICULAR TO DEFLECTION DIRECTION

(EXCITATION FORCE MEASUREMENT)

STATOR ADJUSTMENT UEA=.0 MM DN/DH=.35 AB=4°18

MR	PSI	SAX	N UPM	TE C	PE BAR	M KG/S	DPT BAR	US N	K2S	K2	FK2 O/O	L1	FL1 O/O
194	2.0	2.8	5000	25	1.1276	2.14	.1160	252	0.28	0.21	5	0.84	3
195	2.5	2.8	5000	30	1.1812	2.46	.2292	372	0.28	0.14	7	0.82	3
196	3.1	2.9	5000	34	1.2355	2.77	.2858	512	0.28	0.11	8	0.66	3
197	3.5	2.9	5000	36	1.2840	3.02	.3333	640	0.28	0.10	10	0.60	3
199	4.1	2.9	5000	38	1.3467	3.32	.3961	817	0.28	0.09	11	0.52	2
200	4.6	2.9	5000	41	1.3994	3.54	.4492	973	0.28	0.09	16	0.45	2
201	5.0	2.9	5000	44	1.4525	3.77	.5025	1138	0.28	0.09	19	0.38	2

STATOR ADJUSTMENT UEA=.0 MM DN/DH=.53 AB=4°21

205	2.0	3.0	5000	29	1.1352	2.15	.1769	256	0.41	-0.13	28	2.18	3
208	2.5	3.1	5000	34	1.1879	2.47	.2299	376	0.41	-0.09	35	1.94	3
211	3.1	3.1	5000	39	1.2435	2.77	.2860	519	0.42	-0.06	52	1.58	3
214	3.6	3.1	5000	40	1.2925	3.03	.3340	648	0.42	-0.05	95	1.47	2
221	4.1	3.1	5000	43	1.3499	3.31	.3939	818	0.42	-0.02	73	1.16	3
224	4.6	3.2	5000	45	1.4022	3.54	.4468	977	0.42	-0.01	297	1.06	3
227	5.1	3.2	5000	49	1.4540	3.74	.4989	1138	0.42	0.001	233	0.94	4

STATOR ADJUSTMENT UEA=.0 MM DN/DH=.70 AB=0

230	2.0	2.9	5000	34	1.1333	2.11	.1752	253	0.55	-0.60	7	1.19	5
233	2.6	2.9	5000	37	1.1900	2.45	.2301	378	0.55	-0.43	9	1.10	3
236	3.1	3.0	5000	41	1.2476	2.75	.2861	517	0.55	-0.38	10	0.97	4
239	3.6	3.1	5000	45	1.2946	2.99	.3325	644	0.55	-0.43	6	0.97	4
245	4.2	3.1	5000	51	1.3521	3.24	.3895	810	0.55	-0.42	6	0.89	9
248	4.6	3.1	5000	43	1.4187	3.58	.4561	992	0.55	-0.41	8	0.87	4
251	5.0	3.1	5000	40	1.4723	3.83	.5107	1147	0.55	-0.35	4	0.75	4

TABLE A16 STAGE C VARIATION OF THE PRESSURE COEFFICIENT AND THE HUB RATIO

FORCE MEASUREMENT PERPENDICULAR TO DEFLECTION DIRECTION
(EXCITATION FORCE MEASUREMENT)

ROTOR ADJUSTMENT UEA=.0 MM DN/DM=.35 AB=4*18

MR	PSI	SAX	N UPM	TE C	PE BAR	M KG/S	DPT BAR	US N	K2S	K2	FK2 O/O	L1	FL1 O/O
185	1.9	2.8	5000	26	1.1265	2.13	.1743	249	0.77	2.82	1	-0.28	18
186	2.5	2.9	5000	30	1.1800	2.46	.2270	368	0.75	2.69	1	-0.14	15
187	3.1	2.9	5000	35	1.2243	2.76	.2841	511	0.72	2.57	1	-0.12	14
188	3.5	2.9	5000	37	1.2825	3.01	.3311	637	0.69	2.51	2	-0.16	12
191	4.1	2.9	5000	44	1.3396	3.27	.3909	809	0.66	2.25	2	-0.15	20
192	4.6	2.9	5000	44	1.3938	3.51	.4438	963	0.64	2.17	2	-0.14	13
193	5.0	3.0	5000	46	1.4468	3.73	.4977	1129	0.62	2.08	1	-0.09	13

ROTOR ADJUSTMENT UEA=.0 MM DN/DM=.53 AB=4*21

206	2.6	3.0	5000	30	1.1355	2.15	.1770	257	0.73	2.70	2	-0.32	18
209	3.9	3.1	5000	35	1.1878	2.46	.2299	377	0.70	2.67	3	-0.19	21
212	5.1	3.1	5000	39	1.2434	2.77	.2859	519	0.67	2.63	1	-0.18	31
215	3.6	3.1	5000	41	1.2928	3.03	.3348	651	0.65	2.51	1	-0.18	43
222	4.1	3.1	5000	43	1.3494	3.30	.3940	819	0.62	2.24	2	-0.15	21
225	4.6	3.2	5000	46	1.4019	3.53	.4465	976	0.60	2.10	2	-0.11	63
228	5.1	3.2	5000	50	1.4537	3.74	.4986	1138	0.57	2.05	2	-0.12	61

ROTOR ADJUSTMENT UEA=.0 MM DN/DM=.70 AB=0

231	2.0	2.9	5000	34	1.1335	2.11	.1759	254	0.72	2.86	2	-0.54	7
234	2.6	2.9	5000	38	1.1912	2.45	.2307	379	0.70	2.85	1	-0.47	11
237	3.1	3.0	5000	42	1.2471	2.75	.2857	517	0.68	2.67	1	-0.52	8
240	3.6	3.1	5000	45	1.2943	2.99	.3324	645	0.65	2.53	2	-0.47	7
246	4.2	3.1	5000	52	1.3515	3.23	.3886	809	0.63	2.51	2	-0.33	10
249	4.6	3.1	5000	41	1.4218	3.61	.4592	997	0.60	2.45	3	-0.34	11
252	5.0	3.1	5000	40	1.4719	3.83	.5101	1146	0.59	2.21	4	-0.30	19

TABLE A17 STAGE C VARIATION OF THE PRESSURE COEFFICIENT AND THE AXIAL GAP

FORCE MEASUREMENT PERPENDICULAR TO DEFLECTION DIRECTION
(EXCITATION FORCE MEASUREMENT)

STAGE ADJUSTMENT UEA=.9 M' DN/DH=.35 AB=4018

MR	PSI	SAX	N UPM	TE C	PE BAR	M KG/S	DPT BAR	US %	K2S	K2	FK2 O/O	L1	FL1 O/O
277	2.0	0.6	5000	32	1.1430	2.12	.1792	257	1.01	4.10	5	-0.15	49
280	3.1	0.6	5000	35	1.2591	2.79	.2940	525	0.95	3.80	3	-0.15	59
283	3.6	0.5	5000	38	1.3038	3.01	.3390	645	0.93	3.77	4	-0.33	19
289	4.1	0.5	5000	42	1.3663	3.30	.4015	820	0.90	3.46	8	-0.30	44
292	5.0	0.5	5000	45	1.4726	3.76	.5104	1142	0.83	2.87	13	-0.79	42
256	2.0	1.7	5000	27	1.1430	2.13	.1782	252	1.01	3.02	2	0.33	21
259	3.1	1.6	5000	30	1.2601	2.82	.2941	521	0.96	2.73	1	0.09	49
262	3.5	1.6	5000	32	1.3113	3.08	.3448	654	0.93	2.62	2	0.21	47
268	3.5	1.6	5000	32	1.3120	3.09	.3467	658	0.93	2.52	6	0.08	69
271	4.1	1.6	5000	38	1.3696	3.34	.4036	821	0.90	2.46	3	0.14	33
274	5.0	1.5	5000	42	1.4800	3.80	.5153	1151	0.83	2.34	6	0.00	999
295	2.0	2.8	5000	34	1.1426	2.11	.1806	259	1.01	2.66	3	0.48	10
310	2.6	2.7	5000	38	1.1932	2.42	.2303	373	0.99	2.64	3	0.52	14
298	3.1	2.7	5000	36	1.2550	2.77	.2899	517	0.95	2.73	3	0.34	13
301	3.6	2.7	5000	40	1.3036	3.01	.3389	647	0.93	2.38	6	0.20	48
328	4.1	2.7	5000	42	1.3614	3.28	.3979	810	0.90	2.16	7	0.29	21
331	5.0	2.7	5000	45	1.4746	3.77	.5114	1145	0.83	1.99	9	0.07	35
334	2.0	3.3	5000	32	1.1426	2.14	.1806	261	1.01	2.72	3	0.74	19
337	3.1	3.4	5000	34	1.2583	2.79	.2933	521	0.96	2.57	7	0.43	13
340	3.6	3.5	5000	37	1.3066	3.04	.3413	651	0.93	2.38	9	0.32	23
346	4.1	3.5	5000	39	1.3662	3.32	.4013	818	0.89	2.24	5	0.40	12
349	5.0	3.4	5000	42	1.4759	3.78	.5119	1139	0.84	2.07	7	0.25	11
352	2.0	4.0	5000	26	1.1436	2.15	.1816	259	1.01	2.75	4	0.76	6
355	3.1	4.0	5000	30	1.2594	2.81	.2938	519	0.96	2.58	7	0.51	2
358	3.5	4.0	5000	34	1.3058	3.04	.3409	644	0.93	2.41	11	0.41	6
364	4.1	3.9	5000	37	1.3663	3.32	.4004	811	0.90	2.12	11	0.31	12
367	5.0	4.0	5000	41	1.4811	3.80	.5156	1147	0.84	1.98	8	0.21	16
370	2.0	4.7	5000	30	1.1434	2.13	.1797	257	1.01	3.13	4	1.12	10
373	3.1	4.7	5000	33	1.2610	2.80	.2944	524	0.95	2.77	9	0.63	7
376	3.5	4.7	5000	36	1.3052	3.03	.3390	643	0.93	2.41	12	0.44	11
382	4.1	4.7	5000	39	1.3672	3.31	.4007	815	0.90	2.21	9	0.46	9
385	5.0	4.6	5000	43	1.4776	3.78	.5119	1141	0.83	1.99	7	0.33	7

TABLE A18 STAGE C VARIATION OF THE PRESSURE COEFFICIENT AND THE AXIAL GAP

FORCE MEASUREMENT PERPENDICULAR TO DEFLECTION DIRECTION
(EXCITATION FORCE MEASUREMENT)

ROTOR ADJUSTMENT UEA=.9 MM DN/DM=.35 AB=4*18

MR	PSI	SAX	N UPM	TE C	PE BAR	M KG/S	DPT BAR	US N	K2S	K2	FK2 O/O	L1	FL1 O/O
276	2.0	0.6	5000	32	1.1426	2.12	.1795	257	0.73	4.12	8	-1.24	6
279	3.1	0.6	5000	35	1.2588	2.79	.2934	523	0.67	3.54	5	-1.05	6
282	3.6	0.5	5000	38	1.3038	3.02	.3391	645	0.64	3.62	6	-1.12	17
288	4.1	0.5	5000	42	1.3666	3.30	.4014	820	0.61	3.13	10	-0.92	10
291	5.0	0.5	5000	45	1.4735	3.76	.5108	1142	0.55	2.79	17	-0.86	21
258	3.1	1.6	5000	29	1.2605	2.82	.2944	521	0.67	2.55	2	-0.69	4
261	3.5	1.6	5000	31	1.3098	3.08	.3432	650	0.64	2.51	1	-0.61	8
267	3.5	1.6	5000	31	1.3110	3.08	.3460	655	0.64	2.41	10	-0.67	9
270	4.1	1.6	5000	37	1.3703	3.34	.4045	823	0.61	2.34	13	-0.48	10
273	5.0	1.5	5000	42	1.4801	3.81	.5160	1152	0.55	2.05	7	-0.44	9
294	2.0	2.8	5000	34	1.1423	2.11	.1802	259	0.72	2.68	2	-0.37	18
309	2.6	2.7	5000	38	1.1927	2.42	.2300	372	0.70	2.66	6	-0.26	19
297	3.1	2.7	5000	36	1.2548	2.77	.2895	516	0.67	2.56		-0.32	12
300	3.6	2.7	5000	39	1.3036	3.01	.3389	647	0.64	2.32	9	-0.30	12
327	4.1	2.7	5000	42	1.3621	3.28	.3972	809	0.61	2.16	10	-0.19	33
330	5.0	2.7	5000	45	1.4747	3.77	.5116	1146	0.55	1.99	10	-0.24	26
333	2.0	3.3	5000	32	1.1420	2.13	.1806	260	0.73	2.65	7	-0.23	23
336	3.1	3.4	5000	36	1.2577	2.79	.2927	520	0.67	2.40	3	-0.21	10
339	3.6	3.4	5000	37	1.3068	3.04	.3412	650	0.64	2.37	5	-0.24	18
345	4.1	3.5	5000	39	1.3666	3.32	.4016	819	0.61	2.23	18	-0.12	112
348	5.0	3.4	5000	42	1.4756	3.78	.5110	1135	0.55	2.00	9	-0.10	37
351	2.0	4.0	5000	26	1.1434	2.15	.1816	259	0.73	2.57	2	-0.20	64
354	3.1	4.0	5000	29	1.2589	2.81	.2939	518	0.67	2.48	6	-0.18	11
357	3.5	4.0	5000	33	1.3073	3.05	.3415	646	0.65	2.38	11	-0.15	24
363	4.1	3.9	5000	37	1.3662	3.32	.4005	811	0.61	2.19	9	-0.18	15
366	5.0	4.0	5000	41	1.4812	3.81	.5160	1147	0.55	1.95	10	-0.18	43
369	2.0	4.7	5000	30	1.1425	2.12	.1792	256	0.73	2.77	8	-0.13	56
372	3.1	4.7	5000	33	1.2595	2.80	.2937	522	0.67	2.53	9	-0.11	13
375	3.5	4.7	5000	36	1.3053	3.03	.3391	643	0.65	2.25	14	-0.16	25
381	4.1	4.7	5000	39	1.3670	3.31	.4006	815	0.61	2.07	7	-0.07	41
384	5.0	4.6	5000	43	1.4786	3.79	.5130	1144	0.55	1.97	5	-0.13	22

TABLE A19 STAGE C VARIATION OF THE PRESSURE COEFFICIENT AND THE AXIAL GAP

FORCE MEASUREMENT PERPENDICULAR TO DEFLECTION DIRECTION

(EXCITATION FORCE MEASUREMENT)

STATOR ADJUSTMENT UEA=.9 MM DN/DM=.35 AB=4*18

MR	PSI	SAX	N UPM	TE C	PE BAR	M KG/S	DPT BAR	US N	K2S	K2	FK2 O/O	L1	FL1 O/O
275	2.0	0.6	5000	32	1.1425	2.12	.1795	257	0.28	0.19	22	1.08	2
278	3.1	0.6	5000	34	1.2579	2.79	.2928	522	0.29	0.24	32	0.89	5
281	3.5	0.5	5000	37	1.3034	3.02	.3393	644	0.29	0.20	25	0.75	5
287	4.1	0.5	5000	41	1.3667	3.30	.4012	818	0.29	0.30	26	0.56	11
290	5.0	0.5	5000	45	1.4725	3.76	.5102	1139	0.29	0.28	32	0.29	23
254	2.0	1.6	5000	26	1.1426	2.13	.1778	251	0.28	0.22	34	0.83	10
257	3.1	1.6	5000	29	1.2594	2.82	.2939	519	0.29	0.07	30	0.77	6
260	3.5	1.6	5000	31	1.3084	3.07	.3429	647	0.29	0.13	28	0.70	5
266	3.5	1.6	5000	30	1.3097	3.08	.3451	652	0.29	0.10	29	0.64	6
269	4.1	1.6	5000	36	1.3700	3.35	.4048	822	0.29	0.13	33	0.51	10
272	5.0	1.5	5000	41	1.4798	3.81	.5157	1150	0.29	0.19	23	0.40	13
293	2.0	2.8	5000	34	1.1416	2.11	.1799	258	0.28	0.13	29	0.81	5
308	2.6	2.7	5000	38	1.1926	2.42	.2302	373	0.28	0.09	30	0.75	3
296	3.1	2.7	5000	36	1.2558	2.77	.2905	518	0.29	0.08	30	0.66	4
299	3.6	2.7	5000	39	1.3036	3.01	.3390	647	0.29	0.07	39	0.53	5
326	4.1	2.7	5000	42	1.3610	3.28	.3970	809	0.29	0.11	26	0.45	6
329	5.0	2.7	5000	44	1.4741	3.76	.5108	1140	0.29	0.14	16	0.28	10
332	2.0	3.3	5000	32	1.1416	2.13	.1804	260	0.28	0.25	13	0.92	4
335	3.1	3.4	5000	33	1.2573	2.79	.2922	518	0.29	0.14	22	0.66	8
338	3.5	3.4	5000	36	1.3064	3.04	.3412	650	0.29	0.13	19	0.56	10
344	4.1	3.5	5000	39	1.3668	3.32	.4018	818	0.29	0.15	19	0.50	7
347	5.0	3.4	5000	41	1.4757	3.78	.5108	1132	0.29	0.12	26	0.38	6
350	2.0	4.0	5000	25	1.1430	2.15	.1812	258	0.28	0.28	21	0.97	4
353	3.1	4.0	5000	29	1.2583	2.81	.2930	516	0.29	0.16	26	0.67	3
356	3.5	4.0	5000	33	1.3067	3.05	.3414	645	0.29	0.12	23	0.55	4
362	4.1	3.9	5000	37	1.3662	3.32	.4010	812	0.29	0.10	13	0.48	6
365	5.0	4.0	5000	40	1.4813	3.81	.5161	1146	0.29	0.10	14	0.36	5
368	2.0	4.7	5000	30	1.1421	2.12	.1788	255	0.28	0.53	10	1.18	2
371	3.1	4.7	5000	32	1.2589	2.80	.2935	521	0.29	0.32	6	0.77	3
374	3.5	4.7	5000	35	1.3058	3.03	.3393	643	0.29	0.28	14	0.64	6
380	4.1	4.7	5000	39	1.3672	3.31	.4008	815	0.29	0.26	8	0.54	3
383	5.0	4.6	5000	42	1.4785	3.79	.5129	1142	0.29	0.16	14	0.43	4

TABLE A20 STAGE C VARIATION OF THE ROTATION RATE, THE PRESSURE COEFFICIENT AND THE HUB RATIO

FORCE MEASUREMENT PERPENDICULAR TO DEFLECTION DIRECTION
(EXCITATION FORCE MEASUREMENT)

STAGE ADJUSTMENT UEA=.9 MM DN/DH=.35 AB=4#18

MR	PS2	SAX	F LPM	TE C	PE BAR	M KG/S	DPT BAR	US N	K2S	K2	FK2 O/O	L1	FL1 O/O
316	3.9	2.8	3000	37	1.0813	1.78	.1161	269	0.92	2.15	2	0.24	12
313	3.5	2.7	3900	36	1.1501	2.23	.1868	364	0.93	2.38	3	0.31	30
307	3.7	2.7	4400	39	1.2237	2.64	.2005	517	0.92	2.35	5	0.25	8
301	3.6	2.7	5000	40	1.3036	3.01	.3389	647	0.93	2.38	6	0.20	48
325	4.0	2.7	4650	40	1.2871	2.95	.3228	658	0.90	2.23	6	0.20	20
322	4.3	2.8	4350	40	1.2706	2.90	.3066	659	0.88	2.13	6	0.13	69
319	4.9	2.7	4000	39	1.2543	2.84	.2915	672	0.86	1.89	8	0.08	31

STAGE ADJUSTMENT UEA=.9 MM DN/DH=.53 AB=4#21

388	2.0	1.0	5000	27	1.1390	2.15	.1807	259	1.15	3.58	3	1.81	10
391	2.6	1.0	5000	29	1.1974	2.49	.2376	385	1.12	3.50	6	1.34	24
394	3.1	1.0	5000	31	1.2554	2.82	.2959	529	1.09	3.34	5	1.28	13
397	3.5	1.0	5000	34	1.3020	3.04	.3412	650	1.07	3.18	1	1.11	13
403	4.1	1.0	5000	39	1.3614	3.32	.4020	822	1.04	3.02	5	0.95	26
407	4.6	1.0	5000	38	1.4229	3.60	.4611	988	1.01	2.83	8	0.90	13
410	5.0	1.0	5000	41	1.4754	3.80	.5144	1147	0.98	2.70	4	0.76	31

STAGE ADJUSTMENT UEA=.9 MM DN/DH=.70 AB=0

413	2.0	3.1	5000	27	1.1426	2.14	.1800	256	1.29	2.53	6	0.91	8
416	2.6	3.1	5000	29	1.2027	2.49	.2381	384	1.26	2.65	5	0.51	16
419	3.1	3.1	5000	32	1.2613	2.80	.2958	524	1.24	2.46	2	0.39	16
422	3.5	3.2	5000	34	1.3086	3.04	.3426	646	1.22	2.35	6	0.44	26
428	4.1	3.1	5000	36	1.3722	3.34	.4062	822	1.19	2.18	5	0.46	6
431	4.6	3.1	5000	39	1.4294	3.58	.4635	987	1.16	2.00	6	0.43	12

TABLE A21 STAGE C VARIATION OF THE ROTATION RATE, THE PRESSURE COEFFICIENT AND THE HUB RATIO

FORCE MEASUREMENT PERPENDICULAR TO DEFLECTION DIRECTION

(EXCITATION FORCE MEASUREMENT)

ROTOR ADJUSTMENT UEA=.9 MM DN/DM=.35 AB=4#18

MR	PSI	SAX	N UPM	TE C	PE BAR	M KG/S	DPT BAR	US N	K2S	K2	FK2 0/0	L1	FL1 0/0
315	3.9	2.8	3000	37	1.0832	1.79	.1197	253	0.62	2.20	5	-0.30	9
312	3.5	2.7	3900	36	1.1501	2.22	.1867	363	0.65	2.29	8	-0.28	19
306	3.7	2.7	4400	39	1.2234	2.64	.2601	510	0.63	2.33	4	-0.31	14
300	3.6	2.7	5000	39	1.3036	3.01	.3389	647	0.64	2.32	9	-0.30	12
324	4.0	2.7	4650	40	1.2869	2.95	.3226	657	0.62	2.28	8	-0.27	10
321	4.3	2.8	4350	39	1.2703	2.90	.3069	658	0.60	2.16	6	-0.30	14
318	4.9	2.7	4000	39	1.2541	2.84	.2910	671	0.57	1.88	10	-0.30	9

ROTOR ADJUSTMENT UEA=.9 MM DN/DM=.53 AB=4#21

387	2.0	1.0	5000	26	1.1388	2.15	.1804	258	0.73	3.43	4	-1.07	5
390	2.6	1.0	5000	29	1.1971	2.49	.2373	384	0.70	3.21	4	-1.05	7
393	3.1	1.0	5000	31	1.2558	2.82	.2959	527	0.67	2.94	1	-0.94	4
396	3.5	1.0	5000	34	1.3024	3.05	.3411	649	0.64	2.85	3	-1.03	5
402	4.1	1.0	5000	39	1.3619	3.32	.4023	823	0.61	2.59	5	-0.92	5
406	4.6	1.0	5000	37	1.4225	3.60	.4611	987	0.58	2.52	4	-0.76	14
409	5.0	1.0	5000	40	1.4758	3.81	.5146	1148	0.55	2.30	2	-0.63	26

ROTOR ADJUSTMENT UEA=.9 MM DN/DM=.70 AB=0

412	2.0	3.1	5000	27	1.1430	2.14	.1801	256	0.72	3.03	4	-0.52	13
415	2.6	3.1	5000	29	1.2026	2.49	.2379	383	0.70	2.89	4	-0.68	19
418	3.1	3.1	5000	32	1.2611	2.80	.2955	523	0.67	2.64	6	-0.69	21
421	3.5	3.2	5000	33	1.3082	3.04	.3425	646	0.65	2.59	6	-0.60	17
427	4.1	3.1	5000	36	1.3718	3.34	.4059	821	0.62	2.42	8	-0.57	17
430	4.6	3.1	5000	39	1.4296	3.58	.4636	987	0.60	2.26	6	-0.51	13

TABLE A22 STAGE C VARIATION OF THE ROTATION RATE, THE PRESSURE COEFFICIENT AND THE HYB RATIO

FORCE MEASUREMENT PERPENDICULAR TO DEFLECTION DIRECTION
(EXCITATION FORCE MEASUREMENT)

STATOR ADJUSTMENT UEA=.9 MM DN/DM=.35 AB=4*18

MR	PSI	SAX	N UPM	TE C	PE BAR	M KG/S	DPT BAR	US M	K2S	K2	FK2 O/O	L1	FL1 O/O
314	4.1	2.8	3000	37	1.0892	1.84	.1259	272	0.28	0.15	17	0.47	6
311	3.5	2.7	3900	37	1.1499	2.22	.1868	364	0.28	0.10	26	0.38	5
305	3.7	2.7	4400	40	1.2237	2.64	.2603	517	0.29	0.10	25	0.31	5
299	3.6	2.7	5000	39	1.3036	3.01	.3390	647	0.29	0.07	39	0.53	5
323	4.0	2.7	4650	40	1.2870	2.95	.3227	657	0.29	0.07	49	0.47	6
320	4.3	2.8	4350	39	1.2703	2.89	.3062	657	0.29	0.08	31	0.42	7
317	4.9	2.7	4000	38	1.2536	2.84	.2909	670	0.29	0.10	25	0.35	8

STATOR ADJUSTMENT UEA=.9 MM DN/DM=.53 AB=4*21

386	2.0	1.0	5000	26	1.1384	2.14	.1803	257	0.42	0.19	50	2.68	2
389	2.6	1.0	5000	29	1.1965	2.49	.2368	383	0.42	0.30	35	2.15	4
392	3.1	1.0	5000	31	1.2549	2.82	.2949	526	0.43	0.30	34	2.04	4
395	3.5	1.0	5000	34	1.3023	3.05	.3411	649	0.43	0.38	22	1.98	3
401	4.1	1.0	5000	38	1.3621	3.33	.4024	822	0.43	0.40	29	1.73	7
405	4.5	1.0	5000	37	1.4218	3.60	.4604	984	0.43	0.43	16	1.56	5
408	5.0	1.0	5000	40	1.4759	3.81	.5150	1148	0.43	0.40	11	1.53	7

STATOR ADJUSTMENT UEA=.9 MM DN/DM=.70 AB=0

411	2.0	3.1	5000	26	1.1424	2.14	.1797	255	0.56	-0.60	21	1.52	6
414	2.6	3.1	5000	29	1.2026	2.49	.2381	383	0.56	-0.33	27	1.33	5
417	3.1	3.1	5000	31	1.2606	2.80	.2952	522	0.56	-0.26	29	1.19	6
420	3.5	3.2	5000	33	1.3078	3.04	.3421	645	0.57	-0.20	31	1.19	5
426	4.1	3.1	5000	36	1.3719	3.34	.4035	819	0.57	-0.20	24	1.06	3
429	4.6	3.1	5000	38	1.4297	3.58	.4636	987	0.57	-0.17	25	0.96	3

TABLE A23 STAGE C VARIATION OF THE PRESSURE COEFFICIENT AND THE ROTOR LABYRINTH (WEBS)

FORCE MEASUREMENT PERPENDICULAR TO DEFLECTION DIRECTION
(EXCITATION FORCE MEASUREMENT)

ROTOR ADJUSTMENT DEA=.9 M.I DN/DM=.53 AB=4.21 WITHOUT WEB

MR	PSI	SAX	N UPM	TE C	PE BAR	M KG/S	DPT BAR	US M	K2S	K2	FK2 O/O	L1	FL1 O/O
559	2.1	3.0	5000	29	1.1335	2.16	.1839	267	0.73	2.84	2	-0.29	45
562	3.5	3.0	5000	36	1.2879	3.00	.3349	637	0.64	2.27	3	-0.43	11
565	5.0	2.9	5000	43	1.4634	3.78	.5100	1148	0.54	1.70	3	-0.63	14

ALL CHAMBERS WITH WEBS

549	2.0	3.0	5000	38	1.1373	2.10	.1754	255	0.73	0.11	76	-0.00	999
552	3.6	3.4	5000	50	1.2910	2.93	.3282	636	0.64	0.06	81	0.23	5
555	5.0	2.8	5000	52	1.4547	3.67	.4923	1107	0.54	0.02	110	0.31	16

FIRST CHAMBER WITH WEBS

568	2.1	3.0	5000	35	1.1330	2.15	.1838	273	0.73	-1.67	6	-0.02	536
571	3.6	2.9	5000	42	1.2824	2.97	.3314	640	0.64	-0.94	16	0.17	58
574	3.2	2.9	5000	51	1.4587	3.74	.5088	1163	0.52	-0.57	13	0.20	29

TABLE A24 REACTION STAGES

FORCE MEASUREMENT IN DEFLECTION DIRECTION

STAGE ADJUSTMEN STAGE A

MR	PSI	SAX	I UPM	TE C	PE BAR	M KG/S	DPT BAR	US M	K1	FL1 O/O	L2	FL2 O/O
71	3.6	1.6	3000	31	1.0772	3.71	.1129	487	0.61	10	0.43	5
67	3.6	2.1	3000	35	1.0751	3.74	.1109	487	0.56	20	0.44	3
80	3.8	3.6	3000	28	1.0908	3.90	.1188	528	0.04	133	0.71	2

STATOR ADJUSTMENT STAGE B

469	2.5	3.3	4000	31	1.1153	2.40	.1395	284	-0.34	7	1.08	4

ROTOR ADJUSTMENT STAGE B

470	2.4	3.3	4000	30	1.1141	2.39	.1384	280	-3.60	5	-0.66	35

STAGE ADJUSTMENT STAGE B

471	2.5	3.3	4000	27	1.1196	2.44	.1441	294	-3.86	9	0.30	35

STAGE ADJUSTMENT 3-STAGE GROUP

511	6.9	2.8	2000	42	1.2541	2.17	.3026	1078	-2.83	4	0.43	19
497	2.5	2.9	4000	72	1.3943	2.47	.4347	899	-3.69	6	0.77	25
509	2.3	2.8	4000	39	1.3908	2.61	.4364	859	-3.59	6	0.62	33
512	2.4	2.8	4000	50	1.3995	2.58	.4451	898	-3.60	7	0.27	69
513	2.5	2.8	4500	52	1.4337	2.69	.4787	886	-3.84	14	0.29	91

/157

TABLE A25 STAGE C VARIATION OF THE AXIAL GAP AND COVERING

FORCE MEASUREMENT IN DEFLECTION DIRECTION

STAGE ADJUSTMENT UEA=.0 MM DN/DM=.35 AB=4*18

MK	PSI	SAX	I UPM	TE C	PE BAR	M KG/S	DPT BAR	US M	K1	FK1 O/O	L2	FL2 O/O
133	3.5	1.2	5000	34	1.3128	3.09	.3403	652	-0.02	290	0.25	23
141	3.5	2.2	5000	33	1.3154	3.11	.3419	654	-0.17	30	-0.13	30
180	3.5	2.7	5000	33	1.3077	3.08	.3382	645	-0.09	83	-0.21	29
149	3.5	3.2	5000	31	1.3131	3.11	.3411	650	0.14	46	-0.44	11
164	3.5	4.2	5000	32	1.3075	3.09	.3374	642	0.90	10	-0.65	9
172	3.5	5.2	5000	34	1.3019	3.06	.3342	638	1.00	13	0.19	36

STAGE ADJUSTMENT UEA=.9 MM DN/DM=.35 AB=6*18

286	3.6	0.5	5000	40	1.3036	3.01	.3392	648	-1.99	4	2.15	3
265	3.6	1.6	5000	33	1.3181	3.11	.3510	672	-0.37	30	0.18	62
304	3.6	2.7	5000	41	1.3032	3.00	.3389	649	-0.13	52	-0.12	22
343	3.6	3.4	5000	38	1.3057	3.03	.3407	651	0.25	42	-0.29	21
361	3.5	4.0	5000	35	1.3059	3.03	.3409	649	0.46	17	-0.63	10
379	3.5	4.7	5000	38	1.3051	3.02	.3388	644	0.79	14	-0.25	24

ROTOR ADJUSTMENT UEA=.9 MM DN/DM=.35 AB=4*18

285	3.6	0.5	5000	39	1.3041	3.01	.3394	648	-3.01	12	-1.32	16
264	3.6	1.6	5000	32	1.3157	3.10	.3488	666	-1.13	9	-1.44	6
303	3.6	2.7	5000	41	1.3032	3.01	.3389	649	-0.63	14	-1.17	7
342	3.6	3.4	5000	38	1.3062	3.03	.3409	651	-0.34	30	-0.99	5
360	3.5	4.0	5000	35	1.3065	3.04	.3407	646	-0.19	68	-0.90	7
378	3.5	4.7	5000	37	1.3054	3.02	.3387	644	0.14	89	-0.81	7

STATOR ADJUSTMENT UEA=.9 MM DN/DM=.35 AB=6*18

284	3.6	0.5	5000	39	1.3040	3.01	.3392	647	0.78	12	3.32	5
263	3.5	1.6	5000	32	1.3137	3.09	.3471	660	0.65	8	1.58	7
302	3.6	2.7	5000	40	1.3034	3.01	.3392	649	0.39	10	0.98	8
341	3.6	3.4	5000	37	1.3067	3.04	.3410	650	0.55	13	0.62	17
359	3.5	4.0	5000	34	1.3066	3.04	.3411	645	0.66	8	0.45	25
377	3.5	4.7	5000	37	1.3054	3.02	.3390	644	0.71	9	0.46	25

TABLE A26 STAGE C VARIATION OF THE PRESSURE COEFFICIENT AND THE HUB RATIO

FORCE MEASUREMENT IN DEFLECTION DIRECTION

STATOR ADJUSTMENT UEA=.9 MM DN/DM=.53 AB=4*21

MR	PSI	SAX	N UPM	TE C	PE BAR	M KG/S	DPT BAR	US N	X1	FK1 O/O	L2	FL2 O/O
558	2.1	3.0	5000	28	1.1350	2.17	.1843	269	0.99	15	2.02	4
561	3.5	3.0	5000	35	1.2878	3.01	.3346	637	0.51	8	1.64	3
564	5.0	2.9	5000	42	1.4641	3.78	.5109	1149	0.35	7	1.55	2

ROTOR ADJUSTMENT UEA=.9 MM DN/DM=.53 AB=4*21

559	2.1	3.0	5000	29	1.1335	2.16	.1839	267	-0.83	34	-1.19	13
562	3.5	3.0	5000	36	1.2879	3.00	.3343	637	-0.77	16	-0.92	9
565	5.0	2.9	5000	43	1.4634	3.78	.5100	1148	-0.88	9	-0.68	8

STAGE ADJUSTMENT UEA=.9 MM DN/DM=.53 AB=4*21

560	2.1	3.0	5000	30	1.1334	2.15	.1831	267	0.39	39	0.92	13
563	3.5	3.0	5000	36	1.2881	3.00	.3346	638	-0.34	37	0.73	8
566	5.1	2.9	5000	43	1.4629	3.77	.5097	1148	-0.64	21	0.79	5

STATOR ADJUSTMENT UEA=.9 MM DN/DM=.70 AB=0

2	2.0	3.1	5000	31	1.1346	2.09	.1755	248	2.95	9	1.55	10
5	3.6	3.1	5000	45	1.3029	2.98	.3397	653	1.87	8	1.52	9
8	5.2	3.2	5000	60	1.4677	3.65	.5059	1155	1.48	9	1.52	8

ROTOR ADJUSTMENT UEA=.9 MM DN/DM=.70 AB=0

3	2.0	3.1	5000	33	1.1342	2.08	.1750	248	-0.50	49	-0.73	29
6	3.7	3.1	5000	47	1.3016	2.97	.3385	653	-0.67	11	-0.65	7
9	5.3	3.1	5000	63	1.4644	3.63	.5031	1152	-0.83	7	-0.58	8

STAGE ADJUSTMENT UEA=.9 MM DN/DM=.70 AB=0

4	2.0	3.4	5000	34	1.1339	2.07	.1747	248	2.51	11	0.70	31
7	3.7	3.1	5000	48	1.3009	2.95	.3380	653	1.31	13	0.75	16
10	5.3	3.1	5000	66	1.4613	3.60	.4993	1146	0.74	18	0.83	13

TABLE A27 PROTOCOL FOR THE DETERMINATION OF THE DAMPING CONSTANTS

EVALUATION STAGE C MEASUREMENT SERIES 23 DETERMINATION OF DAMPING CONSTANTS

MASS = 111.0 KG

NP	V CM/S	SX1	SX2	SX3	SY1	SY2	SY3	UX 1/S	JY 1/S	DX NS/MM	DY NS/MM	
7203	5,23	47,5	43,5	47,5	47,5	45,5	46,5	-2,760	-2,793	0,306	0,319	FRONT
	5,25	49,5	43,5	46,5	48,5	51,5	53,5	-2,790	-2,952	0,310	0,331	BACK
										0,308	0,325	MEAN VALUE
7211	5,23	43,5	48,5	47,5		45,5	45,5	-2,750	-2,749	0,305	0,304	FRONT
	5,25	55,5	51,5	51,5		53,5	54,5	-3,203	-3,234	0,355	0,359	BACK
										0,330	0,331	MEAN VALUE
7214	5,23	48,5	48,5		48,5	48,5		-2,830	-2,905	0,314	0,322	FRONT
	5,23	52,5			48,5	45,5		-3,131	-2,853	0,347	0,311	BACK
										0,331	0,317	MEAN VALUE

DAMPING CONSTANTS: DX = 0,323 NS/MM +- 4,22 %

DY = 0,322 NS/MM +- 3,42 %

TABLE A28 PROTOCOL FOR THE EVALUATION OF A MEASUREMENT SERIES
(KUNETIC TESTS)

EVALUATION MEASUREMENT SERIES 30 DETERMINATION OF EXCITATION CONSTANTS

(BLADE LENGTH = 41.5 MM)

1	= 185,0 KG			CZ	= 7,014 N/MM			OMK	= 66,173 1/S		F	= 177,6							
CXX	= 197,1 N/MM			CYY	= 208,9 N/MM						A	= 1,060							
CXY	= -10,8 N/MM			CYX	= -10,8 N/MM			K	= -0,395		C	= 1,030							
JX	= 0,307 KS/MM			JY	= 0,450 KS/MM			D	= 0,0719		B	= 1,436							
MP	V CM/S	SX1	SX2	SX3	SY1	SY2	SY3		J 1/S	EJ D/D	Q W/MM	PSI	JS N	K	DS	S			
4031	5,16		19,0	19,5	31,0	31,0	31,0												
	5,16		19,0	20,0	32,0	31,0	31,5		-1,574	10,59	22,7	1,95	637	2,15	,0341	,0577			
4032	5,16	15,5	15,5	15,5	22,0	21,0													
	5,16	15,5	15,5	16,0	21,0	21,0			-1,060	11,33	28,5	1,77	583	2,03	,0230	,0724			
4033	5,16	12,0	12,0	12,0	14,0	15,0													
	5,16	12,0	11,5	12,0	13,5	15,0			-0,766	7,49	32,0	2,05	736	1,81	,0166	,0811			
4034	5,16	12,5	12,5	12,5	15,0	14,0													
	5,16	13,0	12,5	13,0	14,0	13,5			-0,787	4,53	31,7	2,29	865	1,53	,0170	,0805			
4035	5,16	9,0	8,0	8,0	9,5	10,0													
	5,16	9,0	8,5	8,0	8,5	10,0			-0,526	8,38	35,0	2,95	1317	1,43	,0114	,0889			
4036	5,16	2,0		2,0	2,0	2,1													
	5,16	2,0	1,8	2,2	2,0	2,0	2,0		-0,119	3,56	40,6	2,81	1165	1,45	,0026	,1030			
								MEAN VALUES	-0,806	8,40		2,15		1,73					

TABLE A29 ERROR COMPUTATION FOR KINETIC TESTS

		M KG	C N/MM	CXX N/MM	CYY N/MM	CXY N/MM	CYX N/MM	DX NS/MM	DY NS/MM	U 1/S	Q N/MM	
STAGE A MR 1												
INITIAL VALUES		67	70019	196.1	196.1	-2.0	-2.0	0.0758	0.0758	-0.44	7.84	
MEAS.UNCERT.	0/0	1.0	1.0	2.0	2.0	20.0	20.0	5.0	5.0	20.7		
EFFECT ON Q	0/0	-0.9	0.0	11.9	11.9	7.6	-2.4	3.1	3.1	-10.4	21.8	0/0
											TOTAL ERROR	
STAGE C MR 27												
INIT.VALUES		111	70019	196.8	194.0	-7.7	-9.8	0.3203	0.3224	-0.77	30.52	
MEAS.UNCERT.	0/0	1.0	1.0	2.0	2.0	20.0	20.0	4.2	3.4	10.0		
EFFECT ON Q	0/0	-0.7	0.0	2.2	0.0	7.9	-2.8	2.1	1.7	-2.8	9.6	0/0
											TOTAL ERROR	
STAGE C MR 27												
INIT.VALUES		111	70019	183.9	194.0	-7.7	-12.0	0.3310	0.3011	-1.10	37.35	
MEAS.UNCERT.	0/0	1.0	1.0	2.0	2.0	20.0	20.0	2.4	2.5	17.2		
EFFECT ON Q	0/0	-0.3	0.0	-5.9	7.7	6.2	-3.2	0.5	0.7	-3.2	12.4	0/0
											TOTAL ERROR	
3-STAGE GROUP MR 30												
INIT.VALUES		185	70019	197.1	208.3	-10.8	-10.8	0.3072	0.4596	-0.79	31.50	
MEAS.UNCERT.	0/0	1.0	1.0	2.0	2.0	20.0	20.0	1.0	4.4	8.4		
EFFECT ON Q	0/0	-0.5	0.0	-3.2	5.1	11.7	-2.0	0.5	1.2	-2.6	13.6	0/0
											TOTAL ERROR	
3-STAGE GROUP MR 31												
INIT.VALUES		185	70019	205.9	210.4	-11.8	-11.8	0.2592	0.4114	-0.47	32.29	
MEAS.UNCERT.	0/0	1.0	1.0	2.0	2.0	20.0	20.0	3.1	1.5	13.2		
EFFECT ON Q	0/0	-0.4	0.0	-0.5	2.4	12.7	-1.9	1.1	0.4	-2.4	13.4	0/0
											TOTAL ERROR	